

University of Salford

Not to be removed
from the Library

R

Username:	<u>UTS 203</u>
Date added:	<u>02/05/18</u>

Requested Item Collection

Once you have collected your item from the request shelf you should issue it on the self service machines located nearby.

The item will only issue to the user who holds the request against it.

A THESIS SUBMITTED FOR MEMBERSHIP OF THE COLLEGE
OF TECHNOLOGISTS

March, 1967.

FUNDAMENTAL STUDIES OF THE
BEHAVIOUR OF ANTIMONY IN
THE LEAD-ACID BATTERY

by

JOHN LIONEL DAWSON

[University of Salford, Ph.D.]

Department of Pure and Applied Chemistry,
Royal College of Advanced Technology, Salford.

and

Electric Power Storage Co. Ltd., Wynne Avenue,
Clifton, Swinton,
Manchester.

ACKNOWLEDGEMENTS

The author wishes to express his appreciation to Dr. M.I. Gillibrand and Dr. J. Wilkinson for their supervision and encouragement throughout this work. Also to the Directors of Chloride Technical Services Limited and Electric Power Storage Company Limited for the financial support during the period of research.

5600342/505

CONTENTS

<u>ABSTRACT</u>	1
1. <u>INTRODUCTION</u>	3
1.1 The lead-acid battery	3
1.2 'Antimony poisoning' a cause of self discharge	5
2. <u>EXPERIMENTAL</u>	10
<u>2.1 Antimony ions in aqueous sulphuric acid</u>	11
2.1.1 Preparation of solutions	11
2.1.2 Ionic migration of radio-active antimony	13
2.1.3 Spectrophotometric and polarographic analysis	16
2.1.4 Solvent extraction	17
<u>2.2 The deposition of antimony from aqueous sulphuric acid onto pure lead electrodes</u>	19
2.2.1 The lead electrodes	23
2.2.2 The deposition cell	26
2.2.3 The radiation detector and counting equipment	29
2.2.4 Electrochemical measurements	32
2.2.5 Purification of nitrogen	34
2.2.6 Calibration of the radio-activity	35
2.2.7 Deposition studies	36
<u>2.3 Antimony chemistry in the lead-acid battery</u>	36
2.3.1 Production of antimony species from antimonial-lead electrodes	36
2.3.2 The reduction and oxidation of antimony in aqueous sulphuric acid	37
2.3.3 The adsorption of antimony onto lead dioxide and lead-sulphate	37

<u>3. RESULTS</u>	39
<u>3.1. Antimony ions in aqueous sulphuric acid</u>	39
3.1.1. Ionic migration	39
3.1.2. Polarographic analysis	45
3.1.3. Spectrophotometric analysis	56
3.1.4. Solvent extraction	75
<u>3.2. The deposition of antimony from aqueous sulphuric acid onto pure lead electrodes</u>	78
<u>3.3. Antimony chemistry in the lead-acid battery</u>	103
3.3.1. The production of antimony species	103
3.3.2. The reduction and oxidation of antimony	104
3.3.3. The adsorption of antimony onto lead dioxide and lead sulphate	106
<u>4. DISCUSSION</u>	110
<u>4.1. Antimony ions in aqueous sulphuric acid</u>	110
4.1.1. Ionic migration	110
4.1.2. Polarographic determinations	110
4.1.3. Spectrophotometric analysis	112
4.1.4. Solvent extraction	113
4.1.5. Interpretation of results	116
<u>4.2. The deposition of antimony</u>	132
4.2.1. Experimental technique	132
4.2.2. The rate of antimony deposition	135
4.2.3. Electrochemical measurements	144

<u>4.3. Antimony in the lead-acid battery</u>	150
4.3.1. Antimony chemistry	150
4.3.2. The behaviour of antimony in the lead-acid battery	151
4.3.3. The limiting of 'antimony poisoning'	156
5. <u>CONCLUSIONS</u>	159
6. <u>APPENDIX</u>	168
7. <u>REFERENCES</u>	168

Abstract

One of the technological problems associated with the lead-acid battery is the self-discharge of the negative plate as a result of the deposition of antimony onto the sponge lead electrode, a process known as 'Antimony Poisoning'.

The rate of deposition of antimony (III) from aqueous sulphuric acid onto pure lead electrodes was measured using a tracer technique. The deposition rate was found to be independent of the hydrogen overpotential of the electrode and was ascribed to the electrochemical displacement reaction $2\text{SbO}^+ + 3\text{Pb} + 4\text{H}^+ + 3\text{SO}_4^{--} = 2\text{Sb} + 3\text{PbSO}_4 + 2\text{H}_2\text{O}$

In oxygen free electrolyte and under the forced convection conditions of electrolyte flow used, the deposition rate was governed by the equation $\text{Nu} = \text{K Re}^{\frac{1}{2}} \text{Sc}^{\frac{1}{3}}$. Where Nu and Re are the Nusselt and Reynold numbers at the electrode respectively and Sc is the Schmidt number.

Unlike antimony (III), antimony (V) was not deposited onto lead electrodes and neither antimony (III) nor antimony (V) were deposited electrolytically onto lead-lead dioxide electrodes. Tracer experiments showed that both antimony (III) and antimony (V) are adsorbed onto lead dioxide and to a lesser extent onto lead sulphate, the rate of adsorption decreasing with increase of sulphuric acid concentration.

The antimony (III) species formed in sulphuric acid solutions have been investigated by ion exchange, solvent extraction, polarography and ultra-violet spectrophotometry. Comparisons were also made with antimony (V) solutions. The antimonyl ion, SbO^+ , was shown to exist in a hydrated

form $[(H_2O)_2Sb(OH)_2]^+$ below 1.5M sulphuric acid. The observed change in the wave length of the antimony (III) spectra maximum and molar extinction coefficients in 0.25 to 18M sulphuric acid were attributed to the coexistence of the antimony (III) anions $[SbO(OH)_2]^-$, $[SbO_2]^-$ and the antimony sulphato-complexed anions $[SbOSO_4]^-$, $[Sb(SO_4)_2]^-$. Dimerisation of these antimony (III) ions occurred in solutions with an antimony concentration greater than $1 \times 10^{-4}M$.

Antimony (V) was shown to be present as a stable complex anion in sulphuric acid solutions and could be considered as $[Sb_3O_9]^{3-}$. This anion was unaffected by a change of acid concentration over the range 0.5 to 8M sulphuric acid, above 8M sulphuric acid complexing of the anion with the undissociated sulphuric acid occurred.

The results obtained were assessed in conjunction with published data, and a comprehensive picture of the various antimony (III) and antimony (V) reaction paths occurring in the lead-acid battery has been presented. The placing of a suitable ion-exchange material between the separator and the negative plate, with the object of removing antimony (III), could be a feasible method of limiting the problem of 'Antimony Poisoning'.

1. INTRODUCTION

1.1 The Lead Acid Battery

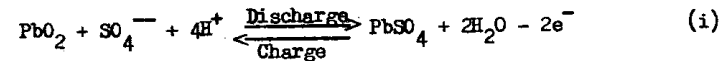
The lead acid battery, in its present day commercial form consists of a series of positive and negative plates immersed in aqueous sulphuric acid electrolyte, contact between each plate being prevented by a porous non-electrically-conducting separator. The plates consist of a lead alloy grid, often antimonial lead, which acts as a take-off contact for the external circuit and as the support framework for the active material. The active material is lead dioxide in the positive plate and sponge lead in the negative plate.

Antimony is added to the grid alloy to improve its mechanical properties, such as hardness, castability and resistance to creep. The use of antimony alloys also reduces "shedding" or loss of the positive active material, since the anodic corrosion products of these antimony alloys appear to have good adhesion properties with respect to the positive active material.

The lead acid battery is a secondary cell. Its accepted reaction mechanism, based on the "double sulphate" was first been put forward by Gladstone and Tribe⁽¹⁾ and later confirmed by Vinal and Craig⁽²⁾, and Beck and Wynne-Jones⁽³⁾, a detailed derivation being given by Vinal⁽⁴⁾.

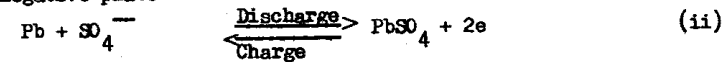
The reactions taking place are:-

at the positive plate



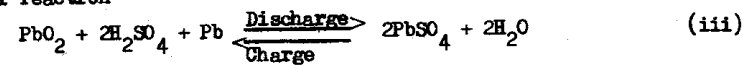
$$E_o = 1.685 \text{ volts}^*$$

at the negative plate



$$E_o = 0.356 \text{ volts}^*$$

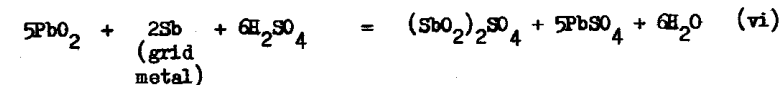
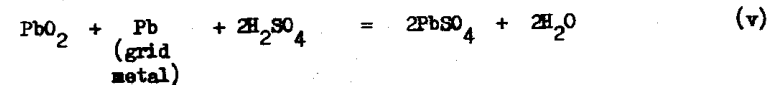
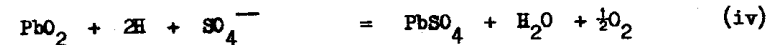
overall reaction

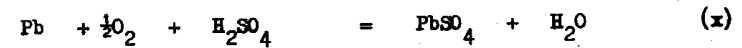
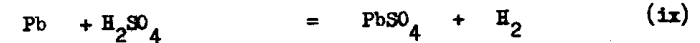
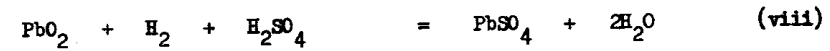
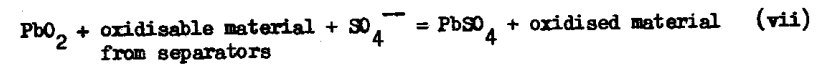


$$E_o = 2.042 \text{ volts}^*$$

(* See appendix 1 for electrode potentials)

In addition to the principal electrode reactions which take place in the lead acid battery, there are other, secondary reactions which give rise to self discharge of the battery. These processes were investigated by Vinal⁽⁴⁾, and more recently by Ruetshi and Angstadt⁽⁵⁾, who showed that seven different reactions can contribute towards self discharge:-





Self discharge of the negative plates, reaction (ix), is slow in the absence of impurities, but contamination by antimony greatly increases the rate of the reaction, since antimony has a lower hydrogen over-voltage than lead. This increase in the rate of self discharge of the battery is known as "antimony poisoning" of the negative electrode.

1.2 "Antimony Poisoning"

In 1900 Stresser and Gahl⁽⁶⁾ realised that the grid antimony of the negative plate could affect the voltage of the plate. Later Crehnel and Milligan⁽⁷⁾ reported traces of stibine in the gases evolved during charging of lead acid batteries, and they concluded that the presence of antimony on the negative plate resulted in its self discharge. Haring and Thomas⁽⁸⁾ found that the evolution of stibine was increased when charging was completed and over charging began. These results were confirmed by Byfield⁽⁹⁾, who also showed that the amount of antimony present in the active material of the negative grid was far in excess of any quantity which could have diffused from the negative grid itself.

The comparatively recent use of radioactive isotopes afforded the battery technologist an effective technique for the study of the problem of "antimony poisoning". Herrmann and Propstl⁽¹⁰⁾ dosed the grid alloy of standard lead-acid batteries with radioactive antimony, and after formation of the plates and subsequent testing of the cells, studied the resulting distribution of antimony. They found that the majority of the antimony detected in the plates, the separators and in the electrolyte came from the positive plate grid. The greater part of this released antimony was contained in the positive material, whilst a smaller proportion was deposited onto the negative plate, especially after lengthy continuous charging of the battery. Antimony from the negative grid was also detected in both the negative and positive plate materials, in the separators and in the electrolyte, but this was only a fraction of the total antimony released.

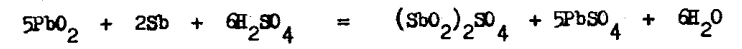
Since it was already known⁽⁵⁾ that the use of different separators could affect the rate of self discharge of the negative plate, Zehender, Herrmann and Leibsalle⁽¹¹⁾ used a radioactive tracer technique to study the influence of the separators on "antimony poisoning". They established that large antimony fluctuations occur in the electrolyte space around the positive plate, particularly during charge-discharge cycles, and also that the positive plate, during charging, takes up a large proportion of the antimony released during the previous discharge

(11)

of the battery. Zehender et al concluded that if the antimony fluctuations could be confined by a suitable separator, limiting the diffusion of antimony into the negative compartment, "antimony poisoning" of the negative plates would be reduced.

During normal operation of the battery, anodic corrosion of the positive grid releases antimony into the electrolyte. Some of this antimony diffuses through the separator and is deposited onto the negative plate. Since antimony has a lower hydrogen overpotential than lead, local action commences, hydrogen is liberated and the sponge lead is converted to lead sulphate, resulting in a gradual discharge of the negative plate, reaction (ix).

The above overall mechanism of "antimony poisoning" has thus been established but the individual reactions involved in each stage of the process have not been studied in detail, apart from the self-discharge reaction (vi).



which was shown⁽⁵⁾ to be dependant upon the solubility of antimony (V) in sulphuric acid.

No information has been published regarding the antimony species formed in the strongly acidic conditions of the lead-acid battery, even though an understanding of these antimony ions is of prime

importance in elucidating the mechanisms of dissolution, transference and deposition of antimony.

The chemical nature of antimony, with its outer electronic configuration of $4d^{10}5s^25p^3$, leads one to expect the existence of both antimony (III) and antimony (V) compounds. However antimony does exhibit valencies greater than three and five by way of the available $4d^{10}$ orbitals; and ions $[SbCl_6]^-$ and $[SbCl_4]^-$ are known to exist⁽²²⁾.

In the solid state, compounds such as antimony trioxide, Sb_4O_6 , antimony trisulphate $Sb_2(SO_4)_3$, and antimony pentoxide Sb_2O_5 are well known. The antimony (V) salts are based on a co-ordination number of six and contain either the $[Sb(OH)_6]^-$ ion or the complex oxide group SbO_6 ;⁽¹²⁾ some of the antimony (III) salts are thought to contain the discrete ion SbO^+ e.g. $(SbO)_2SO_4$, which, on treatment with water gives "antimonyl" solutions.

The aqueous chemistry of antimony is based on the co-ordination of four or six oxygen atoms resulting, for example, in ions such as $[Sb(OH)_4]^-$ and $[Sb(OH)_6]^-$. The formula of the "antimonyl" cation is normally expressed as SbO^+ , although in aqueous solutions it is more likely⁽¹³⁾ to be hydrated ion $[(H_2O)_2Sb(OH)_2]^+$.

Pitman, Pourbaix and de Zoubov⁽¹⁴⁾ considered that antimony could be present in aqueous solutions as the simple ions SbO^+ , SbO_2^+ , $[Sb(OH)_4]^-$ and $[Sb(OH)_6]^-$ (see Appendix I). They postulated that SbO^+ was the cation most commonly encountered in acidic solutions

and that SbO_2^+ was formed under acidic oxidising conditions. $Sb(OH)_6^-$ was found in weakly acidic and in alkaline solutions, whereas $Sb(OH)_4^-$ occurred only in alkaline solutions with a pH greater than 11. No mention was made of the possibility of the acid complexing with antimony to produce, for example, the anion $[Sb(SO_4)_2]^-$ in sulphuric acid⁽¹⁵⁾. There is also evidence⁽¹⁶⁾ that in acidic solutions $[Sb(OH)_6]^-$ ions condense to give $[Sb_3O_{16}]^{3-}$ and an increase in the hydrogen ion concentration causes further condensation to give $[Sb_4O_{13}]^{6-}$.

Since modern battery technology requires a more comprehensive understanding of the problem of "antimony poisoning", it was decided that a detailed investigation into the mechanism of the deposition of antimony onto lead electrodes, together with a study of antimony ions in aqueous sulphuric acid solutions, should be undertaken.

2. EXPERIMENTAL

'Analar Grade' reagents were used throughout the experimental work, except for the antimony metal used in the preparation of the standard antimony solutions, which was obtained as 'spectrographically standardised metal' from Johnson Matthey Co. Ltd.

The choice of antimony isotope was limited to antimony 122, 124 and 125 and the antimony 124 isotope was selected from a consideration of its half life and cost.

<u>Isotope</u>	<u>Half Life</u>	<u>Cost/mc</u>	<u>Decay Emission</u>
122 _{Sb}	2.74 d	up to 5 mc/£10	Beta & Gamma
124 _{Sb}	60 d	up to 5 mc/£10	Beta & Gamma
125 _{Sb}	2.0 y	up to 0.5 mc/£10	Beta & Gamma

Antimony 124

<u>Type of radiation released</u>	<u>Beta</u>	<u>Gamma</u>
<u>Energy in Mev</u>	0.28 (12%)	0.60 (100%)
	0.63 (56%)	0.99 (5.4%)
	1.07 (4%)	1.38 (6.2%)
	1.68 (6%)	1.71 (46%)
	2.39 (22%)	2.11 (10%)

The isotope was obtained as gramules of irradiated spectrographically standardised antimony metal from the Radio Chemical Center, Amersham.

The isotope was allowed to stand for at least three weeks prior to its

use so that the short lived 122 isotope could decay. The antimony granules were easily removed from their lead container by means of tweezers, weighed on an analytical balance and then dissolved in hot concentrated sulphuric acid to give a stock tracer solution containing the required radioactive antimony concentration. In all the experiments using radioactive measurements a sample of the active solution was kept as a standard which was periodically counted with experimental samples and its decay curve noted. The radio-active measurements obtained during a series of experiments carried out over a period of time could then easily be converted to the antimony concentration, the "standard decay curve" providing the conversion factor for the decrease in count rate with time and also allowed for any variation in the detection efficiency of the counting equipment. The normal safety precautions were observed in all the experiments involving the handling of the radioactive isotope.

2.1 Antimony Ions in Aqueous Sulphuric Acid

2.1.1 Preparation of solutions

Antimony (III) / Sulphuric acid solutions were prepared in the following ways.

- (a) Known weights of antimony trioxide or antimony trisulphate were dissolved in hot dilute sulphuric acid.
- (b) A known weight of antimony metal was dissolved in hot concentrated

sulphuric acid. The solution was cooled, diluted with distilled water and sulphur dioxide was passed through the solution to ensure complete reduction of any antimony (V) to antimony (III). The excess sulphur dioxide was removed by boiling, and the solution was then diluted to the required antimony (III) / sulphuric acid concentration.

Antimony (V) / sulphuric acid solutions were prepared in the following ways.

- (a) Antimony pentoxide in amounts less than 0.5g was dissolved in 1 litre of hot dilute sulphuric acid.
- (b) Small known weights of antimony metal were dissolved in hot fuming sulphuric acid containing 20% w/w sulphur trioxide.
- (c) Antimony (V) sulphate was prepared as follows and subsequently dissolved in dilute sulphuric acid.

5g of antimony trichloride were dissolved in 200 ml of concentrated hydrochloric acid. Chlorine gas was passed through the solution to oxidise the antimony trichloride to antimony pentachloride. The colour of the solution changed from pale yellow through orange to pale green-yellow. Oxidation was considered to be complete when no colour change was observed after passing chlorine for a further hour. The solution was concentrated, cooled in an ice bath and saturated with hydrogen chloride for three hours. A white precipitate of hexachloroantimonic (V) acid was filtered off and added to 400 ml of 50% v/v sulphuric acid. This solution was then placed

in a distillation flask and the water / hydrochloric acid mixture distilled off in a stream of nitrogen. Water was added periodically and the distillation continued until no trace of chloride could be detected in the distillate. The white viscous semi-solid antimony (V) sulphate was filtered off using a sintered glass crucible. Attempts to obtain antimony (V) sulphate as a solid proved unsuccessful. To prepare solutions suitable for analysis, small quantities of the gel-like compound were dissolved in dilute sulphuric acid.

(d) Antimony (III) solutions were oxidised by means of the reactive species produced during irradiation of the solutions with gamma rays from a 4 curie cobalt-60 source.

(e) Dilute antimony (III) solutions were oxidised using hydrogen peroxide. Excess peroxide was then destroyed by boiling with small platinum metal 'boiling aids'.

2.1.2. Ionic migration of radioactive antimony

Tracer experiments were conducted to determine the ionic nature of the antimony species. Initially these experiments were carried out in a perapex cell which was divided into three compartments by means of Porvic I separator material, but in the later experiments, a three compartment cell was used which was made from Pyrex with sintered glass separators, Fig. (2.1).

The outer anodic and cathodic compartments of the cell were fitted

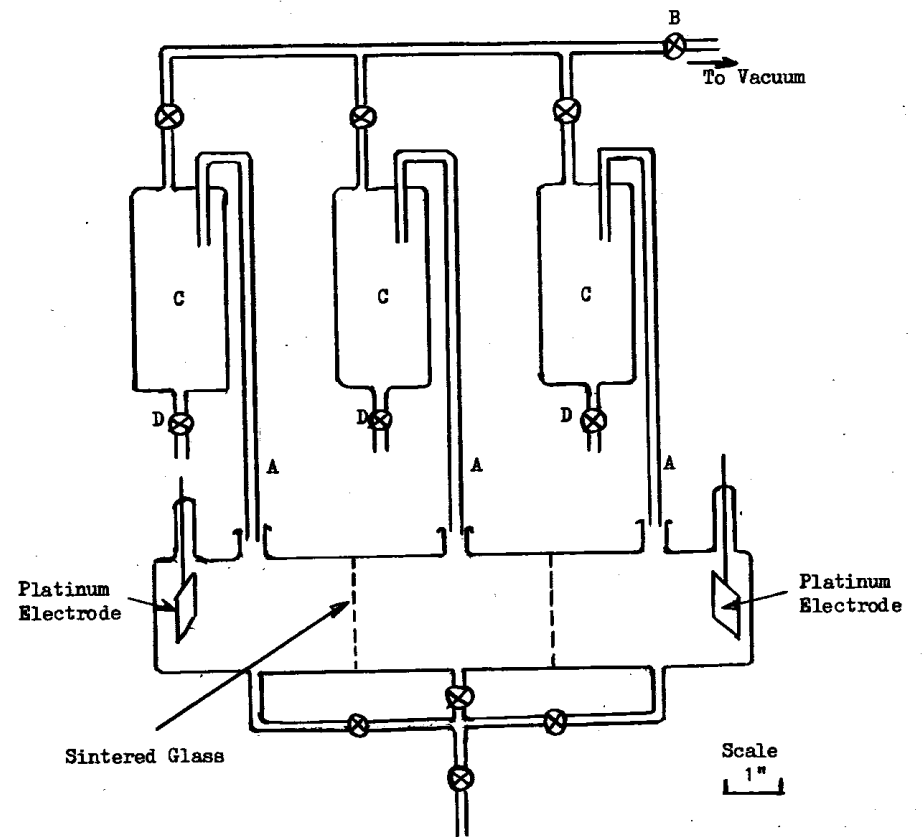


Fig. 2.1 Ionic Migration Apparatus

with platinum electrodes and the cell filled with sulphuric acid containing a known amount of either antimony (III) or antimony (V). The centre compartment was filled with electrolyte of the same composition except that the antimony present included some radioactive antimony. Care was taken to ensure a uniform electrolyte level throughout the cell, and, since the antimony and acid concentrations were the same in each cell, no concentration gradients were set up. Thus, any build up of radioactivity which occurred in the anode or cathode compartments on the passage of an electrical current, would be the result of migration of cationic or anionic antimony (III) or antimony (V). The solutions were periodically removed from the cell using a 'three pipette' system, Fig. (2.1), which emptied the three compartments simultaneously. The stems of the 'pipettes' A, were placed into the compartment and by opening tap B to vacuum the solution in the compartment was drawn up and collected in the bulb C. Tap B was then opened to the atmosphere and samples were obtained through tap D. Samples of the three solutions were counted in an annular type Geiger-Muller tube to determine the amount of radioactive antimony which had diffused from the centre compartment. The solutions were then replaced in the 'pipette' and returned to the cell through taps D. The experiment was then continued. Prior to each experiment, a series of radioactivity measurements was taken to determine the rate of diffusion of the radioactive antimony with no current flowing through

the cell. The results of these 'blank' experiments were subtracted from the results obtained for the rate of diffusion of the radioactive antimony during the passage of current.

2.1.3 Spectrophotometric and polarographic analysis

The solutions prepared as described above were analysed by ultra-violet spectrophotometric and polarographic methods in order to establish that the procedures adopted did, in fact, result in the production of antimony (III) or antimony (V) species. The ultra-violet spectra of the antimony (III) and antimony (V) solutions were measured using an Optika Recording Spectrophotometer over the wave length range 180 - 240 m μ ; 'supersil' cells were used. A 'blank' determination was carried out using sulphuric acid and the wave length scale of the spectrophotometer was checked against a Vikor filter. Since oxygen adsorption occurs in this region of the spectrum, the spectrophotometer was first purged with nitrogen and then with air and the antimony solution spectra obtained in each case were compared. The results indicated that antimony spectra were not affected by purging with nitrogen, also that spectra below 200 m μ were 'true' antimony spectra and not the results of stray light or loss of power due to 'ageing' of the deuterium lamp. Solutions of antimony in fuming sulphuric acid at various dilutions were also examined spectrophotometrically.

The polarographic analysis was first carried out using an Evershed Mark II polarograph with a saturated calomel electrode as the reference anode. Analysis was then repeated on a Southern Instruments Cathode Ray polarograph having a silver / silver chloride reference anode immersed in the test solution within the polarograph cell. This electrode was prepared by the anodisation of a clean silver wire in 0.1N hydrochloric acid.

Standard antimony (III) and antimony (V) solutions, containing 0 to 2×10^{-3} M antimony, in sulphuric acid ranging from 0.2M to 18M were prepared as described previously (Section 2.2.1). These standards were then examined spectrophotometrically and polarographically. Over a period of several days the standards were re-examined to detect any change in the spectra after standing.

2.1.4 Solvent extraction using radioactive antimony

A series of solutions containing 0.5×10^{-5} M to 1×10^{-4} M antimony (III), dosed with antimony 124, in 0.2M to 10M sulphuric and 0.1M to 7M perchloric acid were prepared by dissolving irradiated antimony metal in either hot concentrated sulphuric acid or hot 60% perchloric acid, followed by dilution to the required antimony and acid concentration.

10 ml samples of these solutions were then continuously shaken with an equal volume of an organic solvent containing a complexing agent. The organic solutions used were 1M thenoyl trifluoroacetone (T.T.A.) in

benzene, $2.5 \times 10^{-3}M$ 9-methyl 2,3,7, trihydroxy-6-flurone in benzoyl alcohol and 0.01M thioalide in cyclohexanone. After shaking for 60 min., 1 ml aliquots of the aqueous and organic layers were counted using a sodium iodide well crystal and the distribution coefficients,

$$K_d = \frac{\text{Concentration of antimony in the organic layer}}{\text{Concentration of antimony in the aqueous layer}}$$

were calculated directly from the radioactivity measurements.

2.2 The Deposition of Antimony from Aqueous Sulphuric Acid onto Pure Lead Electrodes.

The rate of deposition of antimony onto lead was investigated by means of a tracer technique using antimony-124. The deposition of antimony was measured continuously by monitoring the lead electrode through the sulphuric acid electrolyte, and, by using a flowing electrolyte system, a constant level of antimony concentration was maintained in the electrolyte at the electrode interface.

Figs (2.2), (2.3), and (2.4) show the final version of the apparatus used. The apparatus consisted of a deposition cell, a constant head device from which the electrolyte flow could be controlled and measured, and a radiation detector. Pyrex glass was used throughout the apparatus, except for the deposition cell and the electrolyte pumps which were made from perspex.

The deposition apparatus components, listed below, have the same lettering in Figs. (2.2), (2.3), and (2.6).

- | | |
|----------------------------|-------------------------------------|
| A - Reservoir | N - Counter Electrodes |
| B - Constant Head Device | O - Araldite Backing |
| C - Pumps | P - Beta Sensitive Plastic Phosphor |
| D - Deposition Cell | Q - Photo Multiplier Tube |
| E - Flow Control Tap | R - Light Pipe |
| F - Differential Manometer | S - Hydrogen Reference Electrodes |
| G - Tap | T - Luggin Capillary |
| H - Tap | U - First Salt Bridge |
| I - Tap | V - Intermediate Vessel |
| J - Lead Electrode | W - Second Salt Bridge |
| K - Gas Trap | X - Valve Voltmeter |
| L - Water Trap | Y - Counting Assembly |
| M - Polythene Spacer | Z - Nitrogen Scrubbing Unit |

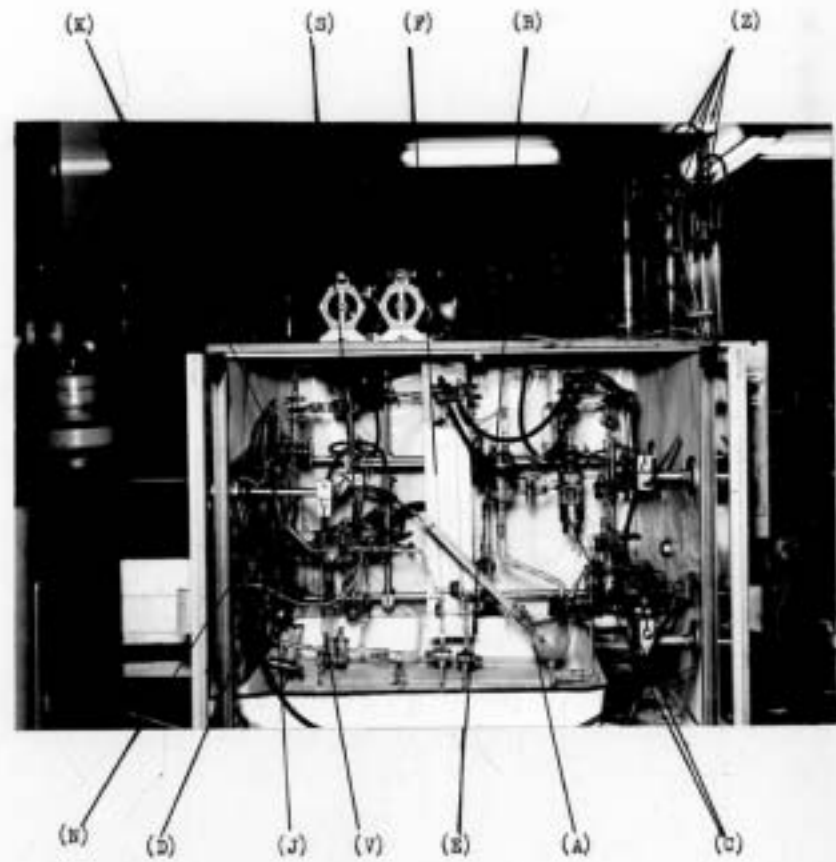


Fig. 2.3 Deposition Apparatus

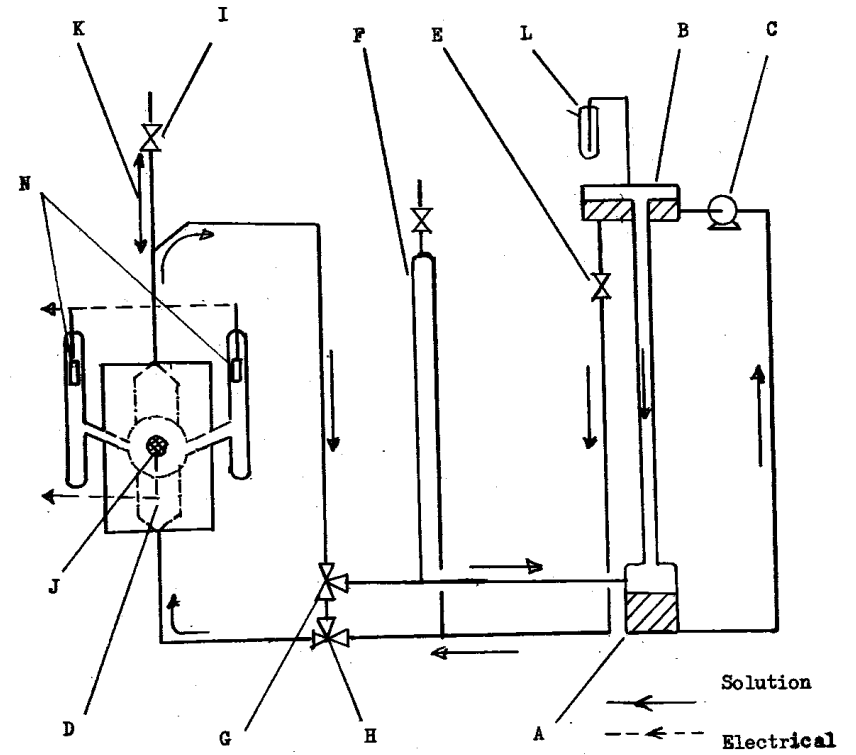


Fig. 2.4 Flow Diagram of the Deposition Apparatus

The antimony-sulphuric acid solution was pumped from the reservoir (A) to the constant head device (B) by the pumps (C). The pumps had a magnetic impeller which was driven by an external magnet attached to a small D.C. motor. The pump design, using the magnetic coupling, eliminated any seepage of the radio-active solution. The solution flowed from the constant head device to the deposition cell (D) and, back to reservoir. The excess solution was returned directly from the constant head device to the reservoir. The solution flow through the deposition cell was controlled by the tap (E) and the flow rate measured on the differential flow manometer (F). Taps (G) and (H) were used when the deposition cell was drained and they also allowed the solution to by-pass the electrodeposition cell when the lead electrode was replaced. The solutions could be continuously purged with nitrogen and the diffusion of air into the apparatus prevented by a number of small water traps (I). The apparatus was housed in a thermostated box, heated by a stream of hot air from an industrial air blower. This thermostating method kept the solution within $\pm 0.2^{\circ}\text{C}$ of any required temperature within the range 25°C to 50°C .

2.2.1. The lead electrodes

(a) Preparation of the Electrodes

To prepare the electrodes, zone refined lead was first cast into a rod 1" diameter. This was then machined into discs $\frac{1}{4}$ " thick with a face area of 4 cm^2 . A tinned copper wire was soldered onto the back face of each lead disc which was



Fig 2.5 The Lead Electrode

The electrode is made of lead and is used in a lead-acid battery. It is a circular disc with a diameter of 1.5 inches and a thickness of 0.1 inches. The electrode is connected to the positive terminal of the battery. The lead electrode is used to convert the chemical energy of the battery into electrical energy. The lead electrode is made of pure lead and is used in a lead-acid battery. It is a circular disc with a diameter of 1.5 inches and a thickness of 0.1 inches. The electrode is connected to the positive terminal of the battery. The lead electrode is used to convert the chemical energy of the battery into electrical energy.

(a) Construction of the Lead Electrode

The lead electrode is made of pure lead and is used in a lead-acid battery. It is a circular disc with a diameter of 1.5 inches and a thickness of 0.1 inches. The electrode is connected to the positive terminal of the battery. The lead electrode is used to convert the chemical energy of the battery into electrical energy.

then cast in araldite. The front face was milled flat to produce an electrode as shown in Fig. (2.5). The circular mould used for casting the araldite was so designed that the lead disc was positioned centrally in the araldite.

(b) Pretreatment of the electrodes to obtain a reproducible lead surface.

A fresh lead surface was used for each deposition study. This was prepared by removing the existing surface on decreasing grades, (360, 420, 600,), of wet emery paper. Fine scratch marks were removed by polishing on a rotating disc polisher, with a 'Selvet' cloth and a metallurgical solution of 'Brasso' in a saturated solution of paraffin wax in paraffin oil. The 'Beilby layer' was removed with a light etch solution of 15 g. of ammonium molybdate in 100 ml. of water mixed with an equal volume of a solution containing 27 ml. of concentrated nitric acid in 100 ml. of water. This treatment resulted in a clean lead surface free from abrasion marks in which the crystal structure of the lead could be seen clearly. At this point, a roughness factor was introduced by lightly polishing the surface with a 'Selvet' cloth and a saturated solution of paraffin wax in paraffin oil. The electrode was then washed in petroleum ether, degreased in trichlorethylene, rinsed in acetone and finally washed free of solvents with distilled water. The final stage in the pretreatment, and the electrochemical

treatment of the lead in 20% v/v sulphuric acid at 25°C resulted in a reproducible lead surface.

The electrode was first anodised at a current density of 20 mA/cm² for 30 mins and then cathodised at a current density of 5 mA/cm² for 30 mins. The electrode was then transferred to the perspex deposition cell where cathodisation was continued at 2.5 mA/cm² for 5 mins, in antimony-free 20% sulphuric acid.

2.2.2. The deposition cell.

The perspex deposition cell (D) is shown in Figs.(2.6) and (2.7). The circular electrode (J) was positioned vertically into an opening in the front face of the cell, and was then clamped tight by means of a retaining screw, thereby ensuring reproducible geometry for the radiation measurements. At the same time the cell was positioned so as to give a gap of approximately 0.5 cm between the lead surface of the electrode and a beta scintillation counter. A polythene spacer (M) placed between the electrode and the perspex of the cell acted as an electrolyte gasket, it also ensured a constant depth (0.077 cm) of electrolyte at the electrode surface. In order to obtain a smooth flow of electrolyte both through the cell and across the electrode surface, the electrolyte channels on each side of the electrode were made approximately 7 cm. long with a rectangular cross-section similar to that of the polythene spacer at the electrode surface.

Two compartments containing the platinum counter electrodes (N) were sealed with araldite into the sides of the cell, and both compartments were purged with nitrogen to eliminate the diffusion

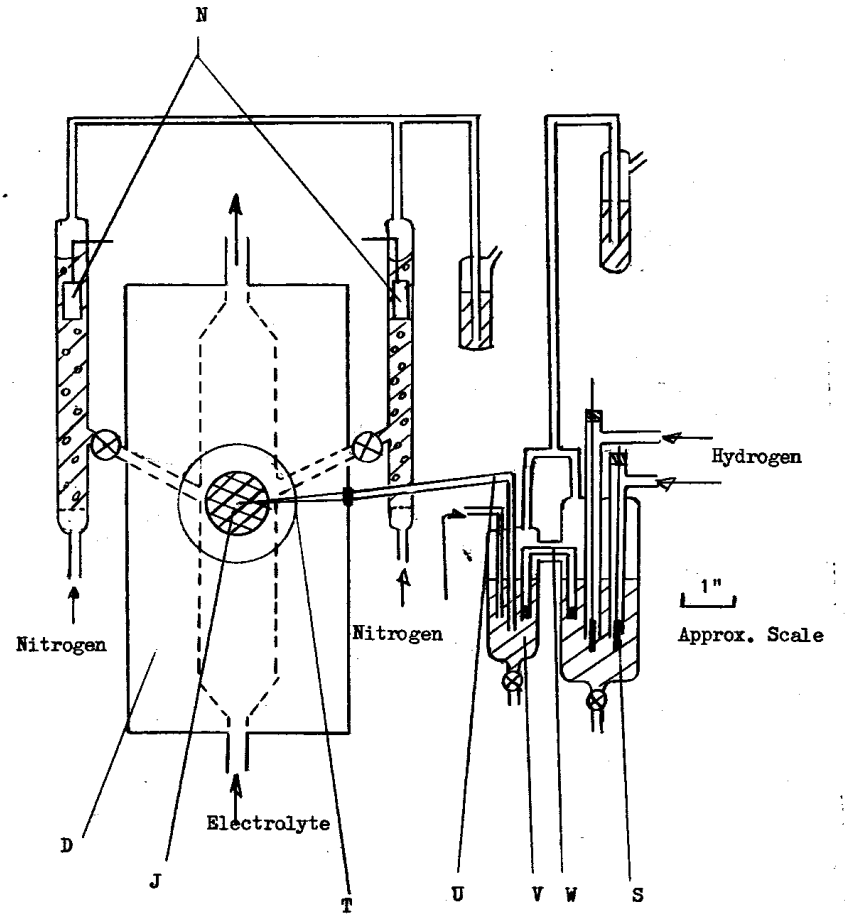


Fig. 2.6 Perspex Cell and Electrode System

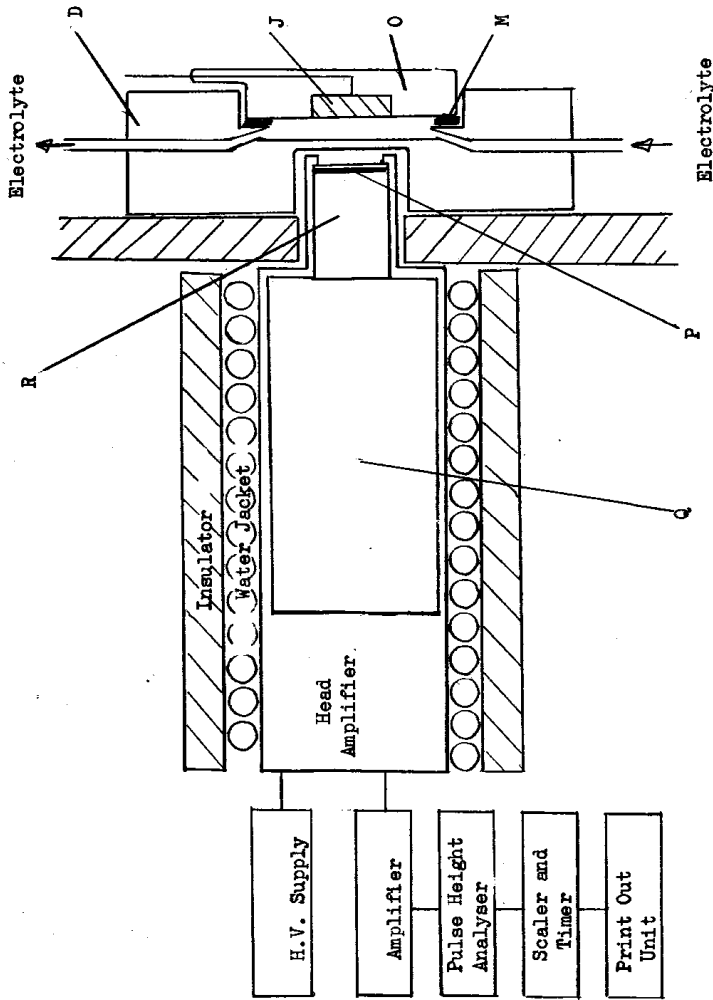


Fig. 2.7 Counting Equipment and Cross-Section of Electrode Cell

of evolved oxygen into the lead electrode compartment.

When nitrogen or air was passed down through tap (I) Fig. (2.4), electrolyte was removed from the cell via taps (G) and (H). In order to prevent interference of the electrolyte flow, any hydrogen evolved during an experiment was carried upwards by the electrolyte and collected in the glass tube below tap (I).

2.2.3. The radiation detector and counting equipment.

The detector assembly, Fig. (2.7), consisted of a Nuclear Enterprises beta sensitive plastic phosphor (P), 1" diameter and 0.010" in thickness, attached to a photomultiplier tube (Q) by means of a light pipe (R). It was found necessary to thermostat the photomultiplier at 25°C since an increase in the count rate of 5% per °C was recorded. The phosphor had a beta efficiency of approximately 95% and a gamma efficiency of 0.1%. For counting purposes, a Nuclear Enterprises 'Edinburgh' series counting assembly (Y) consisting of an amplifier, pulse height analyser, timer, scaler and print-out unit was used. A series of determinations were carried out using a standard source prepared by depositing antimony onto a lead electrode in order to find the most favourable operating conditions for the counting equipment, Figs. (2.8), (2.9). Fig. (2.8) shows the relationship between the threshold voltage of the analyser, the background count, b ; and the source plus background count, s , with 1.0 kV and 1.3 kV supplied to the

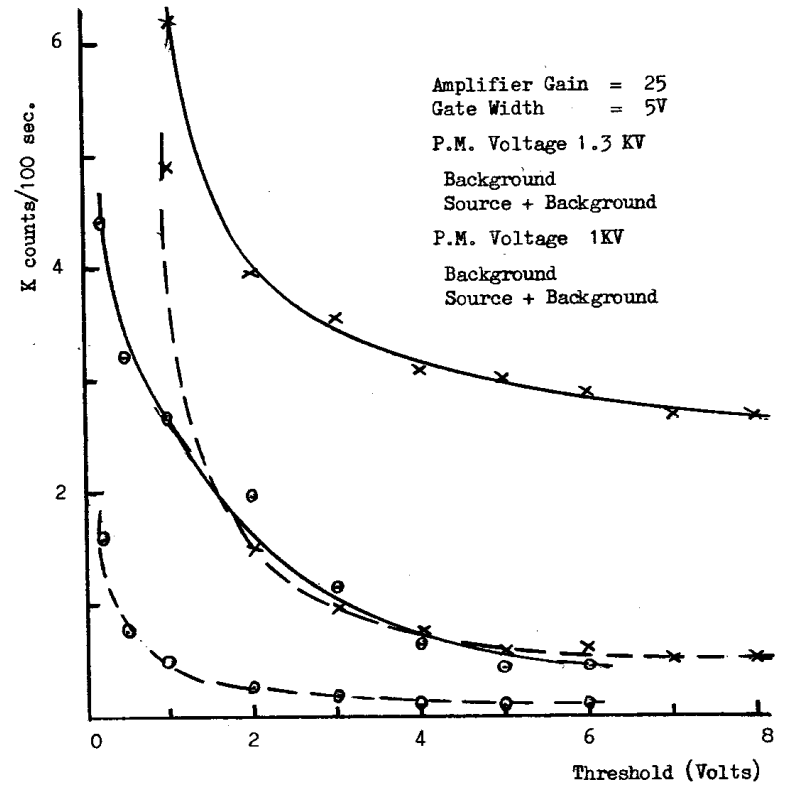


Fig. 2.8 Operating Characteristics of the Counting Equipment

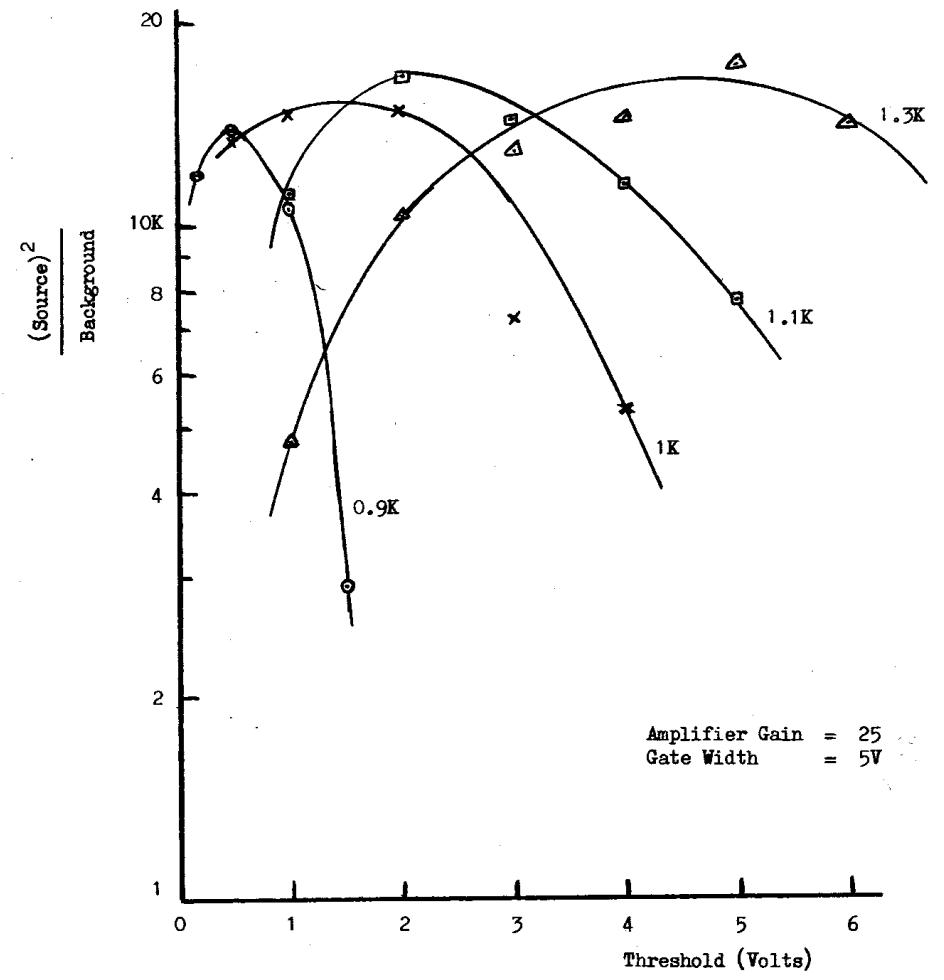


Fig. 2.9 Signal to Noise Relationship of the Counting Equipment

photo multiplier tube. These calibration results were also expressed as a plot of $\frac{S^2}{b}$ against the threshold voltage, Fig. (2.7). The most favourable operating conditions for scintillation counting are normally given by the maxima of the $\frac{S^2}{b}$ plot, but because of the sensitivity of the photomultiplier tube to variations of temperature it was found necessary to operate the equipment on the right hand side of the peak. This position corresponded to the start of the horizontal plateau in Fig.(2.8), a threshold value which eliminated a large proportion of the noise pulses.

By use of a suitable threshold voltage, 3V, on the analyser and a voltage of 1.1 kV on the photomultiplier tube, the initial background count rate of the electrolyte was less than 200 counts per 100 seconds whilst, after a typical deposition experiment of 30 min. duration, the count rate had increased to between 2,000 to 20,000 counts per 100 seconds.

2.2.4. Electrochemical measurements.

The two standard hydrogen reference electrodes (S), Fig. (2.6) (2.3), were prepared by immersing clean platinum wires in an aqueous solution of 0.05% w/v platinum chloride and 0.025% w/v lead acetate. A small D.C. current was passed through the solution and the current density was adjusted by means of a rheostat until evolution of gas commenced. At 15 sec intervals, the current was reversed to produce an even deposit of platinum black on each electrode. The electrodes

washed in distilled water and placed in the pure sulphuric acid solution in the reference electrode compartment of the deposition apparatus.

A luggin capillary (T) was incorporated into the perspex cell and was connected to the reference electrode compartment via two salt bridges containing sulphuric acid solution. The first salt bridge (U) connected the luggin capillary to an intermediate vessel (V) containing a sulphuric acid solution similar to that in the deposition apparatus. The second salt bridge (W) then connected the intermediate vessel and reference electrode compartment. This second salt bridge and the reference electrode compartment were filled with a pure sulphuric acid solution of the same molarity as that in the deposition apparatus. This arrangement was necessary because the electrolyte flowing past the luggin capillary tended to either introduce antimony solution into the reference electrode compartment or remove the sulphuric acid from the reference electrode compartment. The luggin capillary enabled the lead electrode potential to be measured against the hydrogen electrodes by means of (X), a high impedance valve voltmeter (18). The hydrogen electrodes were periodically checked against each other to ensure that true potential measurements were obtained. The platinum counter electrodes were positioned as described previously and current for the electrolysis circuit was supplied by a 12 volt accumulator.

2.2.5. Purification of Nitrogen.

British Oxygen Company "white spot" nitrogen was passed through a series of scrubbing tubes (Z) ; initially through two containing 5% sodium dithionite in 5% sodium hydroxide solution to remove oxygen; through a 10% sodium hydroxide solution to remove any sulphur dioxide formed previously; through a 10% sulphuric acid solution, and finally through distilled water. In order to reduce evaporation losses from the deposition apparatus, the purified nitrogen was not dried prior to its introduction into the apparatus.

2.2.6. Calibration of the weight of deposited antimony against its radioactivity.

Radioactive antimony was deposited onto a lead electrode in the deposition apparatus and the count rate was noted on the scaler. The electrode was then taken from the deposition cell and the antimony removed electrolytically using a few drops of sulphuric acid as electrolyte and a small platinum cathode. This solution was counted in an annular type Geiger-Muller tube and a comparison was made between its activity and the activity of a series of standard antimony 124 solutions in sulphuric acid. The electrode was re-positioned in the cell and re-counted to determine the amount of radioactivity which had been removed. From a series of such determinations, a graph of activity against weight of deposited antimony was obtained, Fig (2.10).

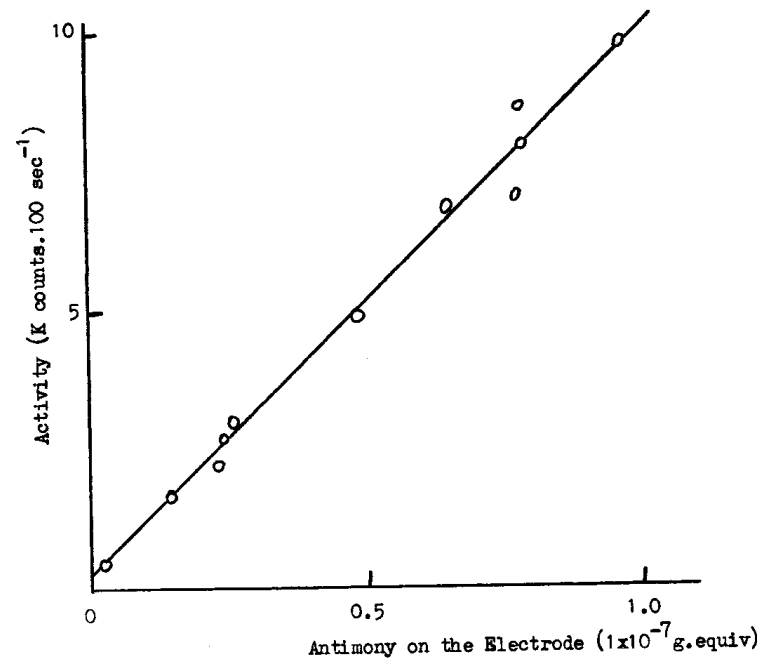


Fig. 2.10 A Typical Calibration Graph used for the Determination of the Antimony on the Electrode

2.2.7. Deposition studies.

Solutions were prepared which contained various concentrations of antimony (III) and sulphuric acid. The rate at which antimony was deposited was determined in each case. These experiments were carried out at varying solution flow rates and at different temperatures. Deposition rates were studied both with current flowing through the electrode and under open circuit conditions.

Experiments were also carried out to determine the rate of deposition of antimony (V) onto lead electrodes and the rate of deposition of antimony (III) and antimony (V) onto lead-lead dioxide electrodes.

2.3. Antimony Chemistry in the Lead-Acid Battery.

2.3.1. The production of antimony species from antimonial-lead electrodes.

The outer anodic and cathodic compartments of the three compartment cell, described in 2.1.2. were fitted with 8% antimonial-lead electrodes, of apparent surface area of 10 cm^2 , and the cell was filled throughout with 4M sulphuric acid. Air was excluded from the cell by the use of water-traps, and nitrogen was bubbled through the electrolyte within the three compartments. A current of 10 mA/cm^2 was passed through the cell for 4 hours and at periodic intervals the electrolyte in the anodic and cathodic compartments was examined for the presence of antimony species by ultra-violet spectrophotometry and polarographic analysis. The centre compartment of the

cell acted as a divider and, as such, limited the contact between antimony produced in the anodic and cathodic compartments. After suitable time intervals, the electrolyte was removed from each compartment as described previously, 2.1.2, and the antimony concentration determined.

The total antimony concentration was measured by counting the radioactivity and the antimony (III) concentration by polarographic determination. The difference between the two results was the concentration of antimony (V) in the electrolyte.

2.3.2. The reduction and oxidation of antimony in aqueous sulphuric acid.

The glass three-compartment cell used previously was filled with either dosed antimony (III) or dosed antimony (V) solutions in aqueous sulphuric acid. Platinum electrodes, surface area 10 cm^2 , were fitted into the end compartments and a current of 0.5 mA/cm^2 was passed through the cell. After suitable time intervals the solutions in the end compartments were examined for any change in the antimony oxidation state by counting the solution and also determining the antimony (III) concentration polarographically.

2.3.3. The adsorption of antimony from aqueous sulphuric acid onto lead dioxide and lead sulphate.

1 g. samples of either "Analar" Grade lead sulphate were placed in test tubes and 15 ml. of a solution of $1.64 \times 10^{-5} \text{ g.}$ of antimony, dosed with antimony 124, in different concentrations of sulphuric

acid. The test tubes were stoppered and shaken daily for five minutes. Solution samples were removed after suitable time intervals, centrifuged to remove any lead dioxide or lead sulphate and an aliquot of the sample was counted to determine the antimony concentration remaining in the solution.

3. RESULTS

3.1 Antimony Ions in Aqueous Sulphuric Acid

3.1.1 Ionic migration

Tables 1 and 5 show the results of tracer experiments conducted in the three compartment perspex cell with Porvic I separators. The tracer experiments were repeated using a glass three compartment cell with sintered glass discs between each compartment, and the results are tabulated below. The migration of radioactive antimony from the centre compartment was measured after a current of 120 mA had been passed between the two platinum electrodes each of which had a surface area of 3 cm².

(a) Antimony (III) species

The cell was filled throughout with antimony (III) in sulphuric acid and the resulting distribution of the radioactivity, expressed as concentration of migrated radioactive antimony is shown below.

Table 1

Initial concentration of antimony (III) = 1.6×10^{-4} M in 4M sulphuric acid

Distribution of Radioactive Antimony in Each Compartment

Time (hrs)	Anode		Centre	Cathode	
	1×10^{-4} M	% of Migrated Antimony	1×10^{-4} M	1×10^{-4} M	% of Migrated Antimony
0	0	0	1.6	0	0
3	0.07	58	1.48	0.05	42
6	0.25	51	1.21	0.24	49
24	0.71	70	0.70	0.30	30

Table 2

Initial concentration of antimony (III) = 1.58×10^{-4} M in 2M sulphuric acid

Distribution of Radioactive Antimony in Each Compartment

Time (hrs)	Anode		Centre	Cathode	
	1×10^{-4} M	% of Migrated Antimony	1×10^{-4} M	1×10^{-4} M	% of Migrated Antimony
0	-	-	1.580	-	-
2	0.015	63	1.562	0.009	37
4	0.032	73	1.541	0.012	27
6	0.051	68	1.505	0.024	32
8	0.060	65	1.489	0.032	35
24	0.197	61	1.257	0.126	39

Blank determination, i.e. 'self diffusion' = 0.003×10^{-4} M Sb per hour
 Average result = 66% anionic species and 34% cationic species.

Table 3

Initial concentration of antimony (III) = $1.58 \times 10^{-4} M$ in 4M sulphuric acid

Distribution of Radioactive Antimony in Each Compartment

Time (hrs)	Anode		Centre	Cathode	
	$1 \times 10^{-4} M$	% of Migrated Antimony	$1 \times 10^{-4} M$	$1 \times 10^{-4} M$	% of Migrated Antimony
0	-	-	1.580	-	-
2	0.015	66	1.557	0.008	34
4	0.027	75	1.544	0.009	25
6	0.038	72	1.528	0.015	28
8	0.053	69	1.502	0.024	31
24	0.185	68	1.207	0.088	32

Blank determination, i.e. 'self diffusion' = $0.003 \times 10^{-4} M$ Sb per hour.
Average result = 70% anionic species and 30% cationic species

Table 4

Initial concentration of antimony (III) = $1.58 \times 10^{-4} M$ in 6M sulphuric acid

Distribution of Radioactive Antimony in Each Compartment

Time (hrs)	Anode		Centre	Cathode	
	$1 \times 10^{-4} M$	% of Migrated Antimony	$1 \times 10^{-4} M$	$1 \times 10^{-4} M$	% of Migrated Antimony
0	-	-	1.580	-	-
2	0.014	74	1.562	0.005	27
4	0.002	71	1.549	0.009	29
6	0.032	73	1.536	0.012	27
8	0.049	69	1.509	0.022	31
24	0.167	75	1.361	0.054	25

Blank determination, i.e. self diffusion = $0.002 \times 10^{-4} M$ Sb per hour.
Average result = 72% anionic species and 28% cationic species.

These results indicate that the antimony (III) solution contained approximately 70% antimony (III) anions and 30% antimony (III) cations.

(b) Antimony (V) species

The cell was filled throughout with antimony (V) in sulphuric acid, the centre compartment containing radioactive antimony and the results are expressed as the concentration of migrated radioactive antimony.

Table 5

Initial concentration of antimony (V) in 4M sulphuric acid = $1.9 \times 10^{-4} M$

Distribution of Radioactive Antimony in Each Compartment

Time (hr)	Anode		Centre	Cathode	
	$1 \times 10^{-4} M$	% of Migrated Antimony	$1 \times 10^{-4} M$	$1 \times 10^{-4} M$	% of Migrated Antimony
0	0	0	1.90	0	0
6	0.20	95	1.69	0.01	5
26	0.61	88	1.20	0.08	12

Table 6

Initial concentration of antimony (V) = 1.58×10^{-4} M in 2M sulphuric acid

Distribution of Radioactive Antimony in Each Compartment

Time (hr)	Anode		Centre	Cathode	
	1×10^{-4} M	% of Migrated Antimony	1×10^{-4} M	1×10^{-4} M	% of Migrated Antimony
0	-	-	1.580	-	-
2	0.021	100	1.568	0.000	0
4	0.032	97	1.547	0.001	3
6	0.046	89	1.528	0.006	11
8	0.059	90	1.513	0.007	10
24	0.154	93	1.414	0.012	7

Blank determination i.e. 'self diffusion' = 0.003×10^{-4} M Sb per hr.

Average result = 94% anionic species and 6% cationic species

Table 7

Initial concentration of antimony (V) = 1.58×10^{-4} M in 4M sulphuric acid.

Distribution of Radioactive Antimony in Each Compartment

Time (hr)	Anode		Centre	Cathode	
	1×10^{-4} M	% of Migrated Antimony	1×10^{-4} M	1×10^{-4} M	% of Migrated Antimony
0	-	-	1.580	-	-
2	0.020	100	1.559	-	0
4	0.029	100	1.550	-	0
6	0.044	98	1.535	0.001	2
8	0.056	95	1.520	0.003	5
24	0.158	95	1.414	0.008	5

Blank determination i.e. 'self diffusion' = 0.002×10^{-4} M Sb per hr.

Average result = 98% anionic species and 2% cationic species.

Table 8

Initial concentration of antimony (V) = 1.58×10^{-4} M in 6M sulphuric acid

Distribution of Radioactive Antimony in Each Compartment

Time (hr)	Anode		Centre	Cathode	
	1×10^{-4} M	% of Migrated Antimony	1×10^{-4} M	1×10^{-4} M	% of Migrated Antimony
0	-	-	1.580	-	-
2	0.018	100	1.562	0.000	0
4	0.027	96	1.561	0.001	4
6	0.041	98	1.538	0.001	2
8	0.050	96	1.528	0.002	4
24	0.149	96	1.434	0.006	4

Blank determination i.e. 'self diffusion' = 0.002×10^{-4} M St per hr.

Average result = 97% anionic species and 3% cationic species

The above results for the antimony (V) solutions show the predominance of an ionic species.

3.1.2 Polarographic analysis

Antimony (V) - sulphuric acid solutions

Polarographic waves were not observed.

Antimony (III) - sulphuric acid solutions

Experiments using a Southern Instruments cathode ray polarograph gave polarograms as shown in Figs. (3.1) and (3.2). In 2-12M sulphuric acid the polarogram consisted of only one peak whereas in acid of less than 1.5M, two peaks were observed.

Since the polarograph was designed as a comparison instrument for analytical use the ordinate of the oscilloscope graticule had to be calibrated to record the diffusion current in amps. This was effected by placing a series of standard resistors across the input terminals of the polarograph and using the voltage sweep of 0.5V of the polarograph itself to give a pulse on the oscilloscope. The pulse height then corresponded to the current, i , where $i = \frac{0.5}{R}$ amps. The value of the standard resistance is expressed as R (ohms); Table 9 and Fig. (3.3).

Antimony (III) results, Table 10, were plotted as diffusion current at the polarogram peak (i_p) against antimony (III) concentration, Fig. (3.4) and (3.5).

The electrochemical diffusion coefficients of these antimony (III) cationic species were calculated from the polarographic results using

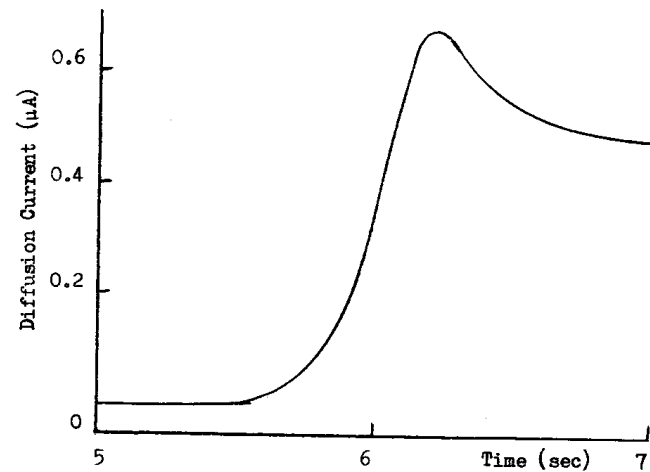


Fig. 3.1 Cathode Ray Polarogram of 0.5×10^{-4} M Sb(III) in 4M H_2SO_4

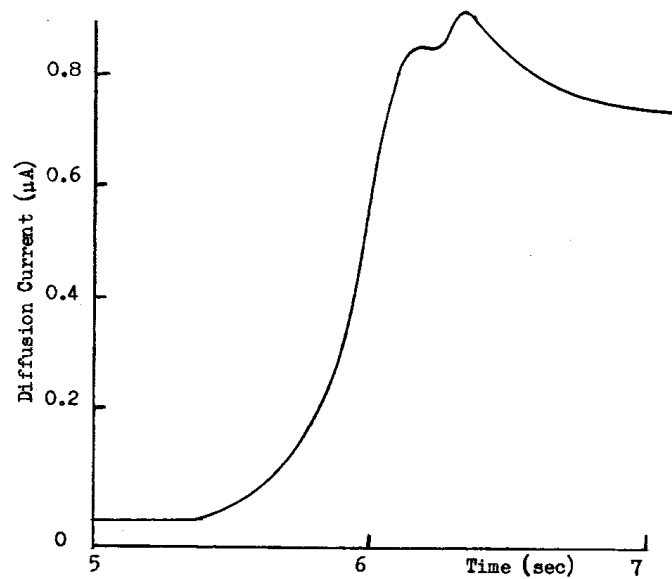


Fig. 3.2 Cathode Ray Polarogram of 0.5×10^{-4} M Sb(III) in 1M H_2SO_4

Table 9

Calibration of Oscilloscope Graticule

Resistance Across Input (Ohms $\times 10^3$)	$i(\mu A)$	Graticule Reading
220	2.27	62
270	1.85	50
390	1.28	35
560	0.89	24
680	0.74	20
820	0.61	16
1000	0.5	14

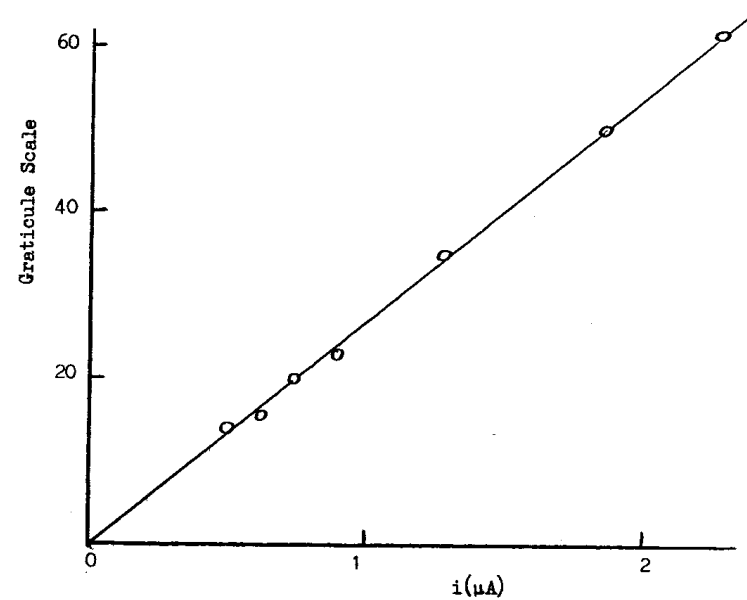


Fig. 3.3 Calibration of Polarograph

Table 10
Determination of the Antimony (III) Diffusion Coefficient

H ₂ SO ₄ M	$\frac{1}{\nu}$ (centipoise ⁻¹)	i _p ' (1x10 ⁻¹ μA) for 1x10 ⁻⁴ MSb(III) Amp. Scale = x 100	t _p (sec)	(t _p) ^{2/3} (sec ^{2/3})	D (10 ⁻⁶ cm sec ⁻¹)
0.4	0.952	1.68	6.16	3.36	4.07
1	0.833	1.71	6.18	3.37	4.21
2	0.681	1.58	6.17	3.36	3.63
3	0.571	1.49	6.16	3.37	3.24
4	0.476	1.36	6.20	3.36	2.66
5	0.385	1.25	6.25	3.38	2.26
6	0.322	0.95	6.21	3.37	1.31
7	0.263	0.94	6.18	3.36	2.27
8	0.213	0.92	6.10	3.34	1.22
9	0.174	0.74	6.02	3.31	0.79
10	0.139	0.73	5.86	3.25	0.78
11	0.109	0.62	5.70	3.19	0.57
12	0.089	0.55	5.63	3.16	0.46
H ₂ SO ₄ M	-	i _p " (1x10 ⁻¹ μA) for 1x10 ⁻⁴ MSb(III)	t _p	(t _p) ^{2/3}	D
0.4	0.952	2.02	6.50	3.53	5.75
1	0.833	1.83	6.35	3.46	4.79

Wt of 50 drops of mercury in 1M sulphuric acid = 0.1554 gm
 Wt of 50 drops of mercury in 10M sulphuric acid = 0.1530 gm
 Average weight of the mercury drop = 0.0031 gm
 Start potential = 0.25 volts vs Ag/AgCl/SO₄²⁻ electrode

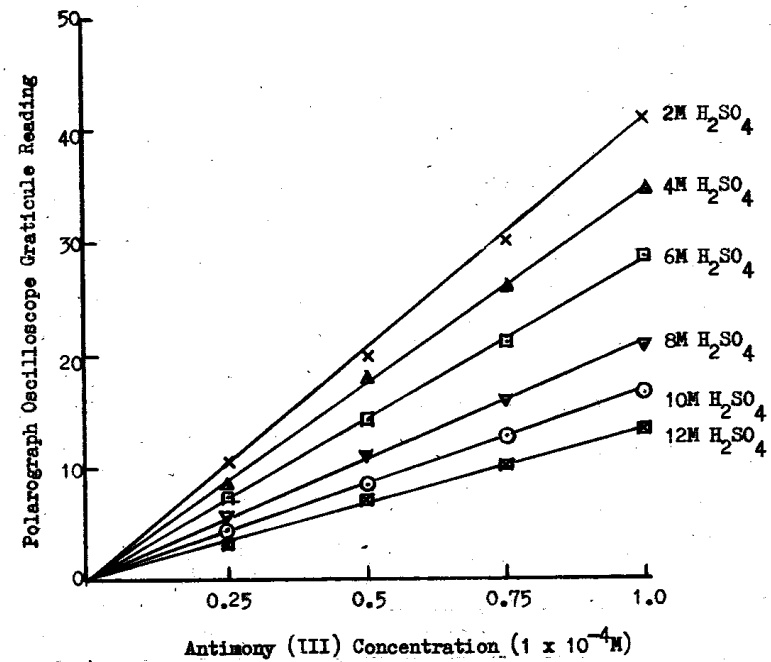


Fig 3.5 Polarogram Peak Height at Various Antimony Concentrations

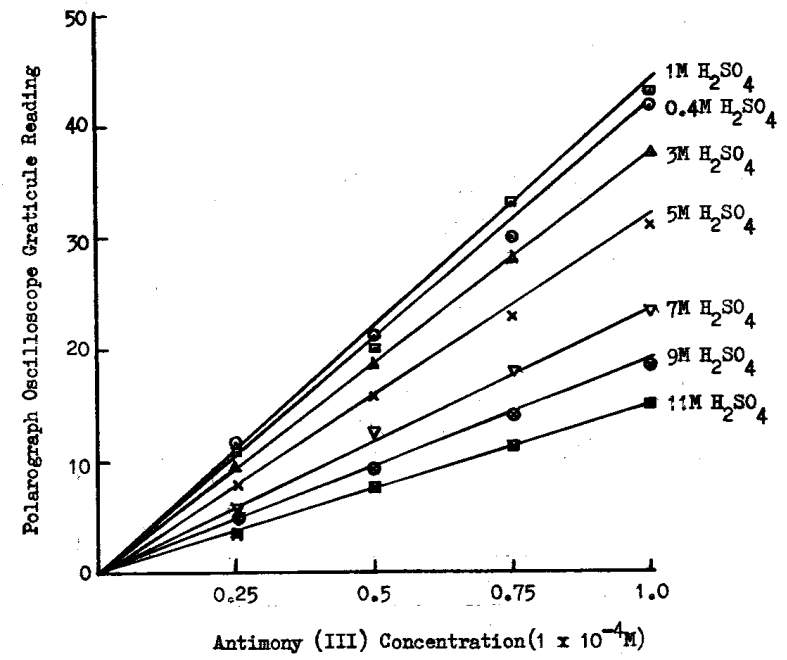


Fig 3.4 Polarogram Peak Height at various Antimony Concentrations

the Randles equation⁽¹⁹⁾:-

$$i_p = \frac{1.24 \pi \cdot F \cdot C_m \cdot \gamma^{\frac{2}{3}} \cdot t_p^{\frac{2}{3}} \cdot n^{\frac{3}{2}} \cdot \alpha^{\frac{1}{2}} \cdot D^{\frac{1}{2}} \text{amps.}}{(0.0118)^{\frac{1}{2}} \cdot 10^3}$$

where i_p = diffusion current at the peak (amps)

F = the Faraday (96,490 coulombs)

C_m = molar concentration of the reacting ions

γ = a constant dependent on the rate of flow of the mercury ($\text{cm}^3 \cdot \text{sec}^{-1}$)

t_p = time at which the peak occurs (sec)

n = electron transfer

α = rate of voltage ($\text{volts} \cdot \text{sec}^{-1}$)

D = diffusion coefficient of the reacting ions ($\text{cm}^2 \cdot \text{sec}^{-1}$)

γ was calculated from the equation $r^3 = \gamma t$, where r = radius of the mercury drop, cm, at the time, t , and t = time, sec, from the commencement of formation of the drop, assuming that the volume of the drop increases uniformly with time.

The volume of a mercury drop is $\frac{4}{3} \pi r^3$ and its radius, r , cm, can be calculated from;

$$r^3 = \frac{3 \cdot m \cdot 1}{4 \cdot \rho \cdot \pi} \text{ cm}$$

where m = weight, g,

and ρ = density, g cm^3

$$\therefore \gamma = \frac{3 \cdot m}{4 \cdot \rho \cdot \pi \cdot t} \text{ cm}^3 \cdot \text{sec}^{-1}$$

The life time of the mercury drop was 7 sec and its weight after 7sec was 0.0031 g.

$$\therefore \gamma = \frac{3 \times 0.0031}{4 \times 13.546 \times 7 \times 3.142} \text{ cm}^3 \cdot \text{sec}^{-1}$$

The polarograms were obtained by applying a voltage increase (0.5 volts) during the final 2 sec of the drop life.

$$\therefore \omega = \frac{0.5}{2} \text{ volts} \cdot \text{sec}^{-1}$$

Assuming an electron transfer of one i.e. $n = 1$, the diffusion coefficient of antimony (III) was calculated from the equation

$$D = \left(\frac{(0.0118)^{\frac{1}{2}} \times 10^{-3} \times 10^{-6}}{1.24 \times 3.142 \times 96490 \times 10^{-4} \left(\frac{3 \times 0.0031}{4 \times 13.546 \times 3.142 \times 7} \right)^{\frac{2}{3}} (0.25)^{\frac{1}{2}}} \right)^2 \left(\frac{i_p (\mu A)}{C(t_p)^{\frac{2}{3}}} \right)^2$$

$$\text{Where } C = \frac{\text{Molar concentration of antimony}}{10^{-4}}$$

$$\therefore D = 2.65 \times 10^{-4} \left(\frac{i_p (\mu A)}{C(t_p)^{\frac{2}{3}}} \right)^2$$

Experimentally, t_p was given as a voltage reading on the oscilloscope graticule and its position depended upon the starting potential

of the voltage sweep. For example, if the starting potential was 0.25 volts and $t = 5$ sec, on completion of the polarogram, t would be 7 sec and the potential $0.25 + 0.5$ volts. Thus if the peak maximum occurred at 0.5 volts, t_p would be 6 sec.

In sulphuric acid solutions less than 1.5M, it was difficult to calculate the antimony (III) diffusion coefficients since the relative concentration of the antimony species producing the two peaks was unknown. The diffusion coefficient of each peak was therefore calculated, t_p' and t_p'' in Table 10, and an average value was assigned to the diffusion coefficient. This average value was later used in the deposition experiments, Tables 11 and 15 to 19.

Using the Stokes-Einstein equation,

$$D = \frac{kT}{6\pi r\eta}$$

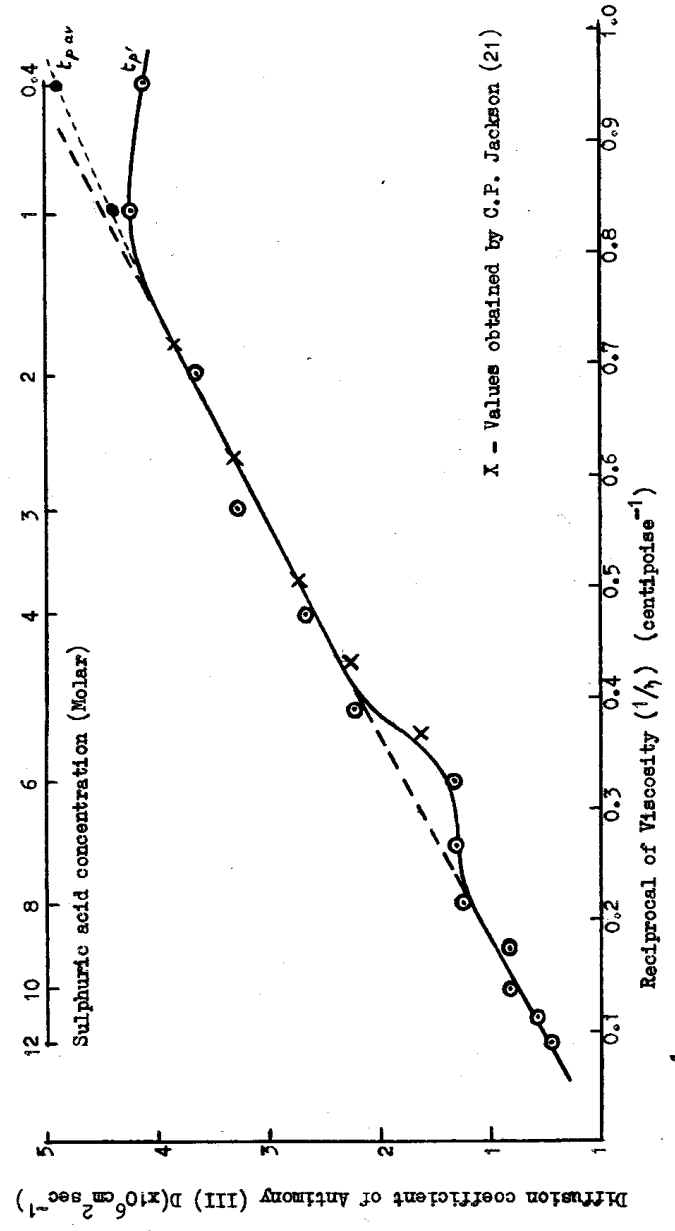
where r = Stokes radius of the ion and η = the dynamic viscosity of the solution, a graph of the antimony (III) diffusion coefficients against the reciprocal of the dynamic viscosity of the sulphuric acid solutions was plotted, Fig. (3.6). The dynamic viscosity values were obtained from the International Critical Tables. The graph proved to be linear over a sulphuric acid range 2 to 12M; except for a slight dip at approximately 7M. The graph also showed that the value of the antimony (III) diffusion coefficient decreased with an increase in

sulphuric acid concentration.

When sulphuric acid solutions above 1.5M were used, only one peak was observed on the cathode ray polarogram. This showed the reduction of one antimony (III) cationic species. Solutions less than 1.5M sulphuric acid gave two polarographic peaks indicating the presence of two antimony (III) cationic species also the value of the diffusion coefficient decreased with a decrease in acid concentration, showing that the Stokes radius of the ion had increased probably due to hydration by the addition of either OH^- or H_2O . The electrochemical diffusion coefficients calculated from the polarographic determinations were similar to those found by Jackson⁽²¹⁾, see Fig. (3.6). The values of the diffusion coefficients obtained from Fig. (3.6) are listed below in Table 11.

Table 11

<u>Sulphuric Acid Concentration</u>	<u>Antimony (III)⁺ Diffusion Coefficient</u>
M	D (cm ² .sec ⁻¹)
0.65	4.90 x 10 ⁻⁶
1	4.50 x 10 ⁻⁶
2	3.68 x 10 ⁻⁶
4	2.50 x 10 ⁻⁶
6	1.70 x 10 ⁻⁶
8	1.12 x 10 ⁻⁶
10	0.71 x 10 ⁻⁶
12	0.46 x 10 ⁻⁶



X - Values obtained by C.P. Jackson (21)

Fig. 3.6. Diffusion Coefficient (D) of Antimony (III) cation against the Reciprocal of the Viscosity of the Sulphuric Acid.

3.1.3 Ultra-violet spectra

(a) Antimony (III) in sulphuric acid

Typical spectra are shown in Fig. (3.7) and (3.8) and consisted of two absorption bands. It was found that the position of the first absorption band varied according to sulphuric acid concentration, Fig. (3.7), whilst the position of the second band remained constant at 208 μ . The dependence of the peak position, λ_{\max} , of the first absorption band on the acid concentration is shown in Fig. (3.9), the projection of the arrows onto the ordinate indicates the variation in the position of λ_{\max} with antimony concentration.

Beer's law was obeyed for antimony (III) concentrations up to 1×10^{-4} M, and sulphuric acid concentration 0.1 to 18M. A typical graph of optical density at 208 μ and λ_{\max} against antimony (III) concentration is shown in Fig. (3.10).

The above antimony (III) spectra were obtained after the solutions had been standing for several days and had reached equilibrium.

A comparison was made, Fig. (3.11), between these normal spectra and spectra obtained within an hour of dilution from a concentrated sulphuric acid solution. The molar extinction coefficient, $(\bar{\epsilon})$, of the antimony (III) at λ_{\max} 190, 195, 200 and 205 μ was calculated for the concentration range obeyed by Beer's Law. The dependence of $(\bar{\epsilon})$ upon

the sulphuric acid concentration is shown in Fig. (3.12).

The spectra of antimony (III) in aqueous perchloric acid, prepared by the dissolution of antimony trioxide, are compared in Fig. (3.13), (3.14) and (3.15).

Table II.

M Sb(III) 1x10 ⁻⁴	λ max m μ	Optical Density.					
		190	195	200	205	210	λ max
<u>0.24M H₂SO₄</u>							
0.20	196.0	-	0.15	0.11	0.05	0.03	0.17
0.40	196.5	-	0.305	0.225	0.10	0.065	0.335
0.60	196.5	-	0.46	0.345	0.155	0.10	0.50
0.80	197.0	-	0.61	0.45	0.205	0.13	0.66
1.00	197.0	-	0.74	0.54	0.24	0.155	0.505
$\bar{\epsilon}$			7700	5600	2550	1650	8400
<u>0.5 M H₂SO₄</u>							
0.20	197	-	0.125	0.09	0.075	0.04	0.16
0.285	197	-	0.165	0.11	0.08	0.06	0.19
0.40	197.5	-	0.22	0.15	0.11	0.07	0.29
0.569	197.5	-	0.33	0.22	0.16	0.09	0.37
0.60	197.5	-	0.345	0.25	0.16	0.10	0.385
0.80	198.0	-	0.49	0.31	0.22	0.13	0.53
0.854	198.0	-	0.505	0.325	0.24	0.15	0.57
1.0	198.0	-	0.58	0.37	0.26	0.17	0.645
1.138	198.0	-	0.63	0.43	0.31	0.20	0.66
1.423	198.5	-	0.73	0.52	0.37	0.25	0.83
1.708	198.5	-	0.82	0.59	0.41	0.29	0.92
$\bar{\epsilon}$			5900	3850	2750	1700	6550

Table II (Contd)

M Sb(III) 1x10 ⁻⁴	λ max m μ	Optical Density					
		190	195	200	205	210	λ max
<u>1.0M H₂SO₄</u>							
0.128	198.5	-	0.02	0.07	0.03	0.02	0.07
0.256	198.5	-	0.03	0.12	0.07	0.05	0.13
0.384	198.5	-	0.09	0.17	0.10	0.06	0.19
0.64	199.0	-	0.09	0.35	0.17	0.09	0.365
0.80	199.0	-	0.11	0.39	0.20	0.14	0.41
1.20	199.0	-	0.14	0.65	0.33	0.23	0.65
1.60	199.0	-	0.22	0.82	0.44	0.32	0.83
1.708	199.5	-	0.23	0.81	0.43	0.35	0.85
2.277	199.5	-	0.26	1.05	0.51	0.40	1.08
\bar{E}		-	1375	4950	2700	1950	5200
<u>2.0M H₂SO₄</u>							
0.285	198.5	-	0.07	0.15	0.06	0.04	0.16
0.569	198.5	-	0.12	0.31	0.11	0.07	0.325
0.854	198.5	-	0.20	0.46	0.15	0.10	0.475
1.0	199.0	-	0.22	0.52	0.18	0.12	0.54
1.5	199.0	-	0.33	0.75	0.32	0.17	0.78
2.0	199.5	-	0.42	0.94	0.37	0.19	0.96
\bar{E}		-	2200	5200	2000	1250	5400
<u>4.M. H₂SO₄</u>							
0.32	197.0	-	0.12	0.13	0.08	0.06	0.15
0.40	197.0	0.01	0.39	0.18	0.10	0.09	0.20
0.64	197.0	0.02	0.25	0.27	0.16	0.15	0.33
1.0	197.5	0.03	0.36	0.425	0.26	0.24	0.50
1.28	197.5	0.04	0.48	0.54	0.33	0.30	0.66
1.50	197.5	0.04	0.55	0.64	0.38	0.35	0.71
2.0	198.0	0.05	0.67	0.82	0.50	0.44	0.92
\bar{E}		300	3700	4200	2600	2350	5100

Table II (Contd).

M.Sb(III) $\times 10^{-4}$	λ max m μ	Optical Density.					
		190	195	200	205	210	λ max
<u>6M.H₂SO₄.</u>							
0.2	194.0	0.09	0.13	0.09	0.08	0.07	0.14
0.4	194.0	0.19	0.29	0.18	0.15	0.15	0.30
0.5	194.5	0.24	0.35	0.23	0.19	0.19	0.35
0.8	194.5	0.35	0.55	0.36	0.32	0.29	0.56
1.0	194.5	0.43	0.66	0.48	0.40	0.38	0.66
1.5	195.0	0.60	0.84	0.65	0.54	0.55	0.84
2.0	195.0	0.68	0.95	0.75	0.63	0.60	0.95
$\bar{\epsilon}$		3200	7000	4700	3900	3700	7100
<u>8M.H₂SO₄</u>							
0.32	193.0	0.12	0.20	0.13	0.11	0.09	0.21
0.50	193.0	0.20	0.30	0.20	0.16	0.15	0.33
0.83	193.5	0.31	0.50	0.32	0.26	0.24	0.52
1.0	193.5	0.37	0.59	0.37	0.32	0.30	0.63
1.28	193.5	0.47	0.65	0.50	0.39	0.36	0.70
1.50	194.0	0.53	0.72	0.54	0.45	0.44	0.76
1.92	194.0	0.60	0.81	0.61	0.55	0.54	0.83
$\bar{\epsilon}$		3700	6100	3800	3200	3000	6400
<u>10M.H₂SO₄</u>							
0.25	191.5	0.15	0.16	0.09	0.08	0.08	0.18
0.50	191.5	0.29	0.32	0.17	0.16	0.15	0.35
0.83	192	0.55	0.50	0.28	0.26	0.24	0.56
1.0	192	0.62	0.65	0.33	0.30	0.29	0.69
1.25	192.5	0.74	0.70	0.42	0.40	0.38	0.80
1.64	192.5	0.85	0.80	0.53	0.49	0.47	0.92
$\bar{\epsilon}$		6200	6600	3300	2900	3100	7000

Table II. (Contd).

M Sb(III) 1x10 ⁻⁴	λ max m μ	Optical Density.					λ max
		190	195	200	205	210	
<u>12M.H₂SO₄</u>							
0.25	191.0	0.19	0.18	0.09	0.07	0.08	0.22
0.50	191.5	0.39	0.35	0.19	0.16	0.17	0.43
0.75	191.5	0.58	0.54	0.28	0.23	0.25	0.65
1.00	192.0	0.75	0.68	0.35	0.30	0.32	0.82
∞		7800	7150	3700	3100	3400	8600
<u>14M.H₂SO₄</u>							
0.25	191	0.22	0.19	0.11	0.09	0.10	0.25
0.50	191	0.45	0.38	0.23	0.20	0.21	0.49
0.75	191.5	0.67	0.56	0.32	0.28	0.29	0.74
1.00	191.5	0.85	0.71	0.42	0.34	0.32	0.92
∞		9000	7500	4400	3700	4000	9800
<u>16M.H₂SO₄</u>							
0.25	191	0.24	0.20	0.13	0.11	0.11	0.23
0.50	191	0.48	0.41	0.25	0.22	0.23	0.51
0.75	191	0.73	0.59	0.38	0.32	0.33	0.76
1.00	191	0.91	0.72	0.47	0.41	0.43	0.96
∞		9700	7850	5000	4300	4450	10200
<u>18M.H₂SO₄</u>							
0.25	191	0.25	0.20	0.14	0.12	0.12	0.23
0.50	191	0.50	0.41	0.27	0.23	0.25	0.51
0.75	191	0.74	0.60	0.39	0.35	0.37	0.77
1.00	191	0.92	0.76	0.41	0.43	0.46	0.96
∞		9900	8050	5300	4600	4900	10300

Table 12.

M.Sb(III) 1x10 ⁻⁴	λ max m μ	Optical Density.					
		λ max	190	195	200	205	210
0.5M. HC10₄							
0.2	194.0	0.25	0.07	0.23	0.14	0.07	0.05
0.4	194.0	0.55	0.15	0.54	0.26	0.13	0.07
0.6	194.0	0.75	0.22	0.73	0.40	0.20	0.12
0.8	194.5	1.0	0.29	0.96	0.52	0.25	0.15
1.0	194.5	1.2	0.35	1.10	0.62	0.30	0.18
\bar{M}		12500	3600	12200	6500	3200	1900
1 M HC10₄							
0.2	194.0	0.21	0.06	0.22	0.13	0.07	0.04
0.4	194.5	0.45	0.12	0.42	0.25	0.13	0.09
0.6	194.5	0.66	0.16	0.65	0.36	0.18	0.12
0.8	194.5	0.89	0.23	0.85	0.48	0.24	0.17
1.0	195	1.05	0.26	1.0	0.57	0.27	0.19
\bar{M}		11000	2800	10600	6000	3000	2100
2 M HC10₄							
0.2	195	0.18	0.04	0.18	0.10	0.06	0.05
0.4	195	0.35	0.06	0.35	0.21	0.12	0.09
0.6	195	0.52	0.10	0.52	0.32	0.18	0.14
0.8	195	0.69	0.13	0.69	0.42	0.24	0.18
1.0	195.5	0.83	0.14	0.83	0.49	0.27	0.21
\bar{M}		8600	1500	8600	5200	2900	2200
3 M HC10₄							
0.2	195.5	0.15	0.02	0.13	0.10	0.05	0.04
0.4	196	0.30	0.02	0.28	0.19	0.11	0.09
0.6	196	0.45	0.03	0.43	0.28	0.17	0.12
0.8	196	0.60	0.03	0.58	0.38	0.23	0.16
1.0	196	0.70	0.04	0.69	0.43	0.26	0.18
\bar{M}		7400	400	7200	4700	2800	2000
4 M HC10₄							
0.2	196	0.13	-	0.13	0.09	0.07	0.04
0.4	196.5	0.26	-	0.25	0.18	0.11	0.08
0.6	196.5	0.39	-	0.37	0.28	0.17	0.12
0.8	196.5	0.51	-	0.43	0.37	0.23	0.16
1.0	196.5	0.60	-	0.57	0.43	0.25	0.18
\bar{M}		6400	-	6100	4600	2800	2000

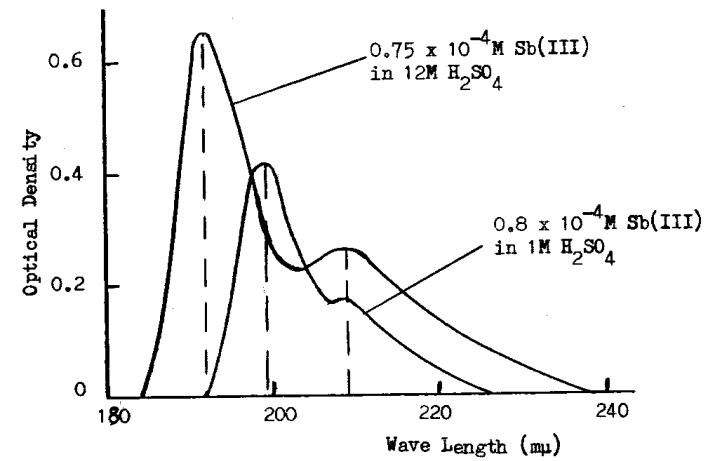


Fig. 3.7 Spectra of Antimony (III) in Aqueous Sulphuric Acid

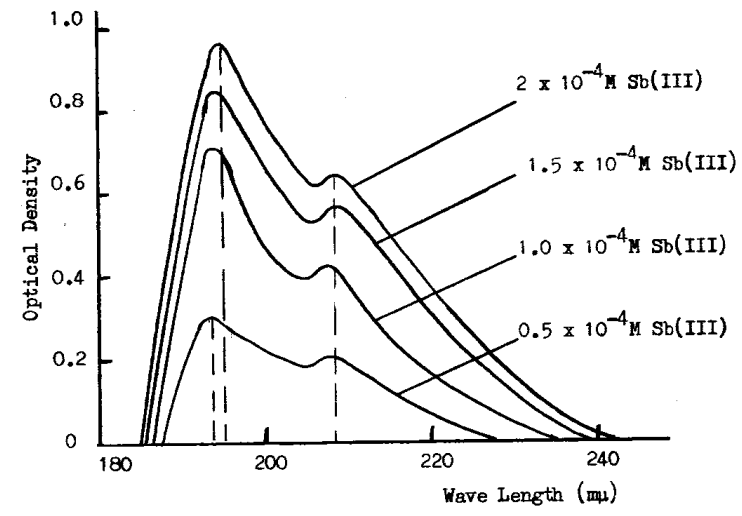


Fig. 3.8 Spectra of Antimony (III) in 6M Sulphuric Acid

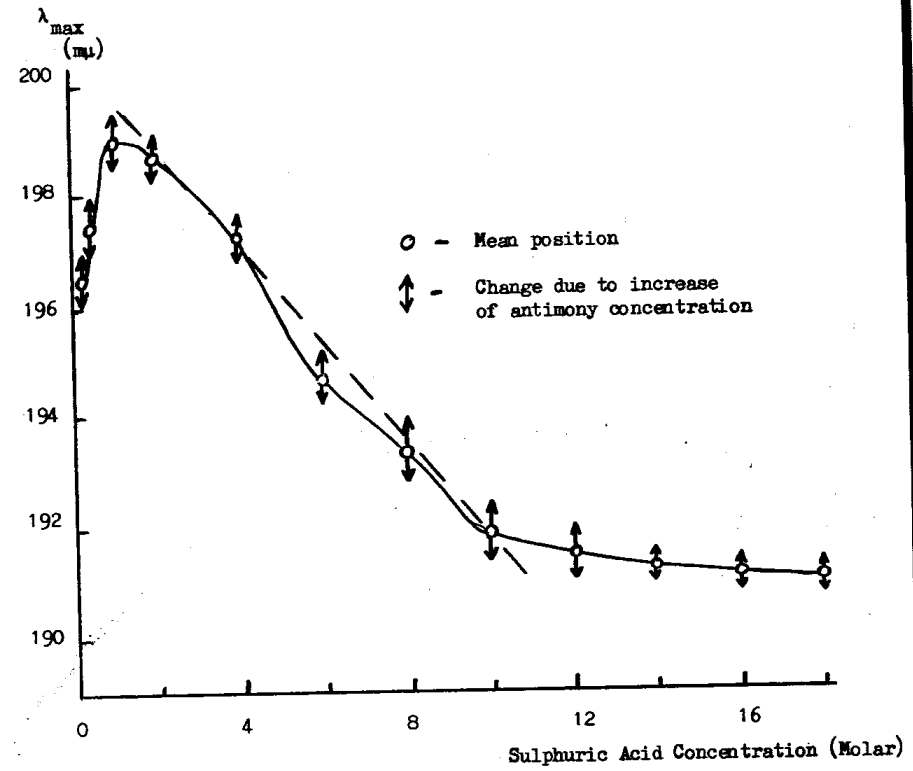


Fig. 3.9 Change of Position of the First Absorption Band of the Antimony (III) Spectra with Increase of Concentration of Sulphuric Acid

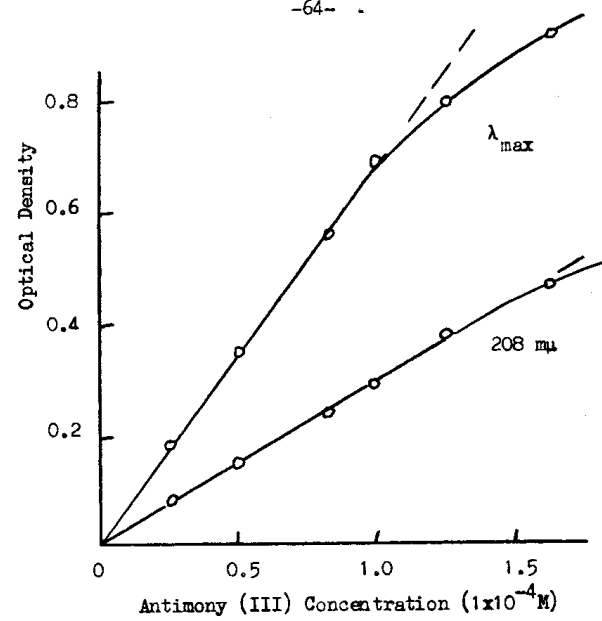


Fig. 3.10 Optical Density v.s. Antimony Concentration (10M Sulphuric Acid)

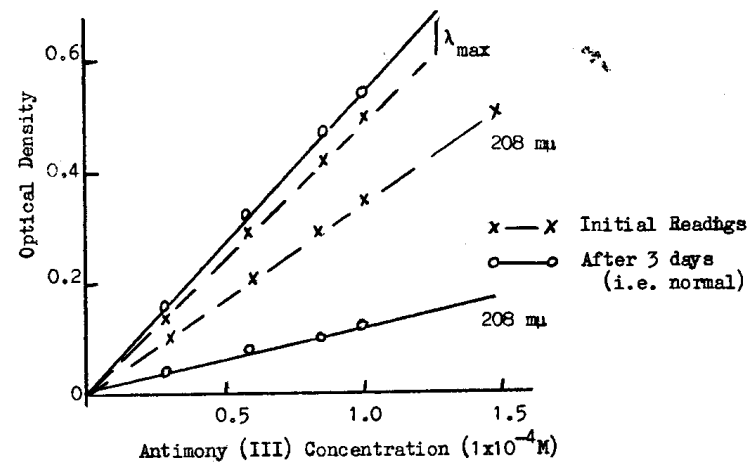


Fig. 3.11 Change of Optical Density Readings with Time (2M H_2SO_4)

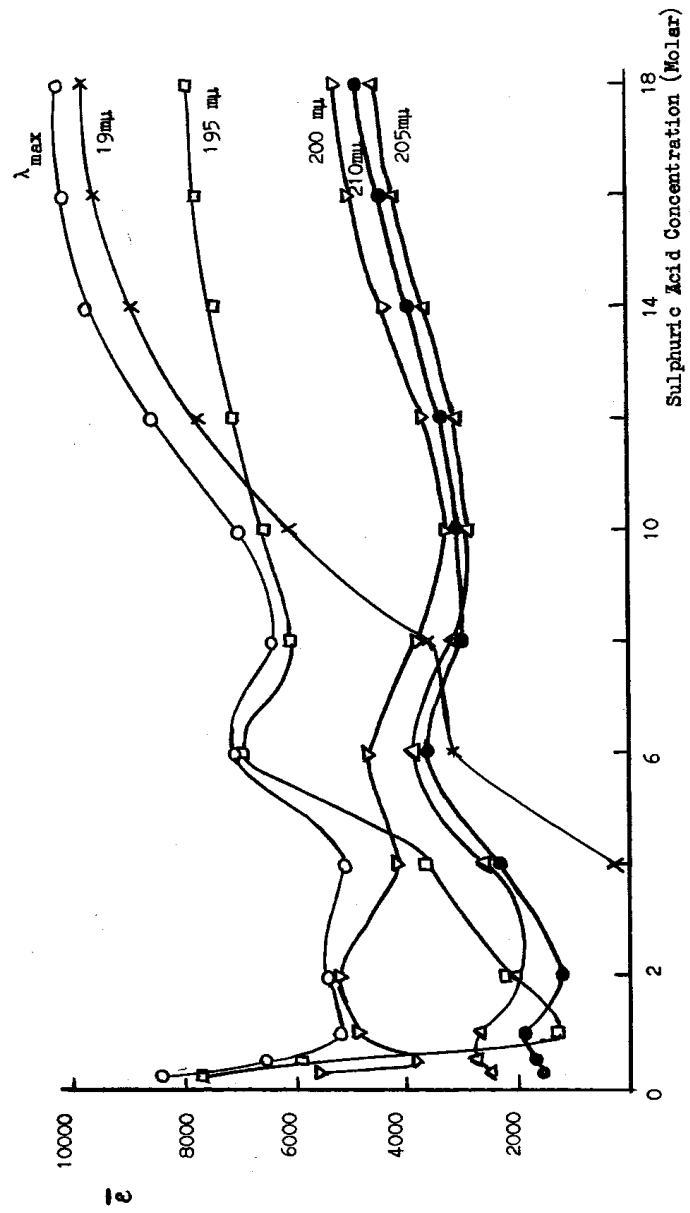


Fig. 3.12 Molar Extinction Coefficient (ϵ) of Antimony (III) at Various Sulphuric Acid Concentrations.

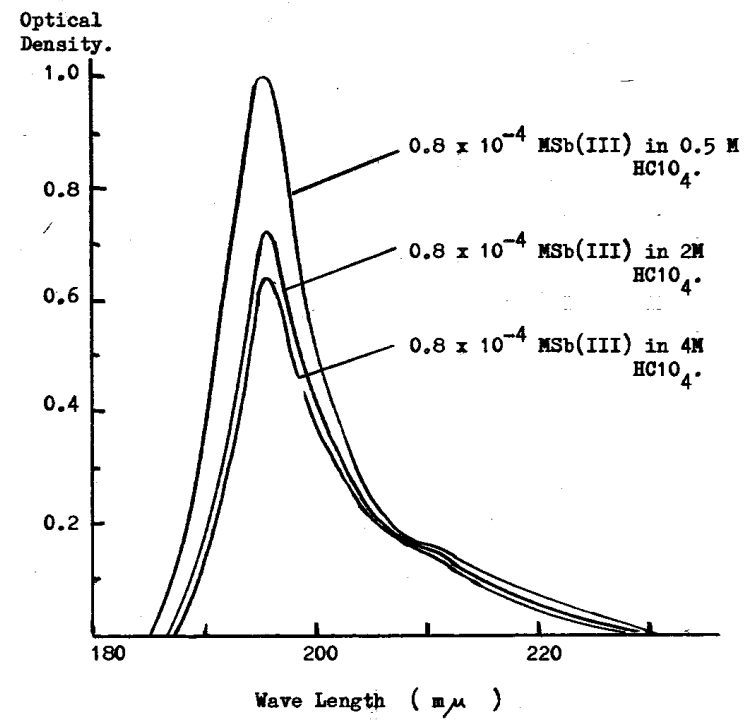


Fig. 3.13. Ultraviolet Spectrum of Antimony (III) in Perchloric Acid.

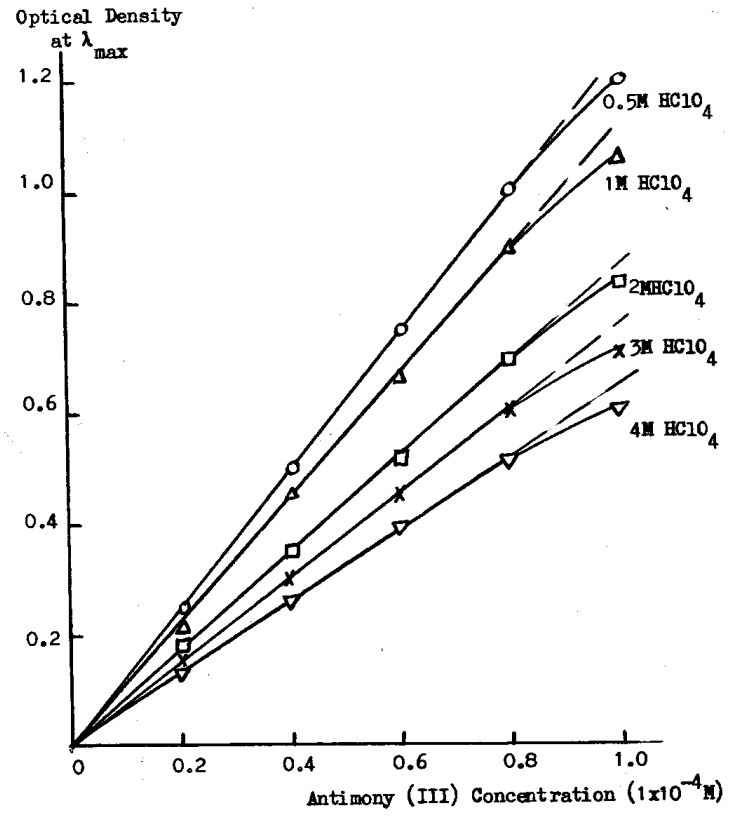


Fig. 3.14 Antimony (III) in Perchloric Acid

Molar Extinction
Coefficient (ϵ)

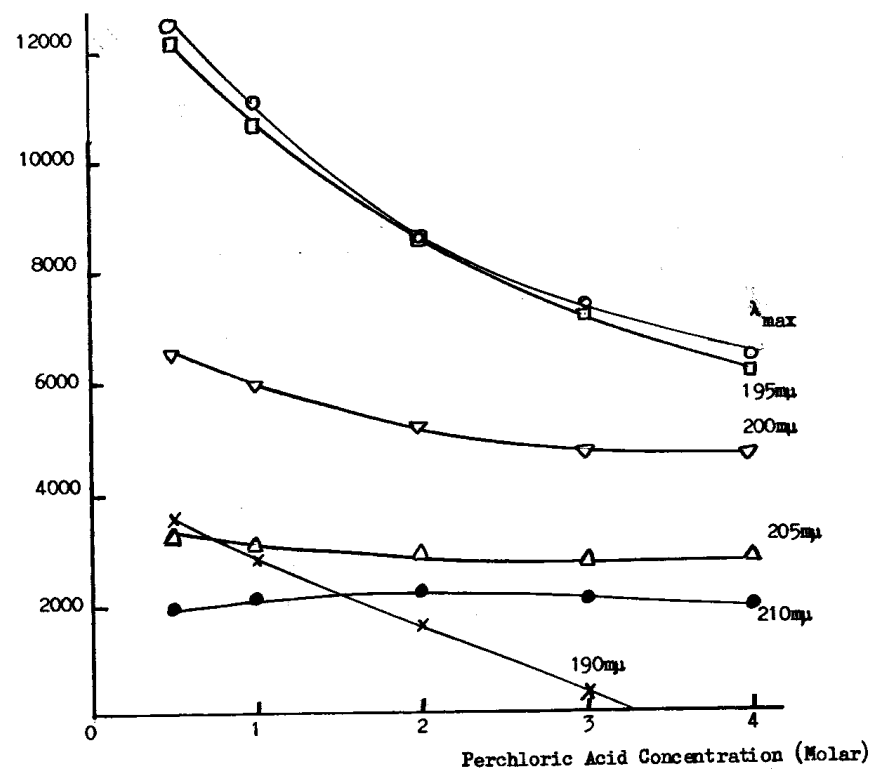


Fig. 3.15 Molar Extinction Coefficient of Antimony (III) in Perchloric Acid

(b) Antimony (V) in sulphuric acid

Antimony (V) in aqueous sulphuric acid solutions gave one absorption band at 193 μ , Fig. (3.16). The position of λ_{\max} at 193 μ was not affected by a change in acid concentration. Beer's Law was obeyed for antimony (V) concentrations 0 to 20×10^{-4} M and sulphuric acid concentrations 1 to 12M, e.g. Fig. (3.17). The dependence of the molar extinction coefficient, $\bar{\epsilon}$, upon the sulphuric acid concentration is shown in Fig. (3.18).

A comparison between antimony (III) and antimony (V) spectra showed that the antimony (V) absorption band was weaker than the corresponding antimony (III) band, Fig. (3.19).

The absorption spectra obtained during the dilution of antimony (V) in fuming sulphuric acid solution are shown in Fig. (3.20) to (3.23).

Table 13.

M Sb(V) 1x10 ⁻⁴	λ max m μ	Optical Density.			
		λ max	190	200	210
<u>0.5 M H₂SO₄</u>					
3.0	195.5	0.18	0.12	0.06	0.04
6.0	195.5	0.35	0.25	0.21	0.10
9.0	195.5	0.53	0.38	0.30	0.15
12.0	196.0	0.71	0.50	0.41	0.19
ε		590	420	340	160
<u>2 M H₂SO₄</u>					
2.0	195.0	0.12	0.07	0.07	0.05
4.0	195.5	0.25	0.18	0.14	0.07
6.0	195.5	0.37	0.25	0.21	0.10
8.0	195.5	0.49	0.32	0.28	0.14
10.0	195.0	0.62	0.42	0.36	0.16
12.0	195.0	0.75	0.51	0.42	0.20
ε		620	420	350	160
<u>4 M H₂SO₄</u>					
2.0	195.5	0.13	0.08	0.07	0.06
4.0	195.5	0.25	0.17	0.15	0.08
6.0	195.5	0.37	0.26	0.23	0.10
8.0	195.5	0.50	0.31	0.28	0.15
10.0	195.5	0.63	0.44	0.37	0.17
12.0	195.5	0.76	0.52	0.42	0.20
ε		630	430	360	170
<u>6 M H₂SO₄</u>					
2.0	195.5	0.12	0.09	0.08	0.06
4.0	195.5	0.26	0.18	0.14	0.07
6.0	195.5	0.38	0.33	0.22	0.11
8.0	195.5	0.50	0.43	0.29	0.15
10.0	196.0	0.64	0.43	0.36	0.16
12.0	196.0	0.76	0.51	0.41	0.19
ε		630	430	360	170

Table 13. (Contd).

M Sb(V) 1 x 10 ⁻⁴	λ max mμ	Optical Density.			
		λ max	190	200	210
<u>8M. H₂SO₄</u>					
2.0	195.5	0.11	0.10	0.08	0.03
4.0	195.5	0.27	0.19	0.17	0.10
6.0	195.0	0.41	0.39	0.25	0.16
8.0	195.0	0.54	0.40	0.33	0.19
10.0	195.0	0.69	0.47	0.41	0.24
12.0	195.0	0.81	0.58	0.49	0.29
∑		680	480	410	240
<u>10M. H₂SO₄</u>					
2.0	195.0	0.16	0.12	0.10	0.08
4.0	195.0	0.35	0.25	0.23	0.16
6.0	195.0	0.52	0.38	0.34	0.25
8.0	195.0	0.69	0.71	0.45	0.34
10.0	195.5	0.95	0.62	0.56	0.39
12.0	195.5	1.00	0.75	0.67	0.48
∑		860	630	560	400
<u>12M. H₂SO₄</u>					
1.25	195.0	0.21	0.13	0.11	0.10
2.5	195.0	0.43	0.27	0.24	0.20
3.75	195.0	0.64	0.41	0.36	0.29
5.0	195.0	0.80	0.55	0.48	0.39
7.5	195.0	0.98	0.82	0.72	0.61
∑		1720	1120	960	780

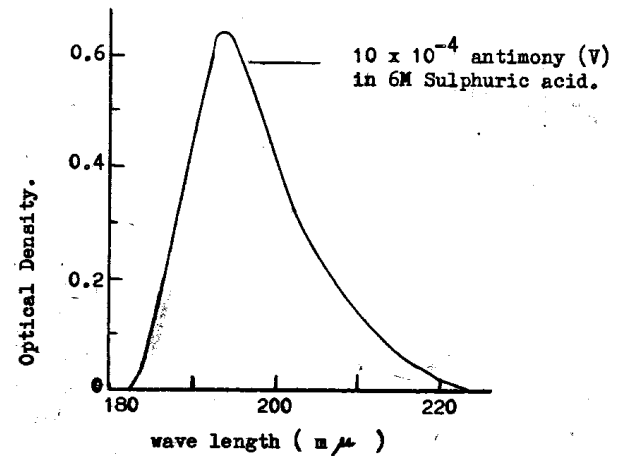


Fig. 3.16. Ultra violet spectrum of antimony (V) in aqueous sulphuric acid.

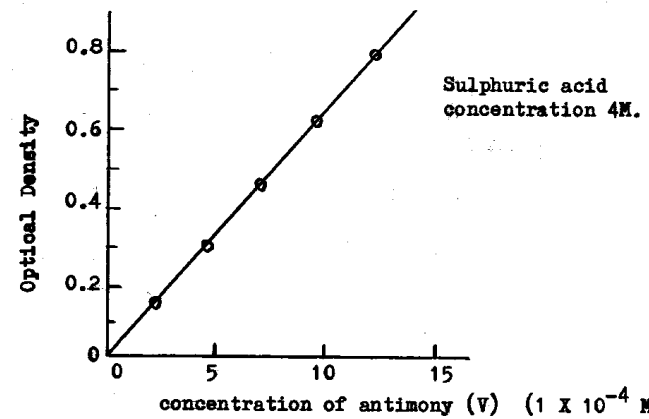


Fig. 3.17. Typical plot of optical density against concentration of antimony (V) in aqueous sulphuric acid.

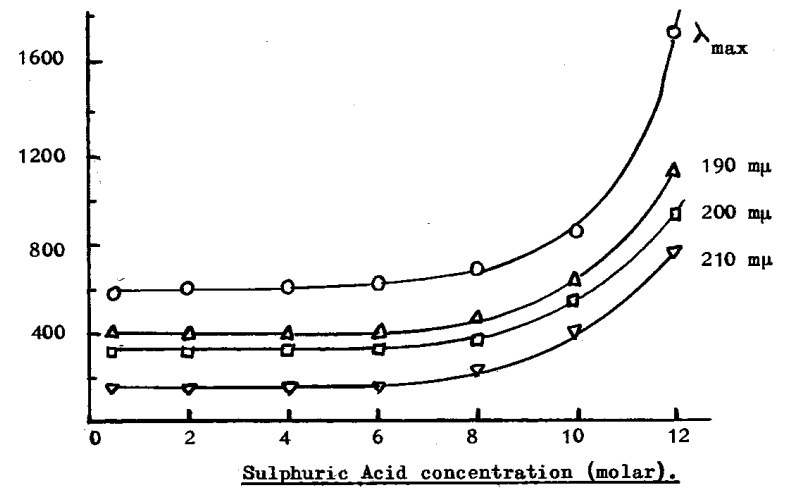


Fig.3.18. Molar extinction coefficients ($\bar{\epsilon}$) of antimony (V).

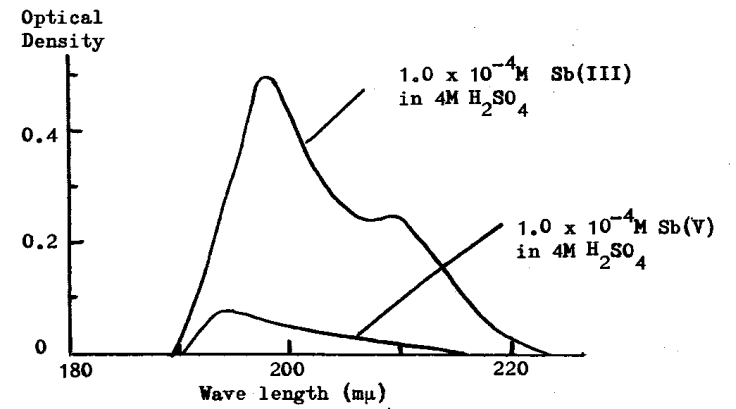


Fig.3.19. Effect of oxidation by the reactive species produced on irradiation with X-rays from Co^{60} .

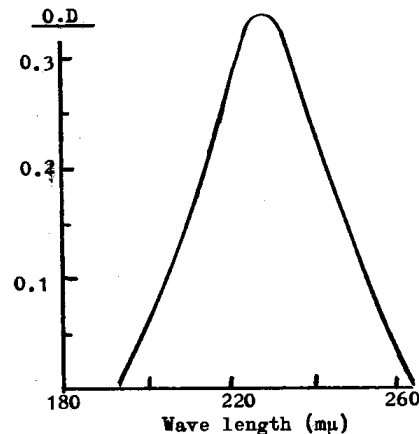


Fig.3.20. Antimony in Fuming Sulphuric Acid.

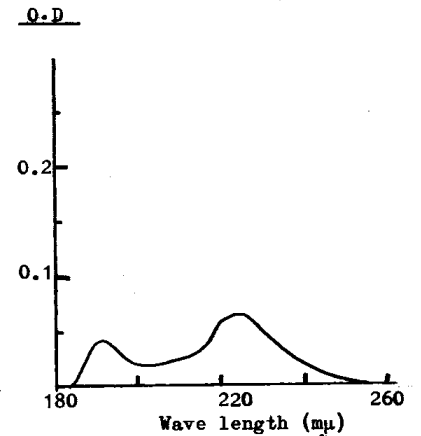


Fig.3.21. Antimony in 90% Fuming Sulphuric Acid.

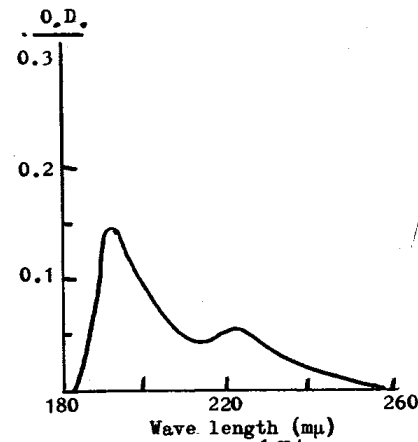


Fig.3.22. Antimony in 80% v/v Fuming Sulphuric Acid.

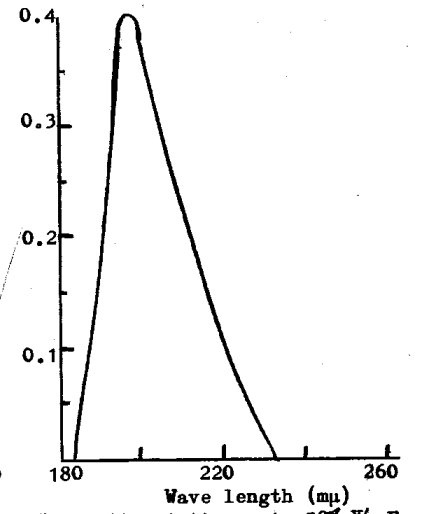


Fig.3.23. Antimony in 50% v/v Fuming Sulphuric Acid.

3.1.4. Solvent Extraction

The results obtained on extracting antimony (III), dosed with antimony 124, by 9 methyl 2, 3, 7, trihydroxy - 6 - fluorone from perchloric acid solutions are shown below in Table 14. The batch distribution coefficient, K_d , was calculated directly from the radioactivity measurements, which had been corrected for the back ground count. The results were expressed as graphs of $\log K_d$ against \log of the fluorone concentration, Fig (3.24), and as $\log K_d$ against \log of the hydrogen ion concentration, Fig (3.25).

Table 14.

HClO_4 M	Sb(III) $1 \times 10^{-4} \text{M}$	fluorone $1 \times 10^{-4} \text{M}$	c.p.100s aq.layer	c.p.100s org.layer	K_d	$\log K_d$	$\log [H^+]$
1.0	1.0	0.5	3,879	10,134	0.261	-0.583	0
1.0	1.0	1.0	8,432	6,871	0.815	-0.089	0
1.0	1.0	1.5	6,242	8,021	1.442	0.159	0
1.0	1.0	2.0	4,011	10,971	2.735	0.437	0
1.0	1.0	2.5	2,419	11,395	4.71	0.673	0
0.1	1.0	2.5	180	11,723	65.1	1.814	-1.0
0.5	1.0	2.5	418	14,000	33.5	1.525	-0.301
0.6	1.0	2.5	780	13,273	17.02	1.231	-0.222
0.8	1.0	2.5	1,242	13,627	10.97	1.04	-0.097
2.0	1.0	2.5	4,371	10,368	2.37	0.375	0.301
3.0	1.0	2.5	6,030	9,000	1.49	0.173	0.477
4.0	1.0	2.5	7,576	8,073	1.065	0.027	0.602
5.0	1.0	2.5	8,075	8,216	1.017	0.007	0.699
6.0	1.0	2.5	8,490	7,782	0.917	-0.038	0.778
7.0	1.0	2.5	8,625	8,253	0.957	-0.019	0.845
8.0	1.0	2.5	7,574	7,847	1.036	0.015	0.903

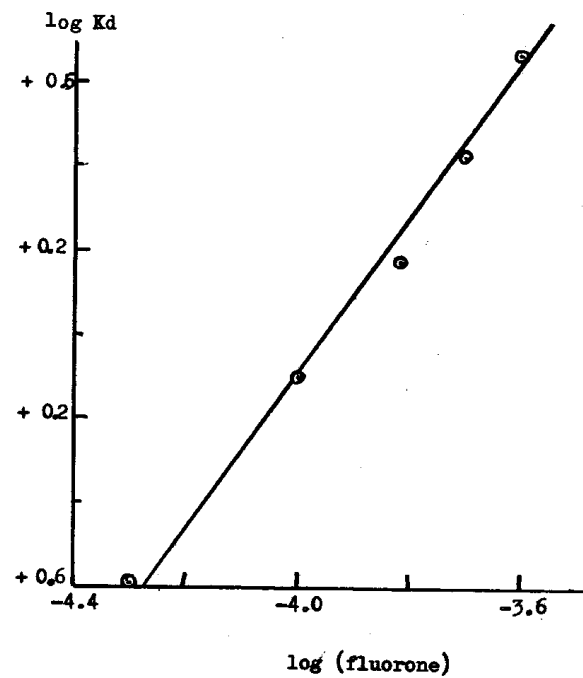


Fig. 3.24. Solvent Extraction of Antimony (III)
from 1M Perchloric Acid.

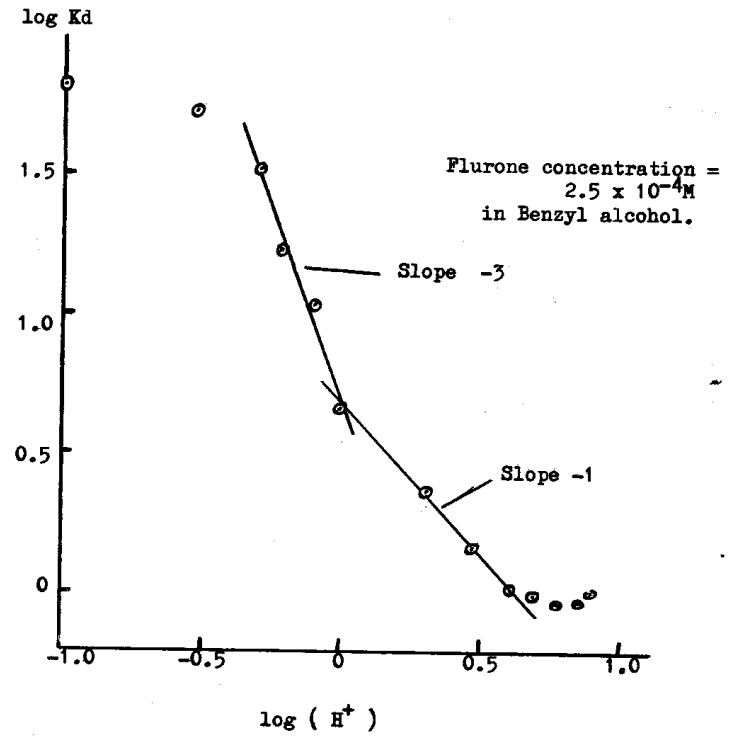


Fig. 3.25. Solvent Extraction of Antimony III expressed as the Distribution Coefficient (Kd) and the Hydrogenion concentration (H⁺).

3.2. The deposition of antimony onto pure lead electrodes

Using the standard electrode pretreatment described in section 2.2.1., the results obtained by depositing antimony from $0.79 \times 10^{-4} M$ antimony (III) in nitrogen saturated 4M sulphuric acid were as shown in Fig (3.26). No current was passed through the cell during the experiment, i.e. the electrode was at open circuit, and the flow rate of the electrolyte was maintained constant at 20 ml. min^{-1} . The amount of antimony deposited, as determined from the radioactivity measurements, was plotted against time and the electrode potential was also noted throughout the experiment. For the first 693 secs. there was a linear increase in the amount of antimony deposited and the electrode potential remained constant at $-0.362V$, the potential of a lead-lead sulphate electrode. The potential of the electrode then increased to $-0.335V$ but the rate of antimony deposition, as measured by the slope of the graph, remained constant for the next 60 sec. and only started to decrease slightly during the next 80 sec. The potential of the electrode rose sharply at 845 sec., the rate of change of potential slowly decreasing until by 1200 sec. a stationary value of $+0.195V$ was obtained. This final potential corresponded to an antimony electrode in the absence of dissolved oxygen or antimony trioxide. The observed rate of antimony deposition also decreased during this period of increase of potential until when the electrode potential was $+0.195V$ the amount of antimony on the electrode surface remained constant. No

Electrolyte = 4M H₂SO₄ containing 0.79 x 10⁻⁴ M Sb(III), Temperature = 25°C, Flow rate = 30.7 ml.min⁻¹

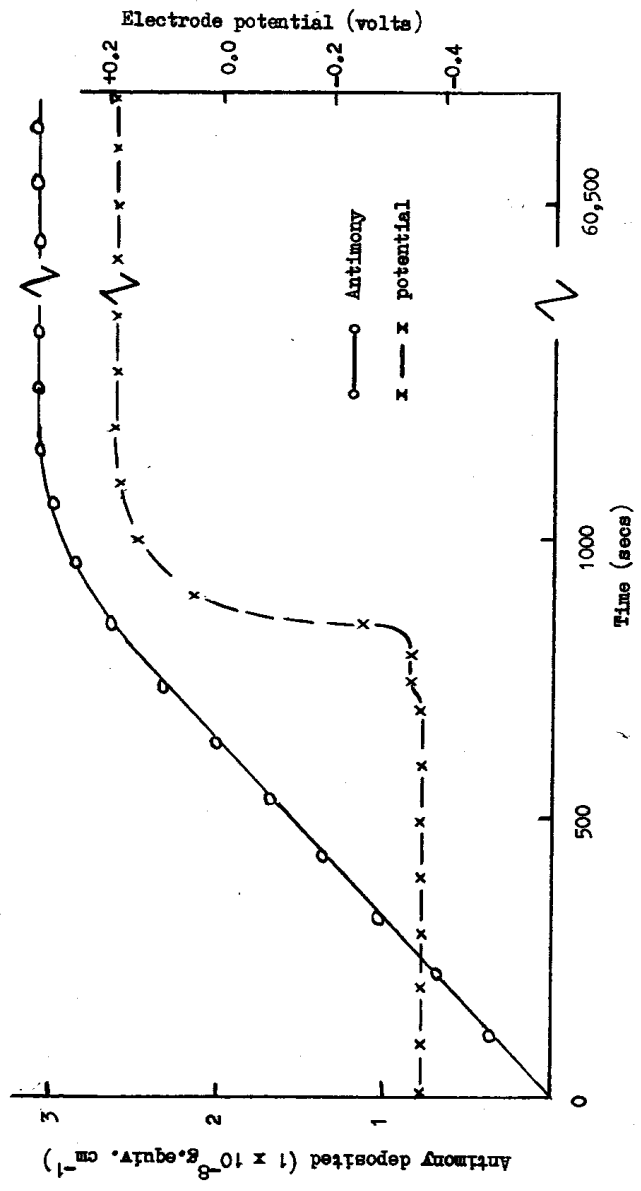


Fig. 3.26. THE DEPOSITION OF ANTIMONY FROM NITROGEN SATURATED ELECTROLYTE

further change in either the amount of antimony on the electrode or the electrode potential was observed either when the electrode remained in contact with the nitrogen saturated electrolyte for 16 hr. or when the electrolyte was replaced with antimony free, nitrogen saturated electrolyte.

All the experiments carried out with nitrogen saturated electrolyte gave results similar to those in Fig (3.26) provided the standard pretreatment of the electrode was used. Altering the pretreatment of the electrode greatly changed the length of time the lead-lead sulphate potential was maintained and also affected to a lesser degree the rate of antimony deposition, this is discussed in greater detail in Section 4.2.1.

The slope of the linear part of the deposition graph gave the rate of antimony (III) deposition and this rate of deposition was dependant on (a) the flow rate of the electrolyte (b) antimony concentration (c) the sulphuric acid concentration and (d) the temperature. These parameters from typical experiments are shown in Figs (3.27) to (3.34) and the results are given in Tables 15 to 19. The flow velocity (cm. s^{-1}) of electrolyte was calculated from the flow rate Q ($\text{cm.}^3 \text{s}^{-1}$) and the mean cross section of the electrolyte flowpath at the electrode (cm.^2). The values of the diffusion coefficients were obtained from the polarographic determinations, and the dynamic viscosity were calculated from the kinematic viscosity and density values quoted in the International Critical Tables. Values of the corresponding Nusselt, Reynold and Schmidt numbers were also calculated.

for the sulphuric acid concentrations employed. The Nusselt and Reynold's numbers were calculated using the hydraulic diameter, d_m , of the electrolyte at the electrode, where

$$d_m = \frac{2 \times \text{cross sectional area}}{\text{wetted perimeter}} = \frac{2 \times 0.077 \times 2.5}{2.577},$$

∴ $d_m = 0.1494$ cm. The dimensionless numbers are given by

$$\text{Nu} = \frac{kd_m}{D}, \quad \text{Re} = \frac{vd_m}{V}, \quad \text{Sc} = \frac{V}{D}$$

where k = mass transfer constant, D = diffusion coefficient of the antimony (III), v = electrolyte velocity at the electrode, and V = the kinematic viscosity of the electrolyte,

These values of Nu, Re and Sc have been included in Tables 15 to 19 for convenience and this aspect of the deposition work is discussed in greater detail in Section 4.2.

The amount of antimony deposited on a lead electrode at different electrolyte flows is shown in Fig. (3.27) and the antimony (III) deposition rates from 4M sulphuric acid at 25°C are plotted against the flow rate and the square root of the flow velocity in Figs. (3.28) and (3.29).

The effect of increasing the antimony (III) concentration in the electrolyte is shown in Figs. (3.30) and (3.31), the rate of antimony deposition increased linearly with increase of antimony (III) concentration. The rate of antimony deposition as a function of sulphuric acid concentration is shown in Figs. (3.32) and (3.33), the deposition rate decreasing with increase of sulphuric acid concentration.

Table 15

0.65M H₂SO₄, Temperature = 25°C, D = 4.91 x 10⁻⁶ cm².s⁻¹

V = 1.075 x 10⁻² cm².s⁻¹, Sc = 2190, Sc^{1/3} = 12.98

[Sb(III)] 1 x 10 ⁻⁴ M	Flow Rate (Q) ml.min ⁻¹	Flow Vel. (v) cm.s ⁻¹	Re _{dm}	Re ^{1/3} Sc ^{1/3}	Dep. Rate R x 10 ⁻¹¹ moles cm ⁻² .s ⁻¹	k x 10 ⁴ (=R/[Sb]) cm.s ⁻¹	Nu _{dm}
0.395	5.20	0.450	6.25	32.4	1.28	3.23	9.8
0.395	12.10	1.047	14.54	49.3	1.85	4.70	14.3
0.395	24.90	2.155	29.99	71.0	2.37	6.00	18.3
0.395	40.00	3.462	41.60	83.0	2.86	7.25	22.1
0.395	52.10	4.510	62.60	102.4	3.47	8.80	26.8
0.63	1.95	0.169	2.34	19.8	1.99	3.16	9.6
0.63	5.50	0.476	6.61	33.3	2.40	3.81	11.6
0.63	12.80	1.107	15.39	50.8	2.94	4.66	14.2
0.63	25.10	2.172	30.16	71.2	3.90	6.20	18.9
0.63	39.80	3.440	47.80	89.5	4.49	7.13	21.7
0.63	51.00	4.410	61.30	101.6	5.50	8.74	26.6
0.79	1.35	0.117	1.62	16.47	1.80	2.28	6.9
0.79	4.50	0.389	5.42	30.20	2.74	3.48	10.6
0.79	8.40	0.727	10.11	41.20	3.04	3.86	11.7
0.79	11.50	0.995	13.84	48.26	3.82	4.90	14.9
0.79	15.60	1.350	18.76	56.15	4.20	5.33	16.2
0.79	20.00	1.732	24.06	63.50	4.38	5.56	16.9
0.79	25.30	2.190	30.45	71.50	5.05	6.41	19.5
0.79	32.00	2.770	38.50	80.40	5.43	6.89	21.0
0.79	41.50	3.590	49.90	91.60	4.86	6.17	18.8
0.79	50.50	4.370	60.75	101.10	6.41	8.14	24.8
0.79	62.00	5.360	74.60	112.00	6.62	8.39	25.6

Table 16

2M H₂SO₄, Temperature = 25°C, D = 3.68 x 10⁻⁶ cm².s⁻¹

V = 1.250 x 10⁻² cm².s⁻¹, Sc = 3400, Sc^{1/3} = 15.04

[Sb(III)] 1 x 10 ⁻⁴ M	Flow Rate (Q) ml.min ⁻¹	Flow Vel. (v) cm.s ⁻¹	Re _{dm}	Re ^{1/2} Sc ^{1/3}	Dep. Rate _s Rx10 ⁻⁵ moles cm ⁻² .s ⁻¹	kx10 ⁻⁴ (-R/[Sb]) cm.s ⁻¹	Nu _{dm}
0.395	3.80	0.329	3.93	29.8	1.13	2.86	11.6
0.395	8.25	0.713	8.52	43.9	1.37	3.47	14.1
0.395	20.10	1.738	20.75	68.5	1.89	4.78	19.4
0.395	24.95	2.156	25.85	76.4	2.02	5.12	20.8
0.395	30.25	2.614	31.20	84.0	2.25	5.69	23.1
0.395	41.00	3.550	42.40	97.8	2.47	6.25	25.4
0.395	50.20	4.390	52.40	109.0	2.82	7.14	29.0
0.63	1.50	0.130	1.552	15.5	0.93	1.48	6.0
0.63	10.00	0.865	10.30	48.3	2.62	4.16	16.9
0.63	21.05	1.822	21.77	70.2	3.16	5.02	20.4
0.63	32.30	2.790	33.30	86.8	3.58	5.68	23.8
0.63	40.90	3.540	42.30	97.7	4.05	6.43	26.1
0.79	2.50	0.216	2.58	24.06	1.31	1.66	9.25
0.79	6.10	0.528	3.51	28.14	1.80	2.28	10.92
0.79	12.50	1.083	4.95	51.60	3.26	4.13	16.79
0.79	18.70	1.62	19.35	66.58	3.46	4.38	17.76
0.79	25.00	2.16	25.80	77.30	3.94	4.99	20.28
0.79	34.00	2.94	35.10	91.40	4.72	5.98	24.28
0.79	45.00	3.90	46.50	105.40	5.09	6.44	26.15
0.79	52.50	4.55	54.4	116.20	5.23	6.62	26.88

Table 17

4M H₂SO₄, Temperature = 25°C, D = 2.50 x 10⁻⁶ cm².s⁻¹
 V = 1.680 x 10⁻² cm².s⁻¹, Sc = 6720, Sc^{1/3} = 18.87

[Sb(III)] 1 x 10 ⁻⁴ M	Flow Rate (Q) ml.min ⁻¹	Flow Vel. (v) cm.s ⁻¹	Re _{dm}	Re ^{1/2} Sc ^{1/3}	Dep. Rate R x 10 ⁻¹¹ moles cm ² .s ⁻¹	k x 10 ⁻⁴ (=R(S)) cm.s ⁻¹	Nu _{dm}
0.63	3.5	0.31	2.75	31.3	0.67	1.87	11.2
0.63	10.1	0.89	7.90	53.0	0.95	2.64	15.8
0.63	20.3	1.79	15.91	75.3	1.23	3.43	20.5
0.63	29.8	2.62	23.28	91.0	1.39	3.85	23.0
0.63	40.0	3.53	31.34	105.7	1.62	4.50	26.9
0.79	1.5	0.13	1.16	20.4	1.11	1.41	8.4
0.79	4.5	0.39	3.47	35.1	1.33	1.68	10.0
0.79	9.8	0.85	7.56	51.9	1.91	2.42	14.5
0.79	16.4	1.42	12.64	67.2	2.33	2.95	17.7
0.79	22.0	1.94	17.25	78.3	2.73	3.46	20.7
0.79	30.7	2.66	23.65	91.7	3.20	4.06	24.3
0.79	40.1	3.47	30.85	104.9	3.39	4.30	25.7
0.79	49.7	4.30	38.20	116.6	3.51	4.45	26.6
1.26	4.0	0.35	3.11	33.2	2.48	1.97	11.8
1.26	9.8	0.86	7.64	52.0	3.38	2.69	16.1
1.26	19.7	1.74	15.45	74.0	4.39	3.49	20.9
1.26	25.6	2.26	20.08	84.3	4.48	3.56	21.3
1.26	32.1	2.83	25.15	94.5	4.98	3.96	23.7
1.26	47.5	4.18	37.10	114.6	5.91	4.70	28.1

Table 18

6M H₂SO₄, Temperature = 25°C, D = 1.70 x 10⁻⁶ cm².s⁻¹

V = 2.330 x 10⁻² cm².s⁻¹, Sc = 13,700, Sc^{1/3} = 23.93

[Sb(III)] 1 x 10 ⁻⁴ M	Flow Rate (Q) ml.min ⁻¹	Flow Vel. (v) cm.s ⁻¹	Re _{dm}	Re ^{1/2} Sc ^{1/3}	Dep. Rate (R x 10 ⁻¹¹) moles cm ⁻² .s ⁻¹	k x 10 ⁻⁴ (=R/[Sb]) cm.s ⁻¹	Nu _{dm}
0.79	1.8	0.156	1.00	23.9	0.84	1.06	9.3
0.79	5.0	0.433	2.77	39.7	1.27	1.68	14.8
0.79	10.4	0.900	5.77	57.4	1.38	1.75	15.3
0.79	18.2	1.576	10.10	76.0	1.96	2.48	21.8
0.79	25.0	2.165	13.87	89.2	2.05	2.60	22.8
0.79	36.1	3.120	20.00	107.0	2.20	2.79	24.5
0.79	50.2	4.350	27.90	126.3	2.69	3.41	29.9
1.26	2.7	0.232	1.50	29.3	1.25	0.99	8.7
1.26	8.3	0.713	4.61	59.5	2.50	1.98	17.4
1.26	17.9	1.537	9.93	75.3	2.70	2.14	18.8
1.26	25.2	2.164	14.00	89.4	3.65	2.90	25.5
1.26	37.5	3.220	20.80	109.0	3.49	3.16	27.7

Table 19

8M H_2SO_4 , Temperature = 25°C, $D = 1.12 \times 10^{-6} \text{ cm}^2 \cdot \text{s}^{-1}$
 $V = 3.25 \times 10^{-2} \text{ cm}^2 \cdot \text{s}^{-1}$, $Sc = 29,000$, $Sc^{\frac{1}{2}} = 30.70$

$[Sb(III)]^{\frac{1}{2}}$ $1 \times 10^{-4} M$	Flow Rate (Q) $\text{ml} \cdot \text{min}^{-1}$	Flow Vel. (v) $\text{cm} \cdot \text{s}^{-1}$	Re_{dm}	$Re^{\frac{1}{2}} Sc^{\frac{1}{2}}$	Dep. Rate ($R \times 10^{-11}$) $\text{moles cm}^{-2} \cdot \text{s}^{-1}$	$k \times 10^{-4}$ ($= R/[Sb]$) $\text{cm} \cdot \text{s}^{-1}$	Nu_{dm}
0.79	2.9	0.25	1.15	31.0	0.86	1.08	14.4
0.79	3.5	0.30	1.38	36.2	0.67	0.85	11.3
0.79	7.2	0.62	2.86	51.8	0.91	1.15	15.3
0.79	16.4	1.42	6.52	69.0	1.39	1.76	23.5
0.79	28.5	2.47	11.34	103.0	1.55	1.96	26.1
0.79	42.2	3.65	16.76	125.0	1.92	2.43	32.4
0.79	57.0	4.93	22.65	146.0	2.46	3.11	41.5
1.26	5.1	0.44	2.03	43.8	1.18	0.94	12.6
1.26	9.9	0.85	3.94	61.2	1.49	1.18	15.7
1.26	19.8	1.70	7.88	86.1	1.95	1.55	20.6
1.26	25.0	2.15	9.94	96.7	2.22	1.76	23.4
1.26	30.1	2.59	12.05	106.3	2.37	1.88	25.1
1.26	39.8	3.42	15.84	122.0	2.78	2.21	29.4

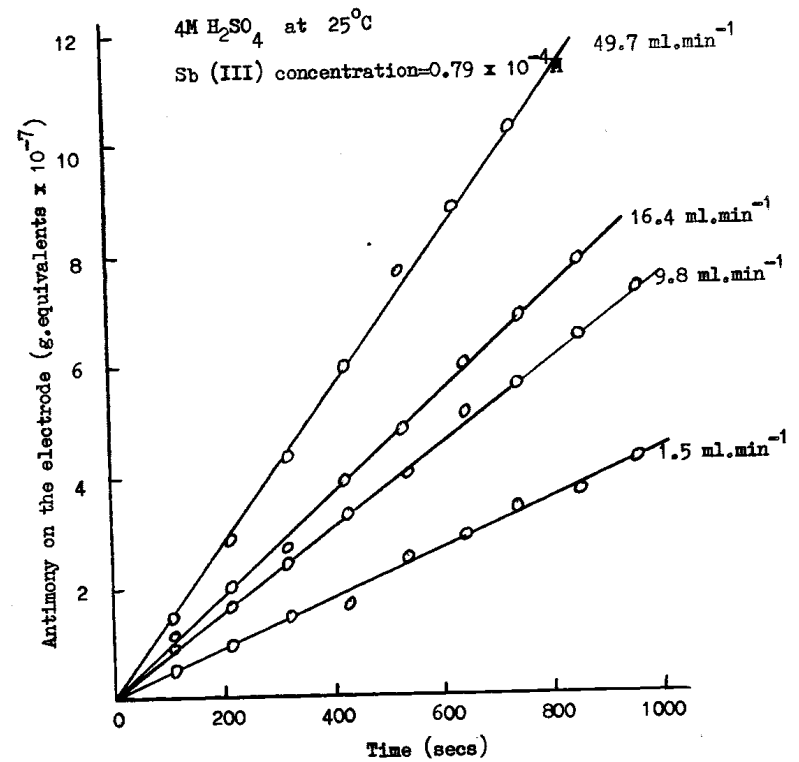


Fig. 3.27. THE RATE OF ANTIMONY DEPOSITION AT VARIOUS FLOW RATES

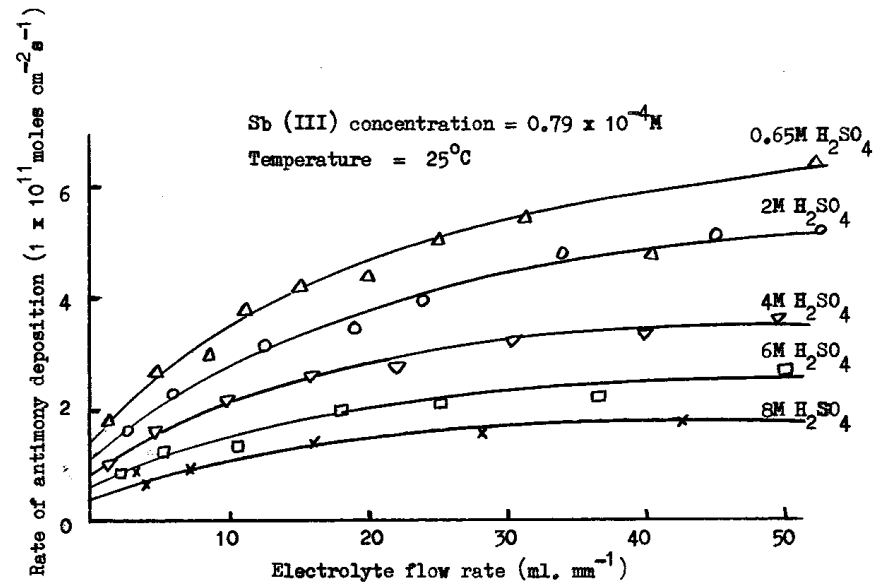


Fig. 3.28. THE RATE OF ANTIMONY DEPOSITION V^S THE ELECTROLYTE FLOW RATE

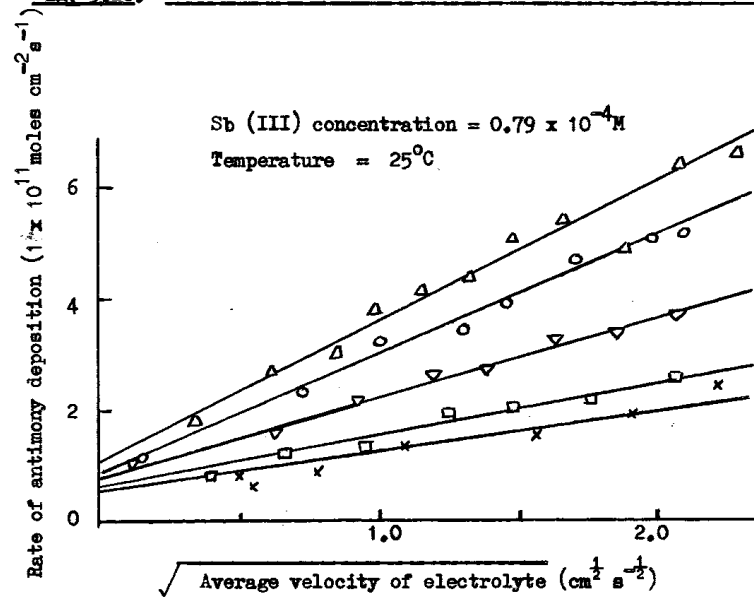


Fig. 3.29. THE RATE OF ANTIMONY DEPOSITION V^S THE SQUARE ROOT OF THE ELECTROLYTE VELOCITY.

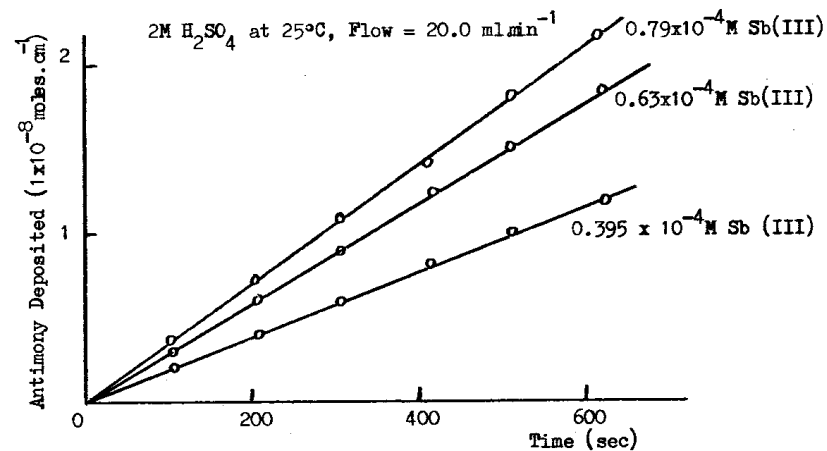


Fig. 3.30 Antimony Deposition at Various Antimony (III) Concentrations

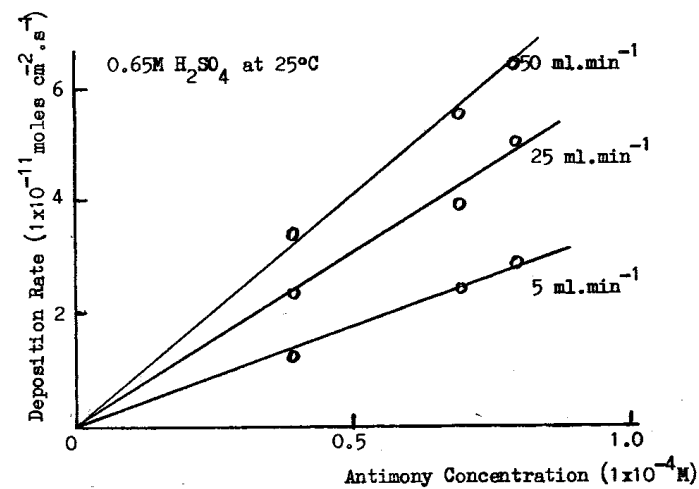


Fig. 3.31 The Rate of Antimony (III) Deposition at Various Antimony Concentrations

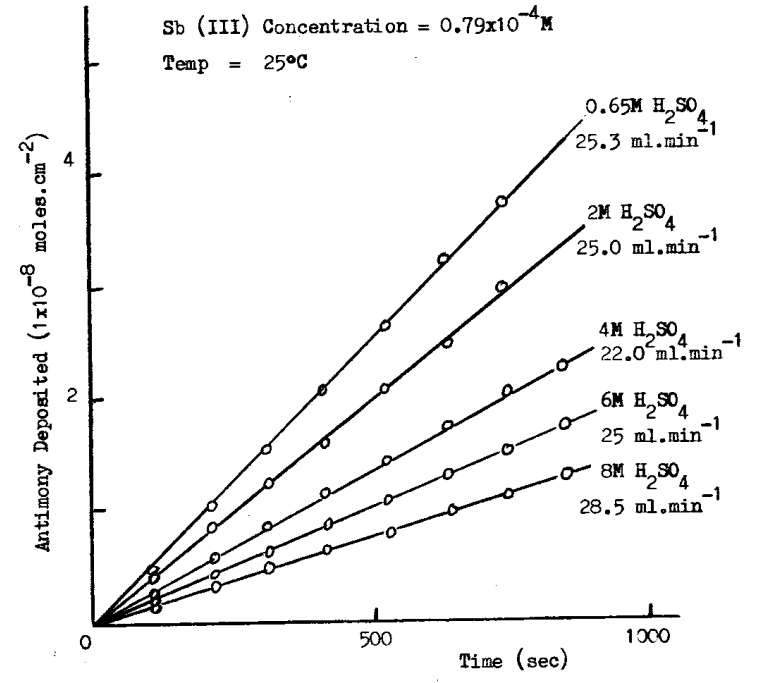


Fig. 3.32 Antimony (III) Deposition at Various Sulphuric Acid Concentrations

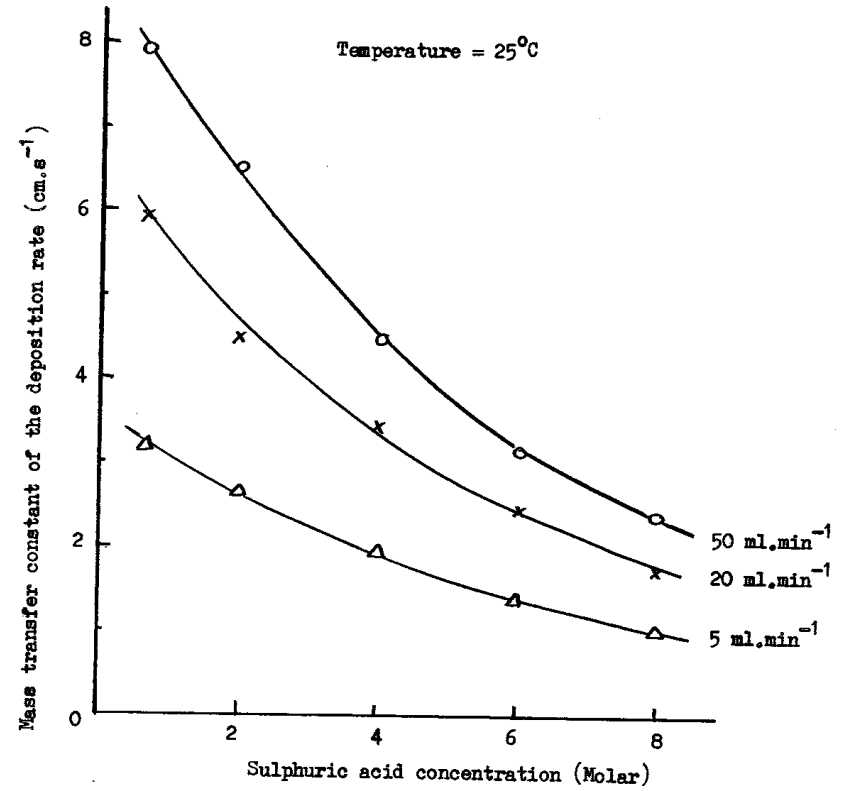


Fig. 3.33. THE RATE OF ANTIMONY DEPOSITION AS A FUNCTION OF SULPHURIC ACID CONCENTRATION

The rate of antimony deposition increased with increase of temperature and from results at various temperatures the activation energy of the reaction was determined from an Arrhenius plot of log rate of deposition against the reciprocal of the absolute temperature, Fig. (3.34). The small activation energies, approximately 2 K cal.mole⁻¹, may be considered as a measure of the resistance to the transport of the antimony (III) ions through the Nernst diffusion layer close to the electrode.

Table 20

Flow rate = 20 ml.min⁻¹

M H ₂ SO ₄	Temp. °C	Rate of Dep. ⁿ k cm.s ⁻¹	Activation Energy K cal.mole ⁻¹
4	20	2.95 x 10 ⁻⁴	1.87
4	25	3.31 x 10 ⁻⁴	
4	35	4.56 x 10 ⁻⁴	
4	40	4.59 x 10 ⁻⁴	
6	20	2.04 x 10 ⁻⁴	2.01
6	25	2.24 x 10 ⁻⁴	
6	35	2.51 x 10 ⁻⁴	
6	40	2.82 x 10 ⁻⁴	
8	20	1.60 x 10 ⁻⁴	2.18
8	25	1.85 x 10 ⁻⁴	
8	35	2.09 x 10 ⁻⁴	
8	40	2.21 x 10 ⁻⁴	

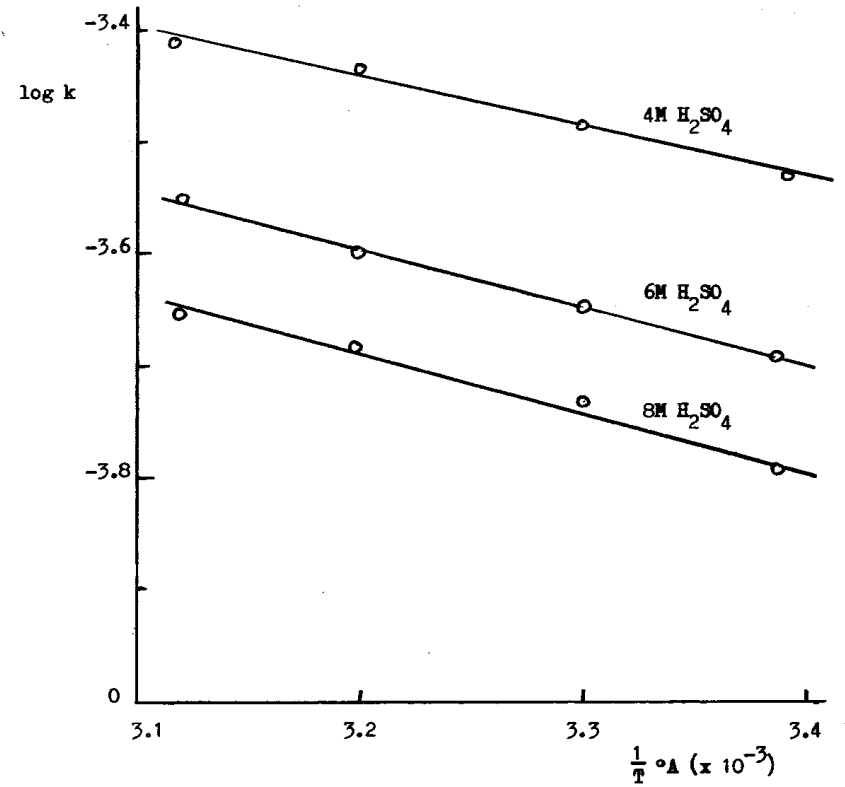


Fig. 3.5 Arrhenius Plot of log of Mass Transfer Constant, k, against the Reciprocal of the Absolute Temperature

No change in the rate of antimony (III) deposition was observed when a cathodic current was passed through the electrode, Fig, (3.36), providing the counter electrode compartment was well purged with nitrogen. The polarisation potential of the electrode was affected by the amount of antimony deposited, the hydrogen overpotential of the lead electrode decreasing with an increased amount of antimony present on the electrode, Fig, (3.36)

Table 21

Hydrogen Overpotential on the Lead Electrode During Deposition

The amount of antimony on the electrode is shown as a percentage required for complete coverage.

Log C.D. (A.cm ⁻²)	Electrode Potential (Overvoltage)				
	0%	10%	40%	80%	90%
-3.602	0.02	-	-	-	-
-3.301	0.06	0.03	0.015	-	-
-2.824	0.12	0.09	0.07	0.05	0.05
-2.699	0.13	0.11	0.085	0.065	0.066
-2.301	0.175	0.16	0.13	0.11	0.11
-1.903	0.225	0.21	0.17	0.165	0.16
-1.602	0.255	0.24	0.23	0.195	0.19

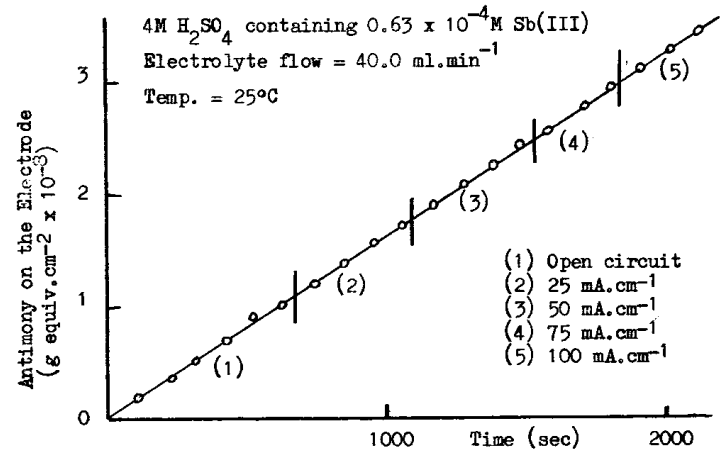


Fig. 3.35 Antimony (III) Deposition at Different Current Densities

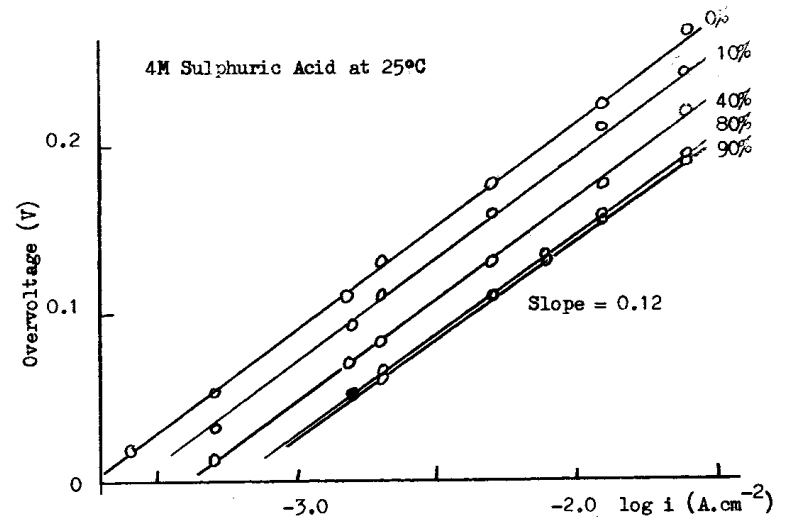


Fig. 3.36 Hydrogen Overpotential on a Lead Electrode with Increasing Deposition of Antimony

The amount of lead available for the sustaining of the discharge reaction $\text{Pb} + \text{SO}_4^{--} \rightarrow \text{PbSO}_4 + 2\text{e}$ decreased as the antimony on the electrode increased. During these discharge experiments the electrode was first subjected to a cathodic current of 25 mA cm^{-2} for 5 minutes prior to the discharge, the current was then reduced to 1 mA cm^{-1} , reversed and the potential of the electrode measured. An initial potential drop of 20 - 30 mV was observed, and the potential then remained fairly constant for a time dependant on the amount of lead present to sustain the discharge reaction, the electrode being considered discharged when the 'knee' of the potential time curve, approximately -0.27V , was reached, Fig (3.37). The electrode was then recharged at 25 mA cm^{-2} and more antimony deposited onto it. It will be seen from Fig (3.38), where the amount of deposited antimony was plotted against the length of the discharge plateau, that the amount of lead available for the discharge reaction appeared to be a function of the amount of antimony present.

Table 22.

<u>Antimony on the electrode</u> <u>(1×10^{-8} g. equiv. cm^{-1})</u>	<u>Discharge Plateau</u> <u>(mins.)</u>
0.15	6.1
0.70	6.0
1.10	5.1
2.20	4.1
2.70	3.7
3.35	1.1
3.65	0.6

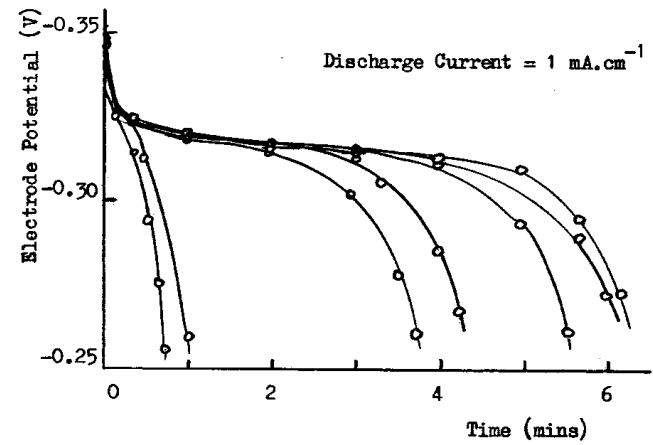


Fig. 3.37 Discharge of Electrode During Deposition

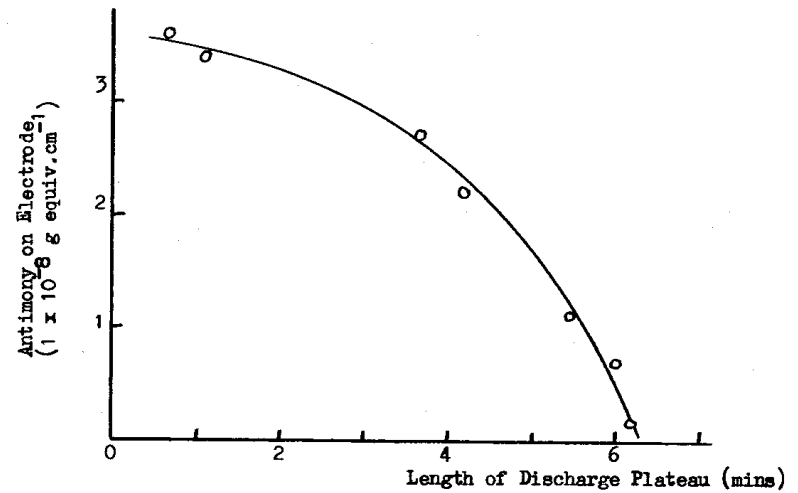


Fig. 3.38 Effect of Deposited Antimony on the Electrode Discharge

In some experiments the electrode was completely reversed and anodic corrosion of the antimony deposited occurred, Fig. (3.39) shows a typical result and it is interesting to note that the electrode potential at 25 mA.cm^{-2} rose to that of a lead-lead dioxide exhibiting oxygen over potential when the majority of the antimony had corroded from the surface. The corrosion of the antimony appeared to be dependant on the current density but this was not fully investigated.

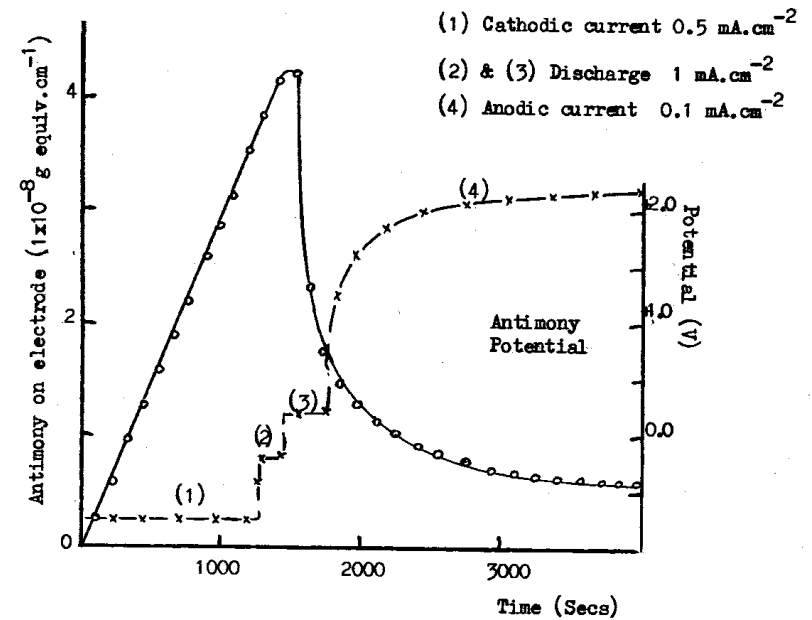


Fig. 3.40 Effect of Reversing the Current

The rate of antimony (III) deposition from oxygen saturated solutions was also investigated, and under open circuit conditions the results were similar to Fig (3.40). The observed rate of antimony (III) deposition appeared to be less than corresponding deposition from nitrogen saturated electrolyte, but it was difficult to obtain an exact comparison of the two rates because of the similarity of the deposition rates. The most interesting aspects of the results from oxygen containing electrolyte was that (a) the "antimony electrode" potential was 10 to 15 mV higher, e.g. +0.212V, than the potentials obtained in oxygen free electrolyte, c.f. +0.195V and (b) the antimony corroded from the electrode when the electrode potential approached this "antimony electrode" potential. The potential decreased only when the majority of the antimony had been removed from the electrode and eventually a static condition was obtained with a small amount of antimony on the electrode and a potential of between +0.05V and +0.15V. The rate of corrosion appeared to depend on the oxygen concentration in the electrolyte and flow rate of the electrolyte but the corrosion rate results were far from conclusive and were therefore not reported.

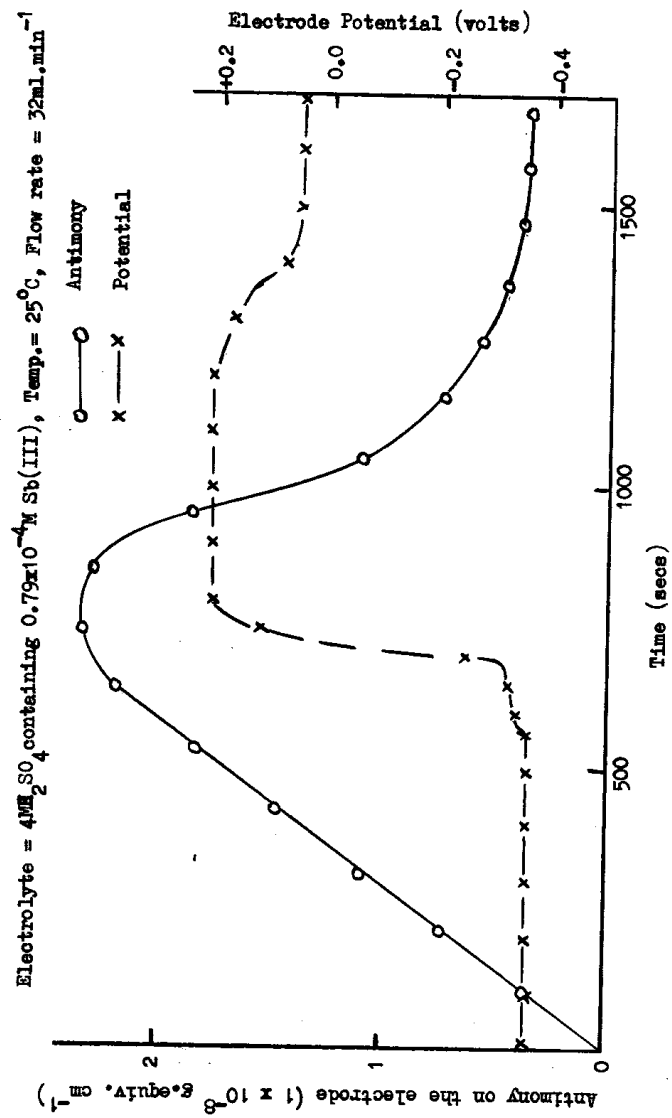


Fig. 3.40. DEPOSITION OF ANTIMONY FROM OXYGEN SATURATED ELECTROLYTE

Table 23

The Rate of Antimony (III) Deposition from Oxygen Saturated Solutions4M H₂SO₄, Temperature = 25°C, Electrolyte Flow = 20.00 ml.min⁻¹

Electrode No.	Mass Transport Constant $k \times 10^{-4} \text{ cm.s}^{-1}$	Electrode No.	Mass Transport Constant $k \times 10^{-4} \text{ cm.s}^{-1}$
1	3.20	6	3.37
2	3.36	7	3.18
3	3.28	8	3.40
4	3.51	9	3.17
5	3.25	10	3.33

$$k_{\text{O}_2 \text{ sat.}} = 3.30 \pm 0.2 \times 10^{-4} \text{ cm.s}^{-1}, \quad k_{\text{N}_2 \text{ sat.}} = 3.42 \pm 0.2 \times 10^{-4} \text{ cm.s}^{-1}$$

Table 24

Hydrogen Overpotential in Oxygen Saturated Electrolyte

The antimony on the electrode, Fig. 3.41, was expressed as a percentage of that required for complete coverage of the electrode surface, Slope = 0.192.

Overpotential (Volts)	Log Current Density (A.cm ⁻²) with Increase of Sb			
	9%	40%	75%	90%
0.04	-2.78	-2.83	-2.84	-2.86
0.08	-2.63	-2.62	-2.64	-2.68
0.15	-2.44	-2.43	-2.46	-2.44
0.25	-2.35	-2.23	-2.18	-2.06
0.35	-1.90	-1.82	-1.75	-1.64
0.45	-1.48	-1.39	-1.30	-1.16
0.55	-1.02	-0.98	-0.88	-0.80

Antimony (V) was not deposited onto the lead electrodes, and neither antimony (V) nor antimony (III) were deposited onto a small lead-lead dioxide electrode.

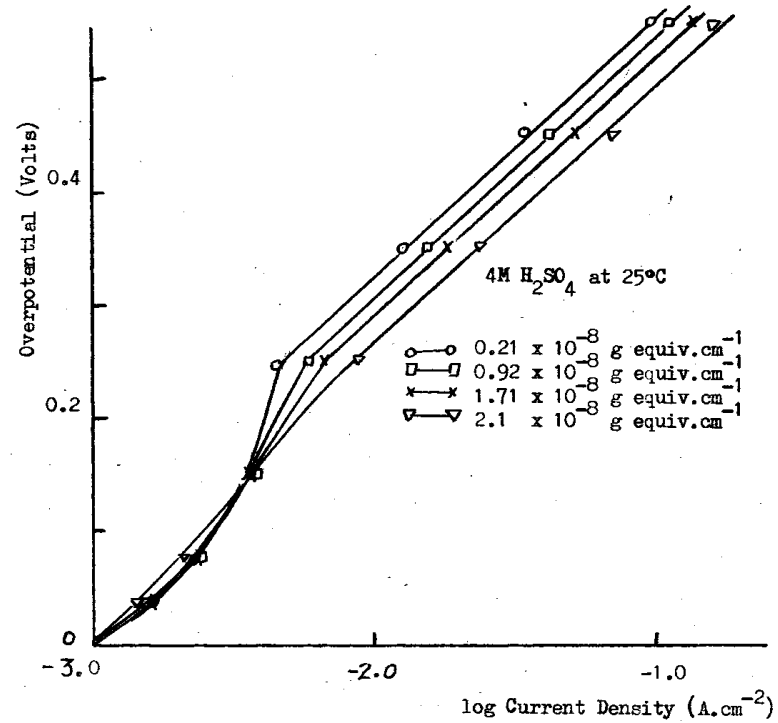


Fig. 3.41 Hydrogen Overpotential on a Lead-Antimony Electrode in the Presence of Dissolved Oxygen

3.3 Antimony Chemistry in the Lead-Acid Battery

3.3.1 The production of antimony species from antimonial lead alloy electrodes

The amount, and the oxidation state, of the antimony formed at 8% antimonial lead electrodes during the electrolysis of 4M sulphuric acid was determined. Samples of electrolyte from the anode and cathode compartments after electrolysis were investigated by spectrophotometric and polarographic analysis. The sample of electrolyte from the cathode compartment gave a well defined antimony (III) polarographic wave, but it was only after reducing the solution with sodium bisulphate, followed by boiling to remove the excess sulphur dioxide, that the antimony content of the anode compartment electrolyte could be estimated polarographically, as shown below in Table 25.

TABLE 25

Antimony formed in 4M Sulphuric Acid from

8% Antimonial Lead Electrodes. Area 10 cm², after a current density of 10 mA/cm² had been passed for 4 hours through the cell

Electrolyte Sample	Amount of Antimony determined, Molar,		
	By ultra-violet Spectra	By Polarography	
		No pre-treatment	After reduction with Sodium Bisulphate
Anode Compartment	$14.5 \times 10^{-4} \text{Sb}^{\text{V}}$	$0.02 \times 10^{-4} \text{Sb}^{\text{III}}$	$15 \times 10^{-4} \text{Sb}^{\text{III}}$
Cathode Compartment	$0.4 \times 10^{-4} \text{Sb}^{\text{III}}$	$0.4 \times 10^{-4} \text{Sb}^{\text{III}}$	$0.42 \times 10^{-4} \text{Sb}^{\text{III}}$

3.3.2 The reduction and oxidation of antimony in aqueous sulphuric acid.

The solutions from the end compartments of the three compartment cell were removed after the time intervals shown. The total antimony concentration was determined by counting the solutions in an annular type Geiger-Muller tube and the antimony (III) concentration was determined polarographically. The cell was fitted with platinum electrodes, of area 10 cm^2 , and the current density used was 0.5 mA/cm^2 .

With the antimony (III) solutions a black deposit of antimony was formed on the platinum cathode but in antimony (V) solutions the physical appearance of the cathode remained unaltered. The results shown below are the average of four experiments.

(a) Antimony (III)

TABLE 26

Initial Antimony concentration = $0.79 \times 10^{-4} \text{ M}$ in
4M Sulphuric Acid.

Time (Hrs)	Anode compartment		Cathode compartment	
	Total antimony concentration, M.	Antimony (III) concentration, M.	Total antimony concentration, M.	Antimony (III) concentration, M.
0	0.79×10^{-4}	0.79×10^{-4}	0.79×10^{-4}	0.79×10^{-4}
2	0.80×10^{-4}	0.75×10^{-4}	0.785×10^{-4}	0.785×10^{-4}
4	0.80×10^{-4}	0.73×10^{-4}	0.78×10^{-4}	0.78×10^{-4}
6	0.81×10^{-4}	0.70×10^{-4}	0.77×10^{-4}	0.77×10^{-4}
8	0.81×10^{-4}	0.69×10^{-4}	0.775×10^{-4}	0.77×10^{-4}

(b) Antimony VTABLE 27

Initial antimony concentration = 0.79×10^{-4} in
4M sulphuric acid

Time (Hrs)	Anode Compartment		Cathode Compartment	
	Total Antimony concentration, M.	Antimony (III) concentration, M.	Total Antimony concentration, M.	Antimony (III) concentration, M.
0	0.79×10^{-4}	0	0.79×10^{-4}	0
2	0.79×10^{-4}	0	0.79×10^{-4}	0
4	0.80×10^{-4}	0	0.79×10^{-4}	0.005×10^{-4}
6	0.80×10^{-4}	0	0.785×10^{-4}	0.005×10^{-4}
8	0.80×10^{-4}	0	0.785×10^{-4}	0.01×10^{-4}

The above results indicate that some of the antimony (III) was oxidised to antimony (V) in the anode compartment and some of the antimony (V) was reduced to antimony (III) in the cathode compartment although the latter was only a trace amount.

3.3.3 The adsorption of antimony from aqueous sulphuric acid onto lead dioxide and lead sulphate.

The radioactivity measurements of the antimony solution samples were corrected for background and decay of the antimony 124, and the results expressed as milligrams of antimony adsorbed per gram of lead dioxide or lead sulphate. The adsorption of antimony by the lead dioxide and lead sulphate is shown as a function of time in Figs (3.42) to (3.45). The rate of adsorption of antimony (III) onto both the lead dioxide and the lead sulphate was greater than the corresponding rate of adsorption of antimony (V). The results also show that lead dioxide is a better adsorbant of antimony than lead sulphate.

Figs. (3.46) and (3.47) show the adsorption of antimony (III) and antimony (V) after various time intervals as a function of the sulphuric acid concentration. The rate of antimony adsorption was greater at low sulphuric acid concentrations.

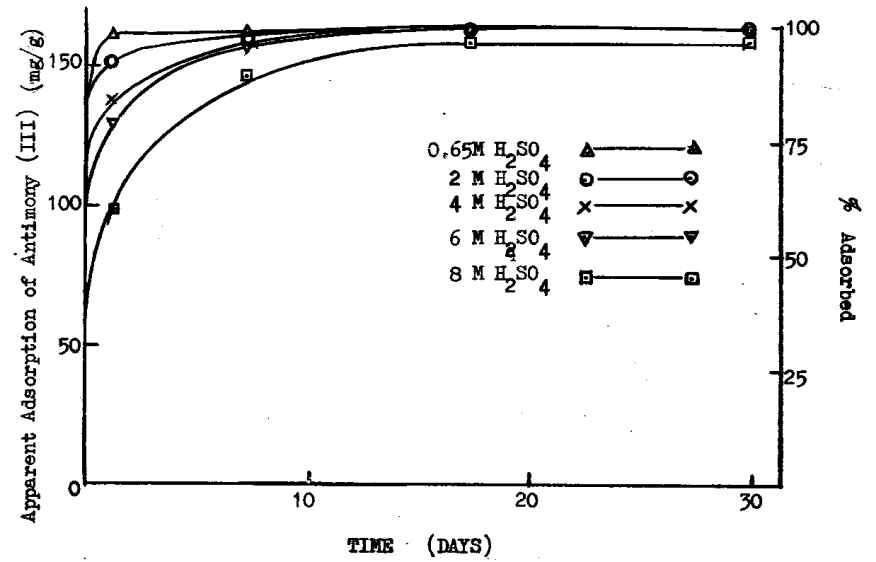


Fig 3.42 The Rate of Adsorption of Antimony (III) onto Lead Dioxide.

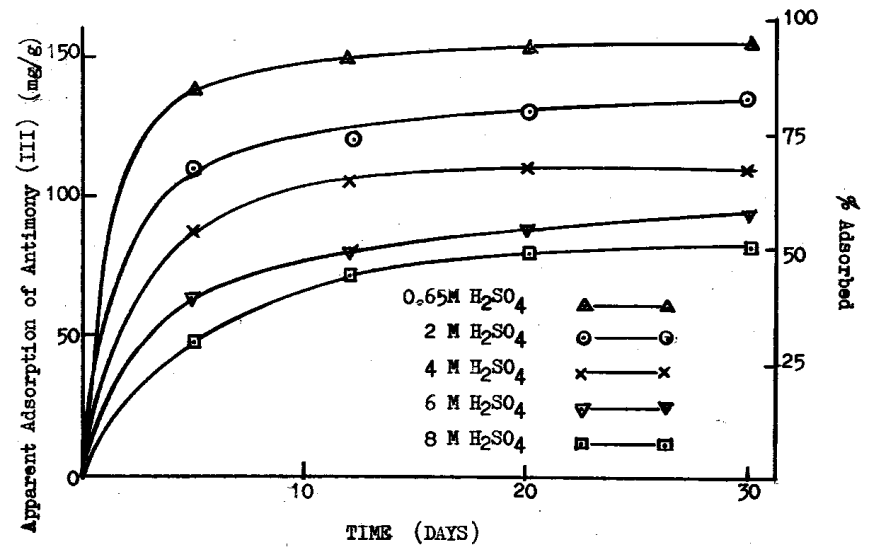


Fig 3.43 The Rate of Adsorption of Antimony (III) onto Lead Sulphate

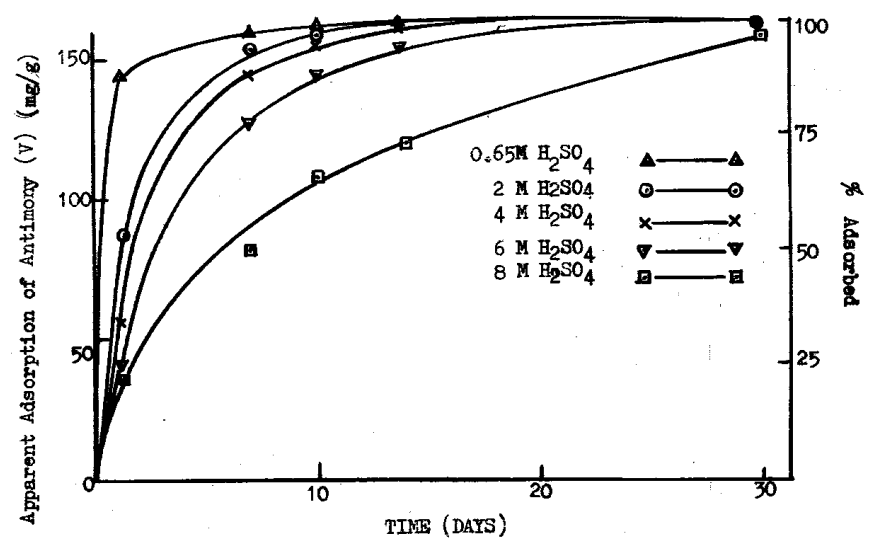


Fig 3.44 The Rate of Adsorption of Antimony (V) onto lead dioxide

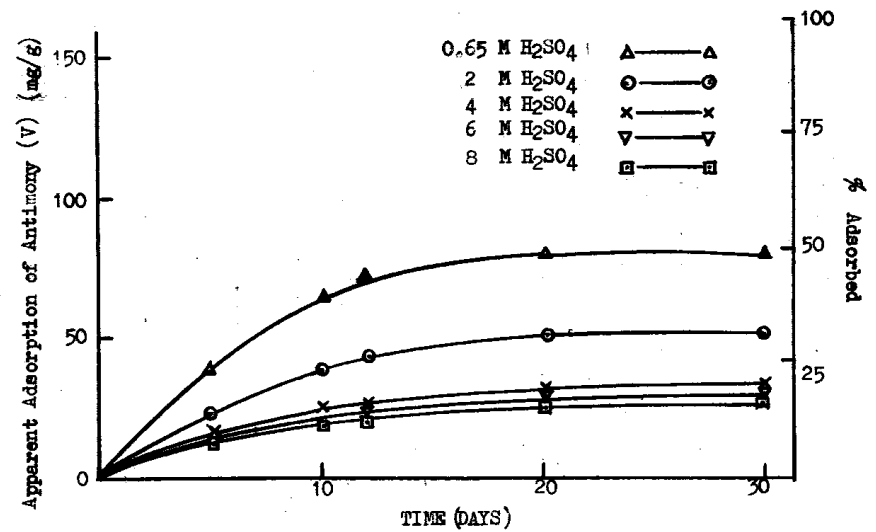


Fig 3.45 The Rate of Adsorption of Antimony (V) onto lead sulphate

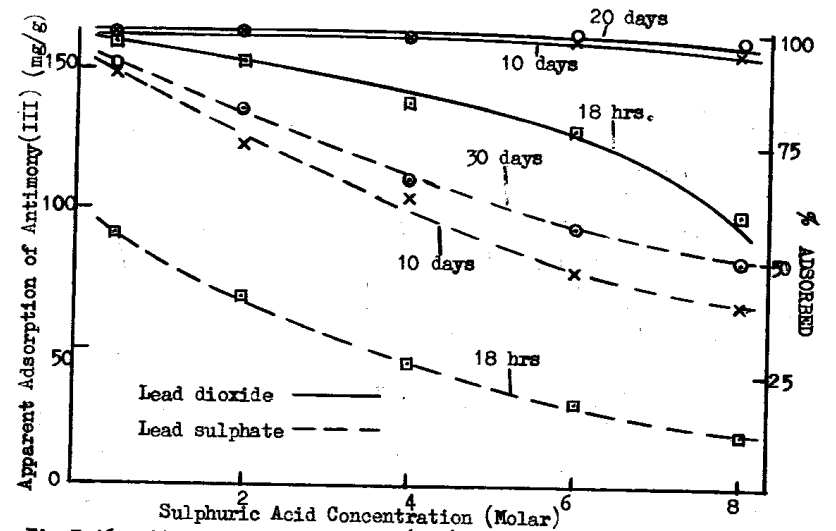


Fig 3.46. Adsorption of Antimony (III) onto Lead Dioxide and Lead Sulphate

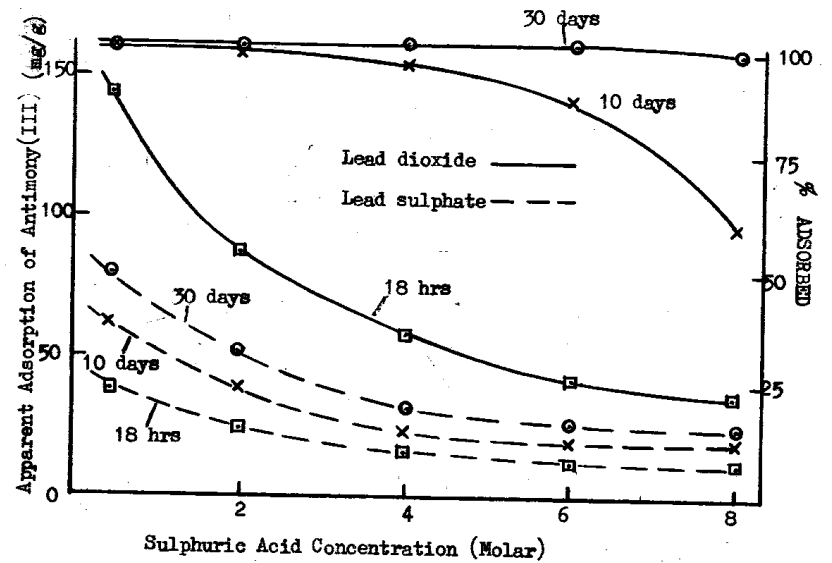


Fig 3.47. Adsorption of Antimony (V) onto Lead Dioxide and Lead Sulphate.

4. DISCUSSION

4.1 Antimony species in aqueous sulphuric acid.

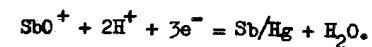
The methods adopted for the preparation of antimony solutions resulted in the formation of either antimony (III) or antimony (V) species in aqueous sulphuric acid.

4.1.1 Ionic migration.

Simple ionic migration experiments using antimony 124 showed that antimony (III) was composed of 70% anionic and 30% cationic species, whereas antimony (V) was 100% anionic species. As the majority of the current was carried by the sulphuric acid and since self diffusion of the antimony occurred, the error in these experiments has been estimated to be $\pm 10\%$.

4.1.2 Polarographic determinations.

Polarographic determinations using an Evershed polarograph showed that antimony (V) was not reduced at the dropping mercury electrode. The polarographic wave observed at -0.3 volts vs. S.C.E. is usually attributed⁽²⁰⁾ to the reduction of the antimony (III) ion at the electrode



The slow rise to the limiting current density of the second part of the polarographic wave, which has been suggested to be indicative of an irreversible reduction⁽²⁰⁾, could be due to a slow Sb (III) anion \rightleftharpoons Sb(III) cation exchange.

The above determinations were repeated using a cathode ray polarograph

before values of the electrochemical diffusion coefficients of antimony(III) were required for the deposition studies. It was considered that the values so obtained would be more representative of the deposition experiments since the cathode ray polarogram was obtained in only 2 sec as opposed to 40 sec using the Evershed polarograph, and would not measure any slow anion-cation exchange.

The values obtained for the electrochemical diffusion coefficients were similar to those of Jackson⁽²¹⁾ whose work was in the smaller sulphuric acid range of 3 to 6 M. Except for a slight deviation at approximately 7M a linear relationship of diffusion coefficient against the reciprocal of the dynamic viscosity was obtained for the sulphuric acid range 2 to 12 M. Below 1.5 M sulphuric acid two antimony cationic species appear to be reduced at the dropping mercury electrode and also the 'Stokes' radius of the ion increased, probably due to the presence of a hydrated species in the diluted sulphuric acid solutions. The deviation from linearity of Fig (3.6) at about 7 M sulphuric acid concentration was probably due to a complexing of an antimony species with the sulphate ions, since the sulphate ion concentration reaches a maximum concentration of \approx 1.0 M at the sulphuric acid concentration of 7 M⁽²⁸⁾; see also the appendix for further details. The influence of the sulphate ion concentration on the antimony (III) species in the region 5 to 9M sulphuric acid was also shown in the ultra violet spectra results and in ion exchange

experiments by Rothwell⁽²⁴⁾.

4.1.3 Ultra-violet Spectrophotometry of Antimony Solutions

(a) Antimony (III) Solutions

In aqueous sulphuric acid, the antimony (III) species gave rise to two absorption bands in the wave-length range 180-250 m μ , Fig. (3.7). As the sulphuric acid concentration increased, the maximum of the larger absorption band was displaced towards the shorter wavelength whereas the position of the second, smaller, absorption band remained constant at 208m μ . The position of the first maximum was also affected, to a slight extent, by the concentration of antimony, being displaced to longer wavelengths with increasing antimony concentration, Fig. (3.8). This shift of the larger absorption band was also observed in the spectra of antimony (III) in perchloric acid solutions. The dependence of the position of the first absorption band on the sulphuric acid concentration was shown in Fig. (3.9), and may be expressed approximately by the empirical equation

$$\lambda_{\max} = 200.5 - 0.88 [M H_2SO_4] \text{ m}\mu$$

over the range 1-10M sulphuric acid.

Beer's Law was obeyed for antimony (III) concentrations up to 1×10^{-4} M in 0.24 to 18M sulphuric acid and in 1.0 to 4M perchloric acid. This was shown, for example, in Figs. (3.10) (3.14) where the optical density at 208 m μ , and λ_{\max} was plotted against the antimony (III) concentration. The molar extinction coefficients ($\bar{\epsilon}$) calculated for λ_{\max}

190, 195, 200 and 205 m μ were for the range of antimony concentrations obeyed by Beer's Law. The dependence of $\bar{\epsilon}$ on the sulphuric acid concentration indicated that a chemical exchange occurred between the antimony (III) species and the acid solvent. Similar spectral changes have been observed in other systems e.g. antimony in hydrochloric acid solutions⁽²²⁾ and cerium (IV) in sulphuric acid solutions⁽²³⁾. The deviation of the antimony (III) spectrum from the Beer-Lambert Law at antimony concentrations greater than 1×10^{-4} M Sb (III), Fig. (3.10), showed that some form of dimerisation or polymerisation of the antimony (III) occurred at higher antimony concentrations. This dimerisation was later confirmed by ion exchange measurements using zirconium phosphate in 0.5 to 2M sulphuric acid⁽²⁴⁾.

Spectra obtained within a few hours of the dilution of a standard antimony (III) in concentrated sulphuric acid solution differed from the normal antimony (III) spectra, Fig. (3.11), showing that slow hydrolysis of the antimony occurred on dilution.

4.1.4 Solvent Extraction

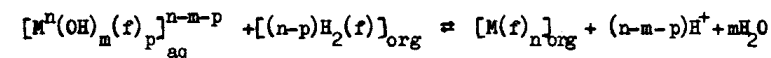
A determination of the number of sulphate ligands attached to the antimony ion was attempted by a solvent extraction technique using 1-(2-Thenoyl)-3,3,3-trifluoroacetone, (T.T.A.) in benzene and aqueous radioactive antimony (III) - perchloric acid solutions, perchloric-sulphate solutions and sulphuric acid solutions. Unfortunately the results were far from conclusive and the only useful solvent extraction results were obtained

by extracting antimony (III) with 9-methyl-2,3,7 trihydroxy-6-fluorone into benzoyl alcohol from aqueous perchloric acid solutions.

The distribution coefficient of the antimony (III), K_d, was obtained directly from the radio activity measurements and is given by

$$K_d = \frac{\text{Antimony (III) concentration in the organic phase}}{\text{Antimony (III) concentration in the aqueous phase}}$$

The equilibrium condition for extraction of a metal ion, M, with fluorone is given by



where (f) = 9-methyl-2,3,7 trihydroxy 6 - fluorone

Then

$$\log K_d = \log K_{ex} + (n-p)\log[H_2(f)] - (n-m-p)\log[H^+]$$

where K_{ex} = the equilibrium constant for the above reaction.

The plot for the antimony (III) solutions of log K_d against log [H⁺] at a constant concentration, 2.5 x 10⁻⁴M, of fluorone gave two straight lines, below the acid concentration of 1M the slope was minus three and above 1M perchloric acid concentration the slope was minus one. These slopes are equal to -(n-m-p) where m and p are the number of hydroxyl groups and fluorone molecules attached to the antimony (III) in aqueous solution. The plot of log K_d against log [fluorone] in 1M perchloric acid solution had a slope of one, thus n-p = 1.

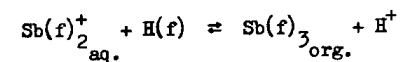
There is also the possibility that the antimony (III) ion could

contain an oxygen atom, $Sb = 0$, thus n could be either +3 or +1. Therefore p could be 2, or 0.

Above 1M perchloric concentration for $n-m-p = 1$ and $n-p = 1$

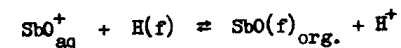
(i) For $n = 3$, $p = 2$. $m = 0$

Extraction equilibrium is

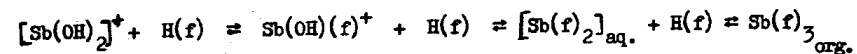


(ii) For $n = 1$ and $n-p = 1$

Extraction equilibrium is



Below 1M perchloric acid concentration the extraction interpretation is complicated since the fluorone-antimony stability constant appears to be stronger than the antimony-hydroxyl stability constant and the following sequence appears to occur



The solvent extraction results from aqueous perchloric acid solutions indicated the presence of $[Sb(OH)_2]^+$ in dilute perchloric solutions, less than 1M, and SbO^+ above 1M perchloric concentration.

Absorption bands in the infra-red region of the spectrum would have given information relating to the antimony-sulphate bonds but the sulphuric acid present in the samples gave strong absorption bands which masked the antimony spectra. Recent ion exchange studies of antimony (III) in 0.4 to 3M sulphuric acid⁽²⁴⁾ have established the presence of a monovalent cation in this acid range but the scatter of results above 1M sulphuric indicated the formation of other antimony species.

Interpretation of the results

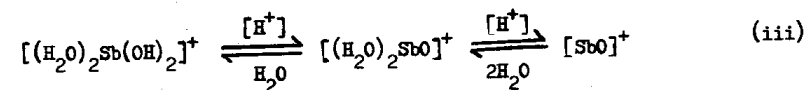
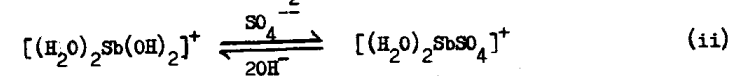
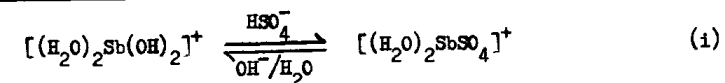
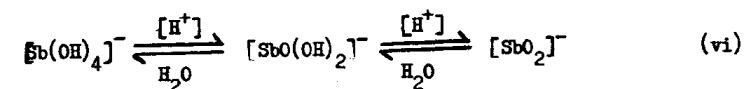
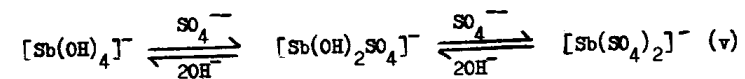
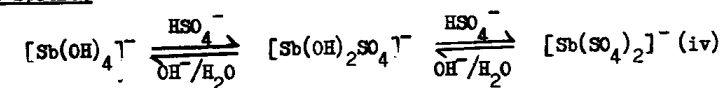
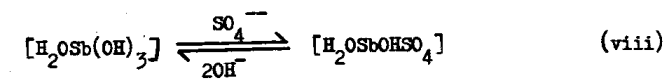
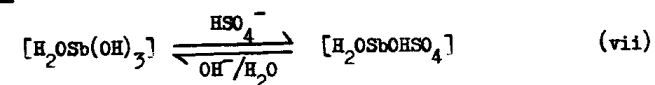
From the results obtained, only probable structures for the antimony (III) species can be suggested since, in aqueous sulphuric acid solutions, numerous combinations of complexing of antimony, water, hydroxyl and sulphate ions are possible. For example, antimony and water could form a unidentate ligand $\text{Sb} - \text{O} \begin{matrix} \text{H} \\ \diagup \\ \text{H} \end{matrix}$.

The sulphate ion could be complexed in three ways; as a unidentate ligand $\text{Sb} - \text{O} \begin{matrix} \diagup \text{O} \\ \diagdown \text{O} \\ \diagup \text{O} \\ \diagdown \text{O} \end{matrix}$; as a bidentate ligand $\text{Sb} \begin{matrix} \diagup \text{O} \\ \diagdown \text{O} \end{matrix} \begin{matrix} \text{S} \\ \diagup \text{O} \\ \diagdown \text{O} \end{matrix}$; and as a

bridged bidentate ligand $\text{Sb} - \text{O} \begin{matrix} \diagup \text{O} \\ \diagdown \text{O} \end{matrix} - \text{Sb}$

other possible bridged structures are $\text{Sb}-\text{O}-\text{Sb}$, $\text{Sb}-\text{Sb}$ and $\text{Sb}-(\text{OH})-\text{Sb}$.

The values of the antimony (III) diffusion coefficients showed that in the sulphuric acid range 2 to 12 M there was one cationic species with a second more hydrated species below 1.5 M sulphuric acid. The solvent extraction of antimony (III) from perchloric acid solutions confirmed the presence of two cationic species. The results from the ionic migration experiments, ultra-violet spectra, and the adsorption from solution onto lead dioxide and lead sulphate indicated the presence of antimony (III) anionic species. Assuming that antimony (III) has a coordination number of four and the sulphate is present as a bidentate ligand, the following simple species may be considered:-

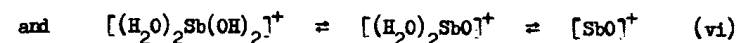
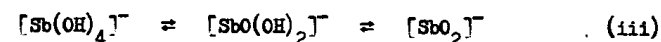
Cationic SpeciesAnionic SpeciesNeutral Species

From spectrophotometric determinations (26) it was found that OH^- ions give an absorption band at 200 to 220 μ whilst the absorption band of SO_4^{--} ions occurs at 190 to 208 μ . In sulphuric acid, the maximum SO_4^{--} concentration of 1.6M occurs at 7M H_2SO_4 and decreases to zero at 12M H_2SO_4 whereas the HSO_4^- ions concentration reaches a maximum of 11.8M at 14M H_2SO_4 and decreases to zero at 18M H_2SO_4 (27)(28).

The polarographic results indicated that only one antimony (III) cation exists in 2-12M sulphuric acid. This ion was unaffected by the change in HSO_4^- concentration since the diffusion coefficients depended only on the viscosity of the solution and this cation is probably therefore the antimonyl ion, SbO^+ . In sulphuric acid of less than 1.5M concentration, a second antimony cation is present and can be ascribed to the hydrated ion $[(\text{H}_2\text{O})_2\text{Sb}(\text{OH})_2]^+$. Absorption spectra of antimony (III) showed that an exchange occurred between some antimony species and the SO_4^{--} and HSO_4^- ions and it is probable that the antimony (III) anion was involved in this reaction. Since the first absorption band was influenced to a greater extent by the change in sulphuric acid concentration a first approximation was to assume that the anion spectra contributes more to this band than to the second absorption band at 208 μ .

The simplest explanation of the first absorption band shift with the increase in sulphuric acid concentration would be either equilibrium

(iv) or (v) :- $[\text{Sb}(\text{OH})_2\text{SO}_4]^- \rightleftharpoons [\text{Sb}(\text{SO}_4)_2]^-$. It was then difficult to explain (a) the increase in the molar extinction coefficient at 6-8 M H_2SO_4 , and (b) the band shift in perchloric acid. The band shift in both 0.24 to 1M sulphuric and 0.5 to 4M perchloric acid solutions and the decrease in the molar extinction coefficients in these acid ranges were therefore ascribed in part to the exchange reactions (iii) and (vi):-



Pitman et al⁽¹⁴⁾ consider that the ion $[\text{Sb}(\text{OH})_4]^-$ is only formed in alkali solutions, in which case the first part of exchange (iii) could be unlikely.

In sulphuric acid the molar extinction coefficients approach a maximum in the acid range 14 to 18 M; this maximum was considered as arising from the ion $[\text{Sb}(\text{SO}_4)_2]^-$. Using this hypothesis the results were treated by the method described by Bugaenko and Huang Kuan-lin⁽²³⁾ in their study of cerium (IV) solutions.

For convenience the antimony (III) sulphato complexes with one and two sulphate groups will be referred to as I and II respectively and the antimony ions with no sulphate as, O.

The equilibrium constant for reaction (iv) will be given by

$$K_{I/II} = \frac{[III]}{[I][HSO_4^-]} \quad (1)$$

Assuming that the absorption of the different complexes was additive, the dependence of the apparent molar extinction coefficient, $\bar{\epsilon}$, on the bisulphate concentration is given by,

$$\bar{\epsilon} = \frac{\epsilon_I + \epsilon_{II} K_{I/II} [HSO_4^-]}{1 + K_{I/II} [HSO_4^-]} \quad (2)$$

where ϵ_I and ϵ_{II} are the molar extinction coefficients of the sulphato complexes I and II.

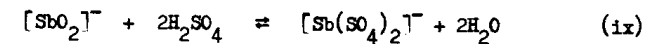
Since the analytical solution of this equation was impossible from the available data a value was assigned to ϵ_{II} which approximated to the maximum value of $\bar{\epsilon}$ in the sulphuric acid range 10 to 18M.

The following equation was obtained from (2)

$$\bar{\epsilon} = (\epsilon_{II} - \bar{\epsilon}) [HSO_4^-] K_{I/II} + \epsilon_I \quad (3)$$

Using the values of the bisulphate ion concentration obtained by Zarakhani and Vinnik⁽²⁸⁾ attempts to solve equation (3) graphically proved unsuccessful.

The calculation was then repeated using the equilibrium



and the equation

$$\bar{\epsilon} = (e_{\text{II}} - \bar{\epsilon})[\text{H}_2\text{SO}_4]_0^2 K_{\text{O/II}} + e_0$$

was solved graphically, Fig. (4.1), for the sulphuric acid range 10 to 18M and the molar extinction coefficients obtained at 190, 195, 200, 205 and 210 μ .

Table 28

M H_2SO_4	$\bar{\epsilon}$	$(e_{\text{II}} - \bar{\epsilon})$	Undiss. H_2SO_4 M ⁽²⁸⁾	$(e_{\text{II}} - \bar{\epsilon})[\text{H}_2\text{SO}_4]^2$
18	9900	60	14	11,740
16	9710	250	6.3	9,910
14	9050	910	3.2	9,310
12	7800	2160	1.8	7,000
10	6300	3660	1.1	4,430
$\bar{\epsilon}$ at 190 μ ; Assumed $e_{\text{II}} = 9960$; From Fig. (4.1) $K_{\text{O/II}} = 0.56$ moles.litre ⁻¹				
18	8050	75	14	14,680
16	7850	275	6.3	10,900
14	7500	625	3.2	6,400
12	7150	975	1.8	3,160
10	6700	1425	1.1	1,724
$\bar{\epsilon}$ at 195 μ ; Assumed $e_{\text{II}} = 8125$; From Fig. (4.1) $K_{\text{O/II}} = 0.08$ moles.litre ⁻¹				
18	5300	100	14	19,600
16	4950	450	6.3	17,860
14	4400	1000	3.2	10,240
12	3700	1700	1.8	5,500
10	3300	2100	1.1	2,540
$\bar{\epsilon}$ at 200 μ ; Assumed $e_{\text{II}} = 5400$; From Fig. (4.1) $K_{\text{O/II}} = 0.12$ moles.litre ⁻¹				

Table 28 (Contd)

M.H ₂ SO ₄	$\bar{\epsilon}$	$(\epsilon_{II} - \bar{\epsilon})$	Undiss.H ₂ SO ₄ M	$(\epsilon_{II} - \bar{\epsilon}) \times$ $[\text{H}_2\text{SO}_4]^2$
18	4600	100	14	19,600
16	4300	400	6.3	15,880
14	3700	1000	3.2	10,240
12	3100	1600	1.8	5,180
10	2900	1800	1.1	2,170
$\bar{\epsilon}$ at 205 μ ; assumed $\epsilon_{II} = 4700$; From Fig.(4.1) $K_0/II = 0.093$ mole litre ⁻¹				
18	4900	100	14	19,600
16	4450	450	6.3	17,900
14	4000	1000	3.2	10,240
12	3400	1600	1.8	5,180
10	3100	1900	1.1	2,300
$\bar{\epsilon}$ at 210 μ ; assumed $\epsilon_{II} = 5000$; From Fig.(4.1) $K_0/II = 0.098$ moles litre ⁻¹				

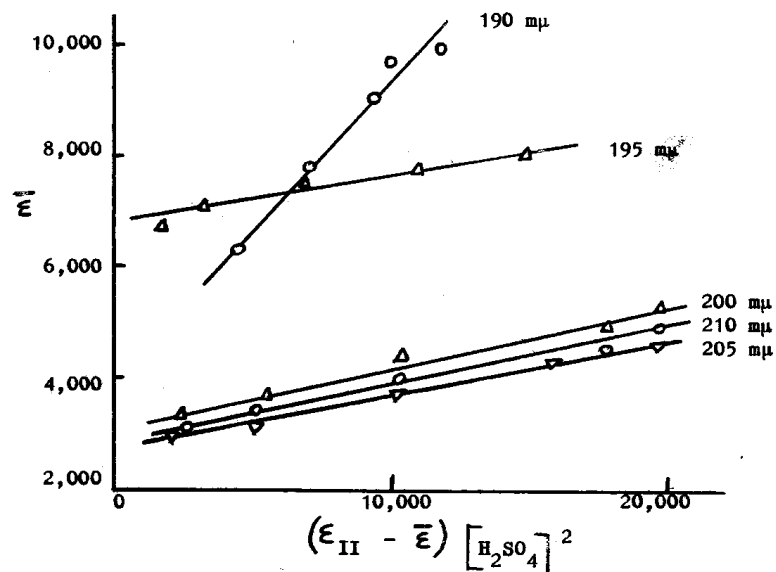


Fig. 4.1. The Molar Extinction coefficient of antimony (III) as a function of the undissociated sulphuric acid concentration.

The calculation of $K_{o/II}$ could not be continued into the sulphuric acid range less than 10M because of the increase of the sulphate ion concentration resulting in the increase of the antimony (III) molar extinction coefficient.

In 6M sulphuric acid the amount of undissociated sulphuric is less than 5% of the total sulphate species and it was therefore assumed that the antimony sulphato complex formed in 1 to 6M sulphuric acid will be the result of complexing of the antimony (III) with the sulphate ions. Assuming the equilibrium constant of equation (v) is given by

$$K_{o/II} = \frac{[I]}{[O][SO_4^{--}]} \quad (5)$$

$$\text{then } \bar{\epsilon} = (\epsilon_I - \bar{\epsilon}) [SO_4^{--}] K_{o/I} + \epsilon_o \quad (6)$$

This equation was solved graphically; however only the values obtained for 195 m μ and the acid range 1 to 4M sulphuric gave a linear relationship, Fig. (4.2), from which a value of $K_{o/I} = 2 \text{ moles.litre}^{-1}$ was obtained. As the concentration of the sulphate ions is small the relative error in its determination from the Raman spectra⁽²⁸⁾ was high, also there are at least four different antimony species in the sulphuric acid range 1 to 6M, these two factors would account for the difficulty in the above interpretation of the antimony spectra.

The exchange reactions involving antimony (III) may now be summarised as:-

Table 29.

M H ₂ SO ₄	$\bar{\epsilon}_{195}$	$(\epsilon_I - \bar{\epsilon}_{195})$	M:SO ₄ ⁻	$(\epsilon_I - \bar{\epsilon}_{195}) \times [\text{SO}_4^-]$
1	1300	6700	0.10	670
2	2250	5750	0.18	1030
3	3000	5000	0.30	1500
4	3700	4300	0.43	1846
5	5200	2800	0.58	1624
6	6900	1100	0.775	852

Assumed $\epsilon_I = 8,000$; From Fig. (4.2) $K = 2$ moles litre⁻¹

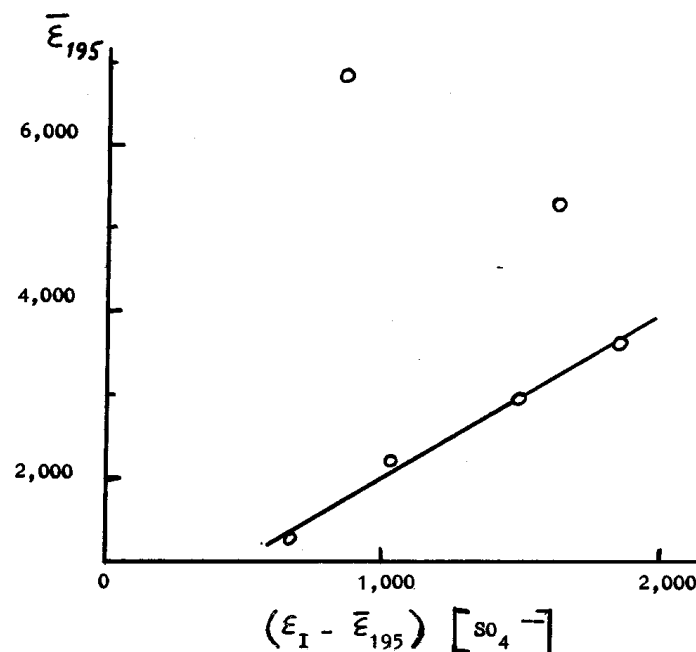
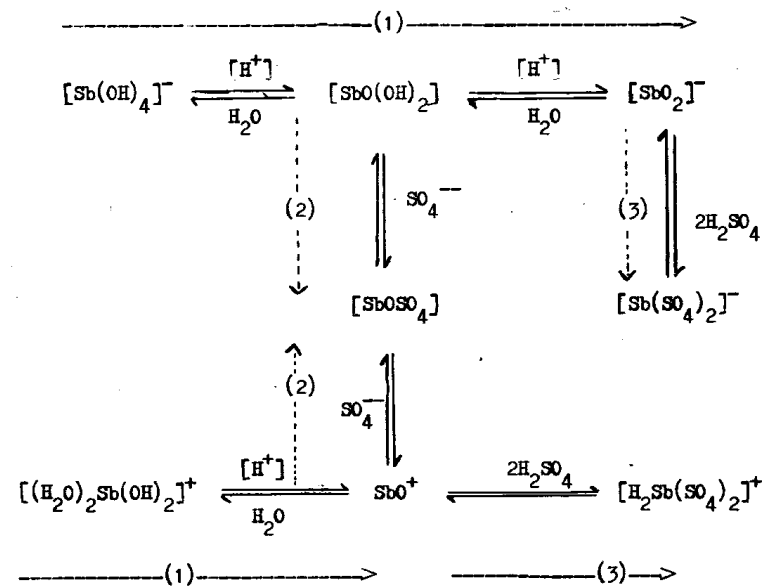


Fig. 4.2. The molar extinction coefficient of antimony (III) as a function of the sulphate ion concentration.



Reaction route (1) is due to the increase of the acidity of the solutions and its effect is observed in (a) the polarograms in less than 2M sulphuric acid, (b) the solvent extraction results and (c) the change of λ_{max} and $\bar{\epsilon}$ in 0.2 to 1M sulphuric acid and 0.5 to 4M perchloric acid. In sulphuric acid the influence of the sulphate ions is superimposed onto (1) to give the sulphato complexed anion $[\text{SbOSO}_4]^-$, reactions (2). The influence of this ion was seen in both the polarographic determination of the diffusion coefficient and in the spectra in 4 to 8M sulphuric acid. The hypothesis of these ions has recently been substantiated by the

X-ray diffraction and microphotographic identification of the antimony sulphates $\text{Sb}_2\text{O}_3 [(\text{SbO})_2\text{SO}_4]$, $\text{Sb}_2\text{O}_3 [(\text{SbO})_2\text{SO}_4]_2$ and $[(\text{SbO})_2\text{SO}_4]_6$ which were formed in 3.5 to 6M sulphuric acid⁽⁴⁴⁾. At the higher sulphuric acid concentrations, 14M to 18M, the antimony complexes with the undissociated sulphuric acid to give the sulphato complexes $[\text{Sb}(\text{SO}_4)_2]^-$ and $[\text{H}_2\text{Sb}(\text{SO}_4)_2]^+$. The proportions of each of the antimony species is shown in Fig. (4.3); however this diagram is only intended to clarify the above discussion and caution must be exercised in its use.

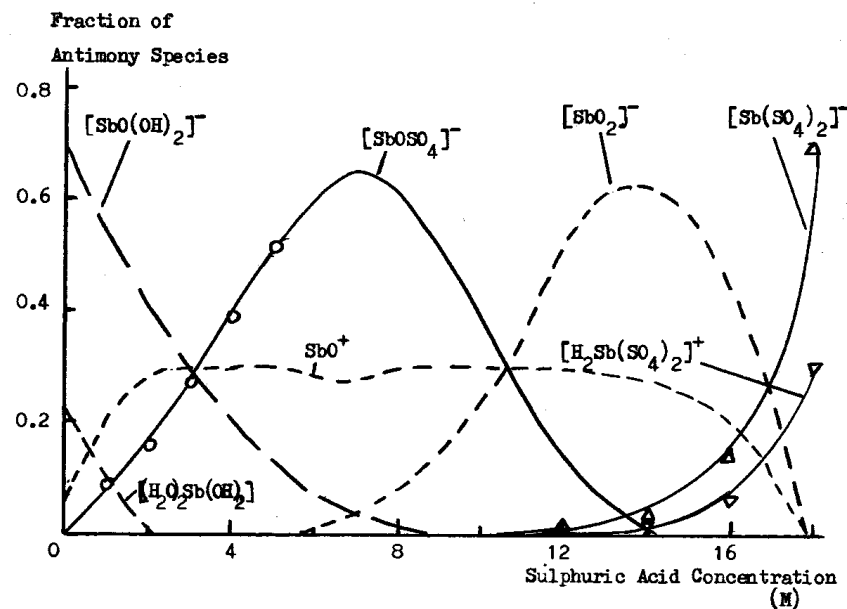


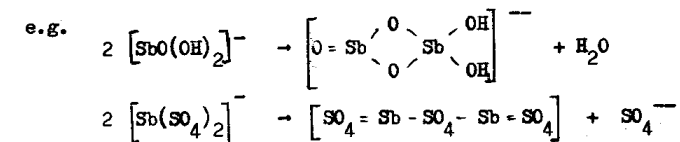
Fig. 4.3 Proportion of Antimony (III) Species in Sulphuric Acid

Dimerisation of Antimony (III)

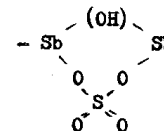
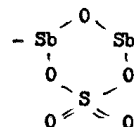
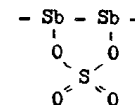
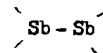
The aggregation of cations normally occurs by the formation of either hydroxo bridges $M \begin{matrix} (OH) \\ \diagdown \\ \diagup \\ (OH) \end{matrix} M$ or an oxo bridge $M \begin{matrix} O \\ \diagdown \\ \diagup \\ O \end{matrix} M$

as a result of an increase of the pH of the solution or an increase in the concentration of the metal ions. Oxolation or the elimination of a molecule of water from two adjacent hydroxo bridges usually leads to the irreversible formation of $M - O - M$.

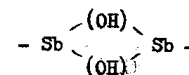
Beer's Law was not obeyed at antimony (III) concentrations greater than 1×10^{-4} molar and showed that some form of aggregation of the ions occurred at these higher antimony concentrations resulting in the formation of at least an antimony (III) dimer. In dilute sulphuric acid and perchloric acid the dimerisation probably involved a di-hydroxo or oxo bridge since antimony trioxide is precipitated from aqueous solutions. Antimony trisulphate is precipitated from concentrated sulphuric acid, therefore as the sulphuric acid concentration increased the mechanism probably involved a bridged bidentate sulphate ligand.



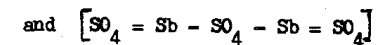
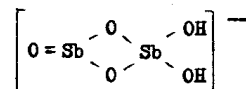
Other possible mechanisms could involve the following structures



and the five or six membered ring structures should have less ring strain than, for example, the dihydroxo bridge,

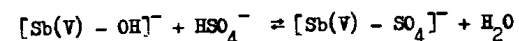


Recent X-ray work on the bismuthyl ion⁽²⁵⁾ has shown its structure to consist of six bismuth atoms each at the corners of an octahedron which are linked together by a hydroxo bridge on each of the twelve edges, to give the ion $[\text{Bi}_6(\text{OH})_{12}]^{6+}$. Thus some of the dimerised antimony (III) species studied in the present work could have a more complicated structure than,



(b) Antimony (V) solutions

The ultra-violet spectrum of antimony (V) species in sulphuric acid had only one absorption band, Fig. (3.16) and the position of this peak was unaffected by the change in the sulphuric acid concentration. The Beer-Lambert plot of antimony (V) concentration, from 0 to 15×10^{-4} Molar, against optical density gave a straight line graph over the acid range 0.5 to 12 Molar, Fig. (3.17). The antimony (V) species did not give as strong a spectra as the antimony (III), Fig. (3.19), indicating that the antimony (V) is probably either polymerised to a greater extent or contains fewer hydroxyl and sulphate groups than the corresponding antimony (III) species. The spectra of the antimony (V) species was not influenced by a change of sulphuric acid concentration over the range 1 to 8 Molar, again suggesting a stable configuration. It is only in almost concentrated sulphuric acid that an exchange with the sulphuric acid occurs probably involving either a dehydration type of reaction



or the addition of undissociated sulphuric acid. Antimony (V) was not reduced at the dropping mercury electrode and was not deposited onto a lead electrode. The ionic migration experiments showed the predominance of the antimony (V) anion.

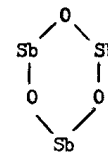
In hydrochloric acid solutions, tracer studies have shown the

existence of a dynamic equilibrium antimony (III) and antimony (V) ions⁽²⁹⁾ involving the ions $[\text{SbCl}_4]^-$ and $[\text{SbCl}_6]^-$. In sulphuric acid the lack of an electron exchange was ascribed to the antimony sulphate-complexes formed⁽³⁰⁾, but due to the lack of experimental evidence it was not possible to elucidate the structure of the antimony species. The formation of a stable complex ion with the antimony held in a double bridge would restrict the electron exchange and from the present experimental work it is probable that the antimony (V) has this type of structure.

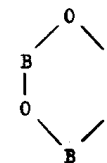
In the solid state there is no evidence⁽¹²⁾ of the finite oxyions SbO_4^{3-} , SbO_3^- and $\text{Sb}_2\text{O}_7^{4-}$. Compounds formerly described as ortho, meta and pyro antimonates all contain antimony (V) coordinated by oxygen either as $[\text{Sb}(\text{OH})_6]^-$ ions in the antimonates, e.g. $\text{K Sb}(\text{OH})_6$, or as antimony-oxygen groups in the complex oxides, e.g. KSbO_3 , PbSb_2O_6 and $\text{Pb}_2\text{Sb}_2\text{O}_7$. Thermodynamic evidence⁽¹⁴⁾ indicates that $[\text{Sb}(\text{OH})_6]^-$ is found in weakly acidic, less than pH 7, or in alkali solutions.

In the present work, over the sulphuric acid range 0.5 to 12 Molar, the antimony (V) anion may be satisfactorily formulated as a derivative of a six membered ring, since antimony has a similar electronegativity as boron; on the Pauling scale $B = 2.0$, $\text{Sb} = 1.8$

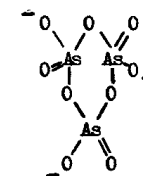
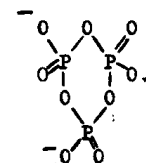
i.e.



c.f.



The antimony (V) anion would have an analogous structure as the cyclic tri-meta phosphates and arsenates, $[P_3O_9]^{3-}$, $[As_3O_9]^{3-}$, reported by Thilo⁽⁴⁵⁾.



The values of the molar extinction coefficient indicate that the ion is stable in 0.5 to 8M sulphuric acid and increasing the sulphuric acid concentration results in the addition of undissociated sulphuric acid.

In fuming sulphuric acid antimony (V) species containing SO_3 must exist since the spectra of these solutions were completely different from those in aqueous solutions, Figs. (3.20) to (3.23).

Further interpretation of the results to completely elucidate the structure of the antimony (V) anion was not possible with the available information.

4.2 The Deposition of Antimony from Aqueous Sulphuric Acid into
Pure Lead Electrodes

4.2.1 The experimental technique

A preliminary investigation⁽¹⁷⁾ had shown that the quantity of antimony deposited on to a small experimental lead electrode was negligible compared with the bulk concentration on the electrolyte and the rate of deposition depended largely on the pre-treatment of the electrode. This preliminary investigation also showed that erroneous electrochemical and deposition results were obtained if the electrode was removed from the solution for counting of the deposited radio-active antimony. The present continuous monitoring system, which counted the radio-activity from the deposited antimony and measured the electrode potential, required considerable development.

Antimony 124 is a strong beta and gamma emitter, but the detection of the beta radiation was considered more feasible since it was difficult to eliminate the gamma radiation originating in the bulk of the sulphuric acid solution. A Geiger-Muller tube was initially used as the beta detector but it was found unsuitable because of the high count rate resulting from the penetrating gamma radiation. The detector assembly was therefore changed to the 'Nuclear Enterprises' beta sensitive plastic phosphor which had the

further advantage of its small size, enabling it to be easily incorporated into the deposition cell. In preliminary experiments, using the beta detector, the counting equipment consisted of an 'E.C.K.O.' N559D cathode follower, an 'E.C.K.O.' N600A amplifier pulse height analyser and rate meter. The count rate then was recorded on a 'Honeywell Brown' chart recorder. This equipment was found to be limited in its use due to a lack of sensitivity in the interpretation of the recorded graph and the majority of the results reported were obtained on the 'Nuclear Enterprises' counting equipment and print-out unit. No correction was made for lost counts since the resolution time of the scaler and detection unit was less than 3μ sec and the maximum count rate was 20,000 counts per minute.

The design of the deposition cell and the lead electrode was determined from a consideration of (a) the counting and electrochemical requirements and (b) the ease of pre-treatment of the lead electrode. The detection efficiency (D) of radio-active counting is given by $D = f_e f_g f_b f_s f_a$, where f_e = efficiency of the counter, f_g = geometry of the system; f_b = back-scatter of the sample; f_s = self adsorption of the sample, and f_a = adsorption in the material between the sample and the detector. The beta detector was approximately 95% efficient and was the same diameter

as the lead electrode. The lead electrode was positioned about 0.5 cm from the detector and this was the smallest practicable distance possible. This arrangement reduced the adsorption of the beta radiation to a minimum and also limited the background count from the intervening radio-active solution. The self absorption of the sample was considered negligible since only a thin film of antimony was deposited. The detector was shielded from the radiation originating in the bulk of the solution by the lead electrode and the electrode also provided a good back-scatter for the deposited radio-active antimony.

The electrode design provided for ease of pre-treatment and also ensured that only one face was presented to the electrolyte. The final electrochemical pre-treatment of the lead electrodes at an anodisation current density of 25 mA/cm^2 for half-an-hour was an optimisation between (a) an electrode surface having a suitable roughness factor to give a measurable rate of antimony deposition and (b) a lack of reproducibility of the results. Anodisation at low current densities, 0.25 to 10 mA/cm^2 , gave a highly reproducible rate of antimony deposition but these deposition rates were small and the self discharge reaction quickly converted the lead to lead sulphate. Anodisation at a higher current density, 50 - 150 mA/cm^2 resulted in an increase

in the rate of antimony deposition and allowed the self discharge reaction to continue well beyond 30 minutes. The latter pre-treatment gave increased deposition rates, which unfortunately were not reproducible; thus although the surface had a large roughness factor, the resulting surface area could not be controlled experimentally.

Corrections for a dilution effect of the antimony during an experimental run were not required since the apparatus contained approximately 200 ml of solution and the bulk antimony concentration was virtually unaltered. In nitrogen purged electrolyte no corrosion of the deposited antimony occurred when the electrode behaved as an antimony electrode and showed that the electrolyte was oxygen free, indicating that the nitrogen scrubbing train, sodium dithionite in sodium hydroxide solution, effectively removed any residual oxygen from the 'B.O.C. white spot' nitrogen.

4.2.2 The rate of antimony deposition

The rate of an electrochemical process on the surface of an electrode is determined by two factors; the rate at which the reactant comes into contact with the electrode; and the rate of the electrochemical reactions on the electrode. Since the rate of antimony (III) deposition was dependent on the solution characteristics the most important factor controlling the deposition was

either the antimony diffusion rate through the boundary layer next to the electrode or diffusion of lead ions from the electrode. Ionic mass-transfer equations for electrolytic processes under flowing electrolyte conditions have been given by Levich⁽³¹⁾ and Wranglen⁽³²⁾. These equations are similar to those used in heat-transfer processes and are based on the boundary-layer theory developed by Prandtl for hydrodynamical studies.

Wranglen derived a more exact equation, although in both cases the final expressions are basically the same. The equations given by Wranglen were derived for the flow along a plane plate and assume that no flow or diffusion occurs perpendicularly to the length direction of the cell. The following notations were used:-

x	= distance along electrode from the leading edge	cm
x_0	= length of inlet channel	cm
δ_d	= thickness of diffusion boundary layer	cm
δ_L	= thickness of laminar hydrodynamic boundary layer	cm
δ_t	= thickness of turbulent boundary layer	cm
δ_{LS}	= thickness of laminar sub layer	cm
v	= velocity in the x - direction	cm.s ⁻¹
V	= kinematic viscosity of electrolyte	cm ² .s ⁻¹

k = mass transfer constant cm s^{-1}
 D = diffusion coefficient $\text{cm}^2 \text{s}^{-1}$

In the present work, k can be determined from the radio active measurements and is given by

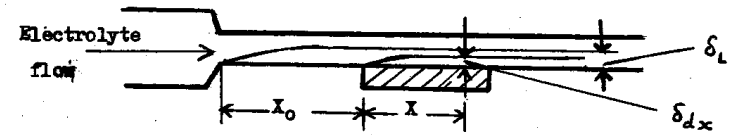
$$k = \frac{R}{A \cdot C}$$

R = rate of deposition moles sec^{-1}

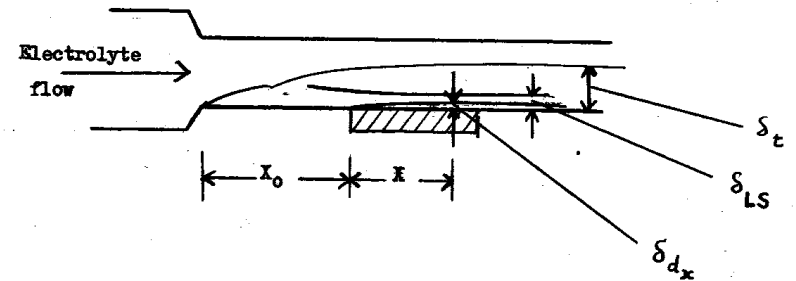
A = area of the electrode cm^2

C = concentration of the reactants in the boundary layer moles cm^{-3}

Diagrammatically the laminar boundary layers can be shown as:-



and for the turbulent boundary layer as:-



The number of variables encountered in diffusion-forced convection controlled electrochemical processes are often large and are better expressed as dimensionless groups or numbers.

These dimensionless groups involve multiplications and divisions of the original variables and there is considerable advantage in expressing the results in the fewer dimensionless numbers. The dimensionless groups of interest are:

The Nusselt number: $Nu_x = \frac{k x}{D}$

The Reynolds number: $Re_x = \frac{v x}{\nu}$

The Schmidt number: $Sc = \frac{\nu}{D}$

The Nusselt number, sometimes called the Sherwood number, relates the kinetic mass-transfer constant to the thickness of the effective diffusion layer at the electrode. The Reynolds number relates the flow of the electrolyte at the electrode to the viscous forces, acting on it. The Schmidt number relates the physical-chemical properties determining (i) the momentum transfer due to the velocity gradient and its viscous effect and (ii) the diffusion mass transfer under a concentration gradient. The resulting mass transfer equations for a cathodic process under forced laminar and turbulent convection as given by Wranglen are:-

(a) Uniform potential (limiting current density)

$$(i) \text{Nu}_{x\text{lam.}} = 0.331 \text{Re}_x^{\frac{1}{2}} \text{Sc}^{\frac{1}{3}} \left[1 - \left(\frac{x_0}{x}\right)^{\frac{2}{3}} \right]^{-\frac{1}{3}}$$

$$(ii) \text{Nu}_{x\text{turb.}} = 0.143 \text{Re}_x^{\frac{1}{2}} \text{Sc}^{\frac{1}{3}} \left[1 - \left(\frac{x_0}{x}\right)^{0.9} \right]^{-\frac{1}{3}}$$

(b) Uniform current density (normal electrolysis)

$$(iii) \text{Nu}_{x\text{lam.}} = 0.417 \text{Re}_x^{\frac{1}{2}} \text{Sc}^{\frac{1}{3}} \left[1 - \left(\frac{x_0}{x}\right) \right]^{-\frac{1}{3}}$$

$$(iv) \text{Nu}_{x\text{turb.}} = 0.170 \text{Re}_x^{\frac{3}{4}} \text{Sc}^{\frac{1}{3}} \left[1 - \left(\frac{x_0}{x}\right) \right]^{-\frac{1}{3}}$$

Where Nu and Re are the local Nusselt and Reynolds numbers at the point x on the electrode respectively.

The above equations were calculated using a linear relationship between the concentration at the electrode, C_0 , and the concentration in the bulk of the electrolyte, C_b . Therefore, the average concentration in the boundary diffusion layer, C, is $\frac{1}{2}(C_b - C_0)$. The equation of interest in the present work is (i), which has been verified by Wranglen from electrochemical measurements on the electrodeposition of copper from flowing aqueous sulphuric acid solutions on to a horizontal cathode in a cell of rectangular cross-section and also by Bazan and Ariva⁽³³⁾ from electrochemical measurements on the electrodeposition of copper on to tubular stainless steel electrodes.

The limiting current density equation for the case in which the hydrodynamical boundary layer is formed simultaneously with the diffusion boundary layer is

$$Nu_x = 0.331 Re_x^{\frac{1}{2}} Sc^{\frac{1}{3}}$$

and when this equation is extended to the whole electrode area it becomes

$$Nu = 0.662 Re^{\frac{1}{2}} Sc^{\frac{1}{3}}$$

The parameters affecting the rate of antimony (III) from nitrogen saturated electrolyte were shown in Figs.(3.26) to (3.33), Section 3.2. Increasing the antimony (III) concentration resulted in a proportional increase in the antimony deposition rate, Figs. (3.30) and (3.31), whilst the deposition rate decreased with the increase in sulphuric acid concentration, Fig. (3.33). The effect of the flow rate was shown in Fig. (3.28) and in Fig. (3.29) where linear plot of the rate of antimony deposition against the square root of the flow rate was obtained. Thus Nu is proportional to $Re^{0.5}$. The log of the mass transfer constant, k, was plotted against $\log Sc$, Fig. (4.4), and the slope of 0.3 showed that Nu was proportional to $Sc^{0.3}$. Thus $Nu = k Re^{0.5} Sc^{0.33}$ as predicted by theory. The Nusselt and Reynold numbers were expressed in terms of the characteristic length, d_m , since it is easier to equate fluid flow in non-circular ducts to the better understood phenomena of flow in circular pipes by means of the hydraulic mean diameter, d_m , where

$$d_m = \frac{4 \times \text{cross sectional area}}{\text{Wetted perimeter}}$$

thus for the rectangular cross section 0.077cm x 2.5cm used, $d_m = 0.1494$ cm. This characteristic length, d_m , was considered to be more informative for electrochemical studies rather than using a value based on the electrode dimensions since from experimental results on the analogous heat transfer equations, the mass transfer equation should contain a term $(\frac{x}{d_m})^n$ which relates the electrode size (expressed as the length x) to the cell dimensions (expressed as d_m). The design of the deposition cell with its fixed electrolyte path and electrode size did not allow the value of the term $(\frac{x}{d_m})^n$ to vary and it was therefore not possible to allow for this "apparatus factor" in the mass transfer equation. The experimental results obtained, Tables 15 to 19, were expressed as Nu_{dm} against $Re_{dm}^{\frac{1}{2}} Sc^{\frac{1}{3}}$ in Fig. (4.5), the value of Nu used in this graph was 2 x the value of Nu in Tables 15 to 19, since k , the mass transfer constant, was originally determined from C_b instead of $\frac{1}{2}(C_b - C_0)$, the average concentration in the diffusion layer. The slope of the graph, Fig. (4.5), was 0.398. Using an effective length, $x = 1.77$ cm, obtained from assuming a rectangular electrode of area 4 cm^2 and having the same width as the diameter of the lead electrode, the slope of 0.398 Fig. (4.5) becomes

$$0.398 \frac{(x)^{\frac{1}{2}}}{(d_m)^{\frac{1}{2}}} = 1.09.$$

This value is 48% greater than 0.662 predicted by theory.

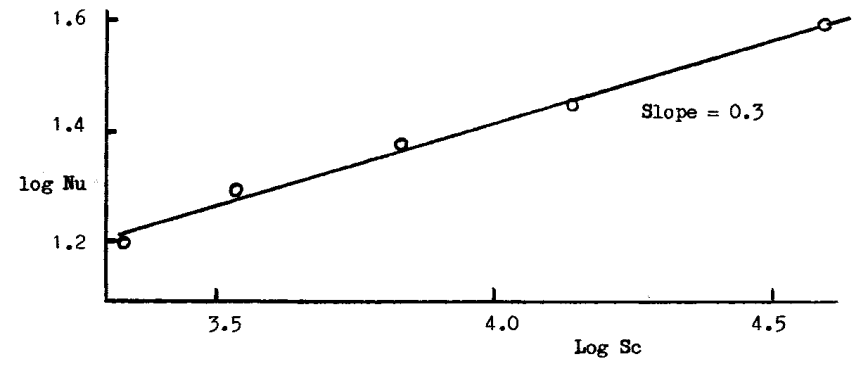


Fig. 4.4 Log-log Plot of Nu v.s. Sc for a Constant Re Number of 24

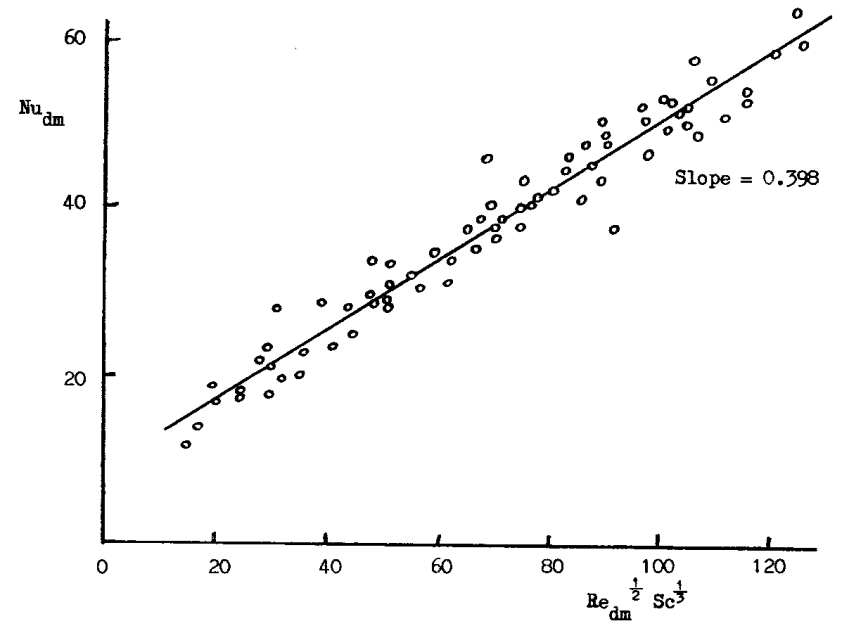


Fig. 4.5 The Rate of Antimony (III) Deposition Expressed as a Nusselt Number against the Reynold and Schmidt Numbers

The relevant velocity, however, is the maximum velocity at the electrode and Wranglen⁽³²⁾ has estimated that the maximum velocity will be about 1.1 times the mean velocity. The disturbances from opposite wall and sides of the cell should also increase the mass transfer process, as was found experimentally.

The spread of results, Fig 4.5, is suggested to be largely the result of the pretreatment of the lead electrode which was a compromise between reproducibility and a large surface area. The mechanical polishing tended to depress the lead at the edge of the electrode whilst the electrochemical pretreatment raised the overall surface from its original level. These two conflicting factors probably contributed the largest error to the results. One other source of error was the calibration procedure adopted for the determination of the amount of antimony on the electrode from the activity measurements although this was minimised by employing a number of determinations for each calibration graph. The combined experimental error, as shown by the results, has been estimated to be $\pm 10\%$.

The spread of results even from nitrogen saturated electrolyte accounted for the difficulty in the determination of the decreased rate of antimony deposition from electrolyte containing oxygen.

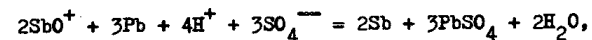
4.2.3 Electrochemical measurements.

Under open circuit conditions the potential of an electrode is controlled by the electrochemical reactions taking place at the electrode and electrolyte interface. Initially the potential of the lead electrode was -0.35V and was governed by the Nernst

Equation

$$E = E_0 - \frac{RT}{nF} \ln \frac{a(\text{PbSO}_4)}{a(\text{Pb}^{++}) a(\text{SO}_4^{--})}$$

'Self deposition' of antimony (III) occurred by an electrochemical displacement reaction; e.g:-



and the deposition continued until sufficient antimony had deposited for the electrode to assume a mixed potential of -0.32V.

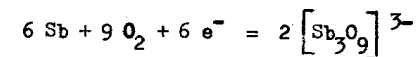
The electrode potential soon rose to about +0.2V indicative of an antimony electrode at which point the deposition ceased and the lead electrode was considered covered with antimony and lead sulphate, there being no lead available to lower the electrode potential.

In the absence of dissolved oxygen the potential of the 'antimony electrode' was +0.195V and there was no 'corrosion' of the antimony. With dissolved oxygen in the electrolyte the potential of the 'antimony electrode' was +0.210V and antimony corroded at an exponential rate from the surface of the electrode

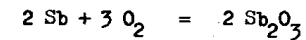
revealing some of the underlying lead. The potential started to fall until sufficient lead was exposed for the electrode to reach equilibrium with an intermediate potential of about +0.1V, a value between the antimony and the lead-lead sulphate electrode potential. During the 'corrosion' process the electrode potential remained at +0.210V and started to fall only when the last 5 to 10% of the 'corroding' antimony remained on the electrode surface, suggesting that the deposited antimony was present as multilayers rather than a monolayer, with the thicker layers of antimony corroding first.

Corrosion of the deposited antimony also occurred if the electrode was made of anodic, Fig. (3.39). Initially the electrode potential was indicative of an antimony electrode showing oxygen overvoltage, the corrosion continued until the majority of the deposited antimony had been removed and sufficient lead was exposed for the electrode to be converted into a lead-lead dioxide electrode exhibiting oxygen overpotential. The removal of the antimony in either the presence of dissolved oxygen or by anodic corrosion is suggested to depend on the presence of the oxygen at the electrode.

Anodic corrosion



Dissolved oxygen



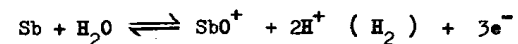
The Appendix contains the equations considered by Pitman, Pourbaix, and de Zoubov ⁽¹⁴⁾ in their study of the antimony system but some of the reactions have not fully elucidated and none of the work reported in the literature has been in the strong acid conditions used in the present work. The potential values obtained by Kolthoff and Hartong ⁽³⁴⁾ on an antimony rod electrode, in the absence of oxygen showed that it behaved approximately as a hydrogen electrode with a H_2-H^+ equilibrium under 0.01 to 1 atmosphere hydrogen pressure; this hydrogen was formed at the electrode surface by minute corrosion of the metal. Mechanical agitation of the solution altered the potential. This change of potential with solution movement has also been reported by Parks and Beard ⁽³⁵⁾ who observed that the electrode potential was displaced negatively by stirring and positively by bubbling oxygen through the solution, a process also observed by the present author ⁽¹⁷⁾.

The work of Tourky and Mousa ⁽³⁶⁾ indicated that oxygen in solution appeared to be an essential component of those antimony electrodes to which no oxide is added. Perley ⁽³⁷⁾ showed that solutions containing oxygen progressively etched antimony, but it is probable that in the conditions used, the antimony was converted to the trioxide.

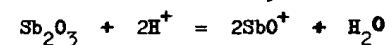
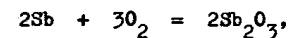
Since the antimony electrode corrodes in solutions containing dissolved oxygen, then oxygen must participate in the electrode reactions and Kan~~w~~and Knappsberg ⁽³⁸⁾ found that the antimony electrode responded to oxygen pressure, although slowly, in the manner of a reversible oxygen electrode.

Gatty and Spooner ⁽³⁹⁾ regarded the surface of the antimony electrode as two areas, the first, bare metal at which anodic dissolution of antimony takes place to give ions in solution and, the second metal covered with an oxide film where electrons can be passed to the oxygen molecules, giving a cathodic area whose potential is determined by the concentration of oxygen, close to the interface. The oxygen electrode reaction is strongly hindered and there is no question of these areas approaching the oxygen electrode potential. Tourky et al ⁽³⁶⁾ also considered the antimony electrode as a continuously corroding system but with the antimony trioxide impermeable to antimony ions, thereby restricting the oxide film growth. This, they suggested an 'overvoltage effect' which hindered the cathodic process. The oxygen, which would form the oxide, remained adsorbed on the oxide surface where it provides a population of 'oxygen doublets', the electrode may then be considered as a 'metal-metal oxide - oxygen' electrode.

In highly acidic solutions, which are oxygen free, the antimony electrode reaction will be



but this reaction is restricted and will cause the electrode to approximate to a hydrogen electrode with the $\text{H}_2\text{-H}^+$ equilibrium reported by Kolthoff and Hartong. Addition of oxygen to the system results in the formation of antimony trioxide, which is unstable in the acid conditions used, and dissolves to give a soluble antimony (III) species;



With a cathodic current flowing through the cell and in the absence of dissolved oxygen the rate of antimony deposition remained the same as it was under open current conditions. This deposition rate was also independent of the cathodic current density. The deposition rate due to the electrochemical displacement could, therefore, be compared to an electrochemical deposition at the limiting current density. There was no decrease in either the rate of antimony deposition or the amount of antimony present on the electrode even at high current densities, 100 mA/cm^2 , indicating that either stibine was not produced at the electrode, or the rate of stibine production was very small as to be undetected by the apparatus used. By means of a tracer technique Tomlinson (40) found that current densities of 4 to 5 A/cm^2 were required to form stibine in appreciable

quantities at lead electrodes in sulphuric acid solutions containing antimony. At these high current densities the rate of stibine formation was independent of the current density but was dependent on the total current flow through the cell, i.e., the total amount of hydrogen produced.

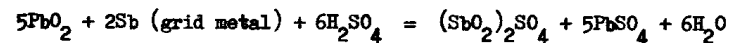
In the absence of dissolved oxygen the electrode behaved as a lead-lead sulphate electrode exhibiting increasing hydrogen overpotential as the amount of antimony on the surface increased, and a linear relationship of overpotential against the log of the current density, typical of a Tafel plot was obtained. In the presence of dissolved oxygen an abnormal Tafel plot below an overpotential of 0.15V to 0.20V was observed indicating that the dissolved oxygen was participating in the electrode reactions. The effect of the presence of dissolved oxygen on the rate of antimony deposited was not fully investigated because of the inherent experimental difficulties, but the observed rate of deposition was slightly less than the deposition from nitrogen saturated solutions, Fig. (3.40). Since the relative rates of deposition in oxygen free and oxygen saturated solutions are very similar it is suggested that the most feasible method of assessing the effect of oxygen would be to measure the rate of removal of antimony from a lead surface on which radio active antimony has previously been deposited.

4.3. Antimony Chemistry in the Lead-Acid Battery

The results obtained in section 3.3. are briefly discussed here and the inference from these simple experiments is used in section 4.4. to clarify the mechanisms which eventually result in 'antimony poisoning' of the negative plate.

4.3.1. The production of antimony species from antimonial lead alloy electrodes.

The results shown in Table 25 indicate that antimony (V) was formed by anodic corrosion of the positive electrode, whilst antimony (III) was produced at the negative electrode and the deposition studies showed that oxygen dissolved in the electrolyte could produce this antimony (III). The formation of stibine with a subsequent decomposition in the sulphuric acid probably occurs although the deposition results with a cathodic current indicated that the formation of stibine was of negligible importance under the experimental conditions used. The formation of antimony (V) at the anode is in agreement with the findings of Ruetshi and Angstadt⁽⁵⁾ in their investigation of the self discharge reaction of the positive plate by the suggested reaction



4.3.2. The reduction and oxidation of antimony in aqueous sulphuric acid

The results in Tables 26 and 27 indicate that antimony (III) could be oxidised to antimony (V) in the anode compartment of a lead acid battery

but it was difficult to reduce antimony (V) to antimony (III) electrolytically .

4.3.3. The adsorption of antimony from aqueous sulphuric acid onto lead dioxide and lead sulphate.

The deposition studies showed that antimony (V) was not deposited electrochemically onto a lead-lead dioxide electrode. The rates of adsorption of antimony onto lead dioxide and lead sulphate, Figs (3.42) to (3.47), indicated a slow chemisorption altering the surface of the solid, together with a physical adsorption on the altered surface. The process was apparently dependant on the nature of the ions being adsorbed since antimony (III) was adsorbed more readily than antimony (V).

4.3.2 Antimony in the lead-acid battery

The overall mechanism of 'antimony poisoning' was discussed briefly, 1.2, but it has never been considered in detail. If the results of previous antimony tracer studies on lead-acid batteries⁽¹⁰⁾⁽¹¹⁾ are used in conjunction with the present work a more comprehensive mechanism, involving the production, transference and deposition of antimony, can be presented.

A critical assessment of the only published data⁽¹⁰⁾ relating to the amount of antimony produced from positive and negative grids leads to the following conclusions. The majority, 90 to 95%, of the antimony released into the battery comes from the positive grid. Overcharging of a battery, resulting in anodic corrosion of the positive grids, causes a higher proportion of the total positive grid antimony to be found in the negative plate material, 26% after continuous overcharge as against 5% after cycling. Although the amount of antimony released from the negative grids, was only 5% to 10% of the total antimony released, it can be a significant proportion of that found in the negative plate material, 6% after formation, 20% after overcharging and 56% after cycling. With no separator present⁽¹⁰⁾, during formation, 72% of the antimony released from the negative was found on the positive plate; whereas with a wooden separator present a smaller

proportion of the negative grid antimony released was found on the positive plate, 15% after overcharging and 27.5% after cycling. If the separator had been restricting the antimony diffusion from the positive to the negative than a greater proportion of the positive grid antimony should have been found in the separator. A later publication⁽¹¹⁾ showed that the influence of a good separator can be reduced in its effectiveness since the design of certain batteries allows the diffusion of the antimony round the sides of the separator.

The present work has shown that the antimony released into the electrolyte by anodic corrosion of the positive plate alloy is present as the antimony (V) anion. Adsorption of antimony (V) onto lead dioxide also occurs and this rate of adsorption is greater than the rate of adsorption of antimony (V) onto lead sulphate. Using a tracer technique, Zehender et al⁽¹¹⁾, observed antimony fluctuations in the positive compartment electrolyte; during charge, antimony was removed from solution and was released again during the subsequent discharge cycle. It would now appear that these antimony fluctuations, involving antimony (V), arose from the different surface properties of lead dioxide and lead sulphate.

During charging of the battery, lead sulphate is converted to lead dioxide and as such can adsorb more antimony (V).

Discharge of the battery converts the surface lead-dioxide to lead sulphate thereby releasing the adsorbed antimony. Although anodic grid corrosion produces antimony in the electrolyte, lead dioxide in the plate can retain antimony (V) at the positive plate, and 73 to 95% of the antimony released from the positive grid of a car battery was found in the positive plate material (10). The charging current will also cause ionic migration of antimony (V) to the positive plate.

It is thought, at present, that both the antimony of the negative grid and the antimony deposited onto the negative plate are released by the formation of stibine. The deposition studies indicated that the production of stibine may not be totally responsible for the removal of antimony since antimony was removed from the experimental electrodes only in the presence of dissolved oxygen or hydrogen peroxide. Ruetschi and Angstadt (5) have shown that dissolved oxygen, produced on charging of the positive plate, can diffuse through the electrolyte to the negative and cause self-discharge. It is suggested that a reaction involving dissolved oxygen might be largely responsible for the removal of antimony from the negative of the lead-acid battery. Antimony (III) is formed, however, from the negative plate antimony, independent of the reaction.

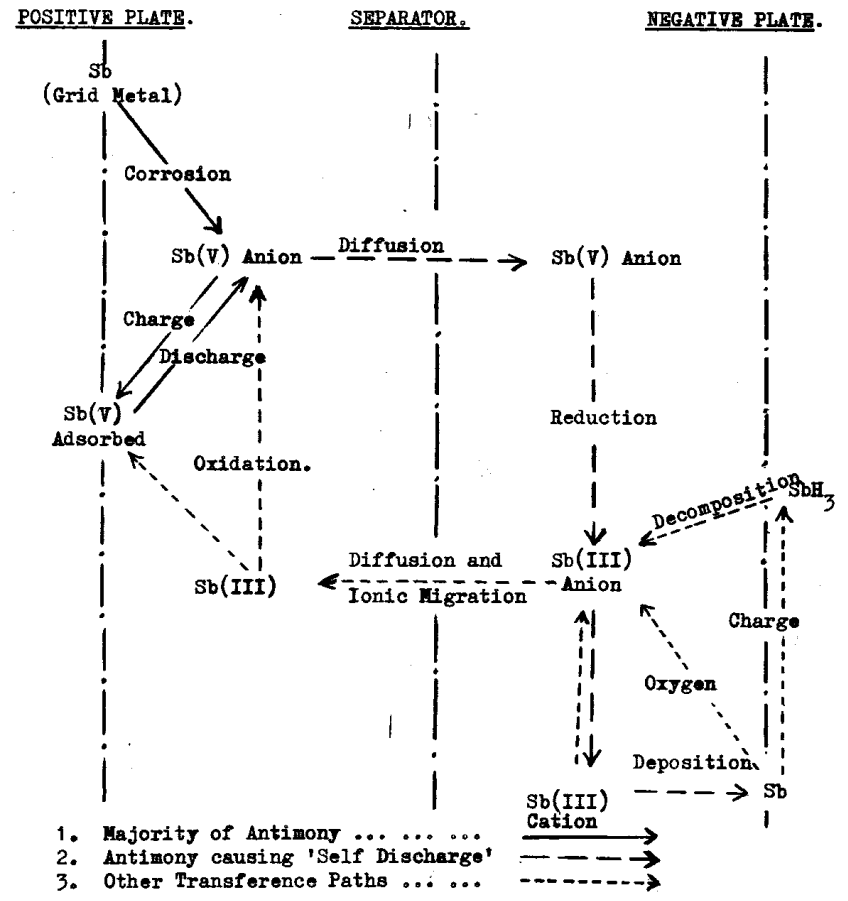


Fig. 4.6. Transference of the Antimony released into the Lead-Acid Battery.

Antimony (III) and antimony (V) can both diffuse through the separator (10). The diffusion of the antimony (III) from the negative will involve ionic migration and the concentration gradient across the separators, whereas the anionic antimony (V) diffusion will be due to the concentration gradient.

Antimony (III) diffusing into the positive plate compartment will be oxidised, either during the charging period or on adsorption on the lead dioxide. When no separator is present, during formation of the battery plates, 72% of the antimony released from the negative grids was found in the positive active material (10).

The present experiments have shown that antimony (V) must be reduced before it deposits onto sponge lead.

The antimony transference and reaction paths discussed above are shown in the schematic diagram, Fig. (4.6), for convenience these ions are shown in their simplest form.

4.3.3 The Limiting of 'Antimony Poisoning'.

From a survey of the literature available it became obvious that previous workers in this field had not considered the chemical nature of antimony in aqueous sulphuric acid when they studied the technological problem of 'antimony poisoning'. The effect of different separator materials on battery performance is well known, but experiments designed to study the influence of these materials

on the diffusion of antimony from the positive compartment must use antimony (V) solution; as shown in previous discussion on the transference of antimony.

Although in the present work the size of the antimony (V) ions were not determined, indications were that these ions should be larger than the antimony (III) ions. The results ⁽¹⁰⁾ from batteries dosed with antimony 124 and containing good wooden separators apparently limited the migration of the antimony (III) from the negative to positive plate rather than reducing the diffusion of the antimony (V) to the negative.

A suitable separator material, as well as being inert to chemical attack, should be impermeable to antimony (V) ions whilst being permeable to sulphate and antimony (III) ions. To be effective the separator should have an envelope construction to completely contain either the negative or positive plate. If the separator eliminated all the antimony diffusion, a certain amount of self-discharge would still occur because of the antimony released from the negative grid being redeposited on the negative plate.

The present work shows that ion exchange materials could be used to advantage in this technological problem by utilisation of the chemical difference between antimony (V) and antimony (III). Other workers ⁽⁴¹⁾ have produced cellulose separators containing

kieselguhr and coated with resins, which reputedly reduced the rate of 'antimony poisoning', presumably by reducing the rate of antimony diffusion, although the actual mechanisms involved were not known. Since approximately 3 gm of antimony ⁽¹⁰⁾ are produced from the positive grids of an 84 Ahr car battery, after 100 charge-discharge cycles the removal of antimony (V) from the positive compartment electrolyte by an ion exchanger would be impractical, due to the amount of antimony involved, and the lead dioxide of the plate already adsorbs an appreciable quantity of antimony.

The amount of antimony found ⁽¹⁰⁾ in the negative plate material was 0.6 gms, therefore, a suitable cationic ion exchanger could remove the antimony (III) from the negative compartment electrolyte, especially if used in conjunction with a good separator material and design. The ion exchange material could be introduced, for example, on a glass wool mat support placed between the negative plate and the separator. The feasibility of separating antimony (III) and antimony (V) in dilute aqueous sulphuric acid solutions on a zirconium phosphate column has already been established ⁽²⁴⁾ and the development of a suitable ion exchange material for use in the strong acidic conditions encountered in the lead-acid battery could prove advantageous in limiting the antimony poisoning of the negative plate.

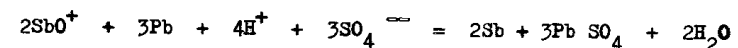
5. Conclusion.

Ionic migration experiments, ultra-violet absorption spectra and polarographic determinations on aqueous sulphuric acid containing less than $1 \times 10^{-4}M$ antimony showed that antimony (III) was present as the ions:- SbO^+ , $[H_2Sb(SO_4)_2]^+$, $[(H_2O)_2Sb(OH)_2]^+$, $[SbO(OH)_2]^-$, $[SbO_2SO_4]^-$, $[Sb(SO_4)_2]^-$ and $[SbO_2]^-$. The cation $[(H_2O)_2Sb(OH)_2]^+$ occurs in solutions with a sulphuric acid concentration less than 1.5M and SbO^+ was the only cation found in the acid range 2 - 12M sulphuric acid. The ions $[Sb(SO_4)_2]^-$ and $[H_2Sb(SO_4)_2]^+$ predominate above 14M sulphuric acid, and $[SbO(OH)_2]^-$ was the anion found in dilute acid below 2M sulphuric. The maximum concentration of the sulphate complexed anion $[SbO_2SO_4]^-$ occurred at 7M sulphuric acid and the anion $[SbO_2]^-$ is suggested to occur in 10 to 14M sulphuric acid. Above an antimony (III) concentration of $1 \times 10^{-4}M$ these ions dimerised to give other species, for example, $O = Sb - SO_4 - Sb = O$.

In 0.5 to 8 M sulphuric acid and from 0 to $10 \times 10^{-4}M$ antimony, the antimony (V) was shown to exist as a stable complex anion containing a double bridge structure and can be considered as $[Sb_3O_9]^{3-}$. At sulphuric acid concentrations greater than 8Molar there was evidence of complexing of the antimony (V) with the undissociated sulphuric acid.

The tracer technique developed to determine the rate of deposition of antimony from aqueous sulphuric acid onto the pure lead

electrodes showed that antimony (III) deposition is a diffusion controlled reaction. The deposition rate was found to be independent of the hydrogen overpotential of the electrode and was ascribed to the electrochemical displacement reaction



In oxygen free electrolyte and under the forced convection conditions of electrolyte flow used, the deposition rate was governed by the equation

$$\text{Nu} = \text{K Re}^{\frac{1}{2}} \text{Sc}^{\frac{1}{3}}$$

Where Nu and Re are the Nusselt and Reynold numbers at the electrode respectively and Sc is the Schmidt number. These dimensionless numbers include the properties of the electrolyte and were given by

$$\text{Nu} = \frac{kx}{D} ; \text{Re} = \frac{v x}{\nu} ; \text{Sc} = \frac{\nu}{D}$$

Where k, the kinetic mass-transfer constant of the deposition reaction equalled the rate of antimony deposition (mol or g equiv. $\text{cm}^{-2} \text{sec}^{-1}$) divided by the antimony concentration in the electrolyte (mol cm^{-3}) or (g equiv. cm^{-3}), x a characteristic length, for example, the electrode height or the hydraulic diameter of the electrolyte flow (cm)

D = the diffusion coefficient of the antimony (III), ($\text{cm}^2 \text{s}^{-1}$)

v = the velocity of the electrolyte (cm s^{-1}) and

ν = the kinematic viscosity of the electrolyte ($\text{cm}^2 \text{s}^{-1}$)

The constant K was dependent on the characteristic length chosen for determining the Nusselt and Reynolds numbers.

The temperature coefficient of the kinetic mass-transfer process corresponded to a heat of activation of 1.96 ± 0.1 K cal mole⁻¹, as determined from an Arrhenius plot of $\log k$ vs $\frac{1}{T}$.

Under open circuit conditions, antimony (III) deposition continued until the electrode was covered with antimony and lead sulphate, the electrode then behaved as an antimony electrode. In the presence of dissolved oxygen corrosion of the antimony occurred, whereas in oxygen free electrolyte no corrosion occurred, a phenomena which can resolve the conflicting theories of the behaviour of the antimony electrode in acid solutions. In oxygen free electrolyte, the electrode potential remained constant at + 0.195 volts, whereas in the presence of dissolved oxygen the potential of the electrode fell to that of a mixed lead-lead sulphate, antimony electrode potential of $\approx + 0.012$ volts, after sufficient antimony had corroded from the electrode surface. Antimony (V) was not deposited onto the lead electrodes but required reduction to antimony (III) before deposition occurred. Neither antimony (III) or (V) were deposited electrolytically onto lead-lead dioxide electrodes. Tracer experiments showed that antimony was adsorbed onto lead dioxide and to a lesser extent on to lead sulphate.

The results obtained were assessed in conjunction with published data, and a comprehensive picture of the various antimony reaction paths occurring in the lead-acid battery has been presented.

The removal of antimony from the negative plate and grid results in the formation of antimony (III) in the electrolyte and probably involves the production of stibine. From the present work however, it would appear that dissolved oxygen, produced at the positive plate is also responsible for the dissolution reaction. This antimony (III) can be re-deposited, although some is adsorbed, with oxidation, on the positive plate.

Anodic corrosion of the positive plate releases antimony (V) into the electrolyte; the majority of this antimony is adsorbed on to the active material of the positive plate.

Antimony (V) ions which diffuse into the negative electrolyte compartment are reduced to antimony (III) prior to deposition on to the negative plate. The requirements of a separator material are that it should be impermeable to antimony (V) ions whilst allowing the diffusion of antimony (III) and sulphate ions. The placing of a suitable cationic ion exchange material between the separator and the negative plate, to remove antimony (III) is suggested as a feasible method of limiting the problem of 'antimony poisoning' of the negative plate.

6. Appendix.

6.1. Electrode Potentials.

Unless stated otherwise, the electrode potentials were measured against a hydrogen electrode in sulphuric acid of the same concentration as used in the particular experiment.

The standard electrode potentials quoted in this thesis have the sign convention adopted by the 'International Union of Pure and Applied Chemistry'. On this convention of the potentials are (a) reduction potentials (b) positive for noble metals (c) identical with the 'European' sign convention.

The electrode potentials of interest are (42) :-

$$\text{Pb} / \text{PbSO}_4 \quad E_o = -0.365 \text{ V}$$

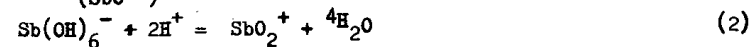
$$\text{Pb} / \text{PbO}_2 \quad E_o = +1.7 \text{ V}$$

Antimony reactions (14),

1. Homogeneous reactions without oxidation

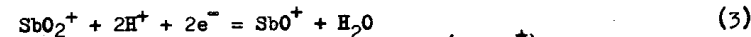


$$\log \frac{(\text{HSbO}_2)}{(\text{SbO}^+)} = -0.87 + \text{pH}$$

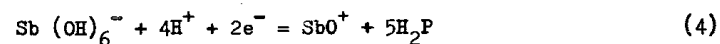


$$\log \frac{(\text{Sb}(\text{OH})_6^-)}{(\text{SbO}_2^+)} = 0.54 + 2\text{pH}$$

with oxidation



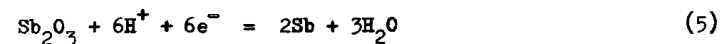
$$E = 0.720 - 0.0591 \text{ pH} + 0.0295 \log \frac{(\text{SbO}_2^+)}{(\text{SbO}^+)}$$



$$E = 0.704 - 0.1182 \text{ pH} + 0.0295 \log \frac{(\text{Sb}(\text{OH})_6^-)}{(\text{SbO}^+)}$$

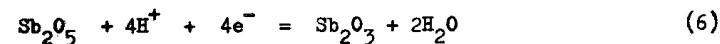
2. Heterogeneous reactions involving two solids,

with oxidation



(cubic) $E = 0.152 - 0.0591 \text{ pH}$

(ortho) $E = 0.167 - 0.0591 \text{ pH}$

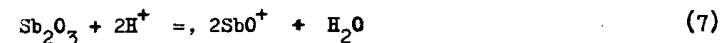


(cubic) $E = 0.671 - 0.0591 \text{ pH}$

(ortho) $E = 0.649 - 0.0591 \text{ pH}$

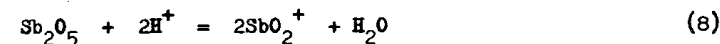
3. Heterogeneous reactions involving one solid

without oxidation

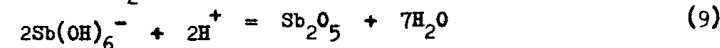


(cubic) $\log (\text{SbO}^+) = -3.05 - \text{pH}$

(ortho) $\log (\text{SbO}^+) = -2.32 - \text{pH}$



$\log (\text{SbO}_2^+) = -4.70 - \text{pH}$

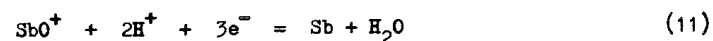


$\log (\text{Sb}(\text{OH})_6^-) = -4.16 + \text{pH}$

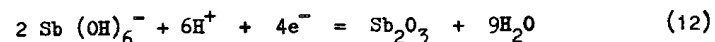
with oxidation



$E = -0.510 - 0.0591 \text{ pH} - 0.0197 \log P \text{ SbH}_3$

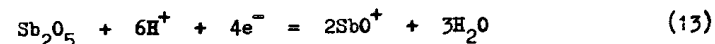


$$E = 0.212 - 0.0394 \text{ pH} + 0.0197 \log (\text{SbO}^+)$$



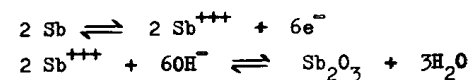
$$(\text{cubic}) E = 0.794 - 0.0836 \text{ pH} + 0.0295 \log (\text{Sb}(\text{OH})_6^-)$$

$$(\text{ortho}) E = 0.722 - 0.0886 \text{ pH} + 0.0295 \log (\text{Sb}(\text{OH})_6^-)$$



$$E = 0.581 - 0.0886 \text{ pH} - 0.0295 \log (\text{SbO}^+)$$

Until recently the accepted mechanism for the Sb/Sb₂O₃ electrode was that suggested by Roberts and Fenwick⁽⁴³⁾ which involved the intermediate Sb⁺⁺⁺ :-



but equation (5) is more likely in the pH range 1-10.

Pitman et al⁽¹⁴⁾ demonstrated that in acid solutions the solid phases involved in the antimony electrode system are stable only under the following conditions,

- (i) Antimony metal - by equations (5) (11) and (10)
- (ii) Antimony trioxide - by equations (11) (5) (6) (7) and (12)
- (iii) Antimony pentoxide - by equation (6) (8) and (9)

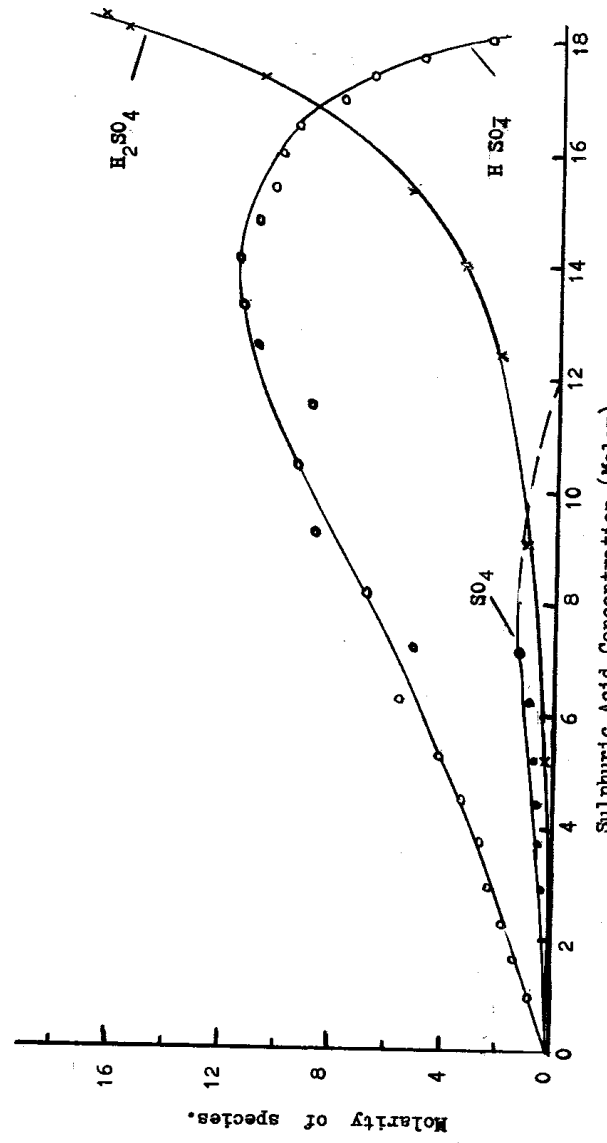
Antimony tetroxide is never thermodynamically stable at 25°C. in the presence of water.

Stibine can be produced by equation (17) but is unstable in the presence of aqueous solutions and decomposes with the formation of antimony (21) and hydrogen.

6.2. Diffusion Coefficients of Antimony (21).

S.G. H ₂ SO ₄	M. H ₂ SO ₄	Diff. Coeff. (cm ² sec ⁻¹)	$\frac{1}{\text{Viscosity}}$ (centipoise ⁻¹)
1.150	2.51	3.84 x 10 ⁻⁶	0.7143
1.200	3.40	3.35 x 10 ⁻⁶	0.6132
1.255	4.41	2.65 x 10 ⁻⁶	0.5089
1.300	5.26	2.22 x 10 ⁻⁶	0.4292
1.340	6.08	1.62 x 10 ⁻⁶	0.3636

The values of the different coefficients were calculated from limiting current measurements on an antimony electrode in antimony (III) - sulphuric acid solutions.



Sulphuric Acid Concentration (Molar).
Composition of the Water/Sulphuric Acid System, (28.)

REFERENCES.

- (1) Gladstone and Tribe; Nature, 27, 583, (1883)
- (2) Vinal and Craig; J. Res. Nat. Bur. Stds. 14, 449, (1935).
- (3) Beck and Wynne-Jones; Trans. Far. Soc. 52, 1260, (1956).
- (4) Vinal, Storage Batteries; 4th Ed. Pub. John Wiley and Sons, New York.
- (5) Ruetshi and Angstadt; J. Elect. Chem. Soc. 105, 555, (1958).
- (6) Strasser and Gahl; Z. Elektro-chem angenphysik Chem. 7, 11, (1900).
- (7) Crennel and Milligan; Trans. Farad. Soc. 27, 103, (1931).
- (8) Haring and Thomas; Trans. Electrochem. Soc, 68, 293, (1935).
- (9) Byfield; Trans. Electrochem. Soc, 79, 259, (1941).
- (10) Herrmann and Propstl; Z. fur Elektrochemi 61, 1154, (1957).
- (11) Zehender, Herrmann and Leibssle; Electrochimica Acta, 9, 55, (1964).
- (12) Wells; 'Structural Inorganic Chem.' 2nd edit. Pub. Oxford Press. (1962).
- (13) Gould; 'Inorganic Reactions and Structure' Pub. Holt, Rinehart and Winston (1962).
- (14) Pitman, Pourbaix and de Zoubov; J. Electrochem. Soc, 104, 594, (1957).
- (15) Cotton and Wilkinson; Inorganic Chemistry. 2nd Edit. J. Wiley (1966).
- (16) Remy; 'Treatise on Inorganic Chem.' Pub. Elsevier, (1956).
- (17) Dawson; Dip. Tech. Thesis, Salford, (1962).
- (18) Gillibrand and Lomax; Electrochemical Acta. 8, 693, (1963).
- (19) Randles; Trans. Farad. Soc. 44, 327, (1948).
- (20) Lingane; Ind. Eng. Chem. Ind. Eng. Chem. Anal Ed. 15, 583, (1943).

- (21) Jackson; R.D.S. Report, Chloride Technical Services Limited. R. & D. Report 12/4, No. 1. (1963).
- (22) Newmann; J. Am. Chem. Soc, 76, 2611, (1954).
- (23) Bugaenko & Huang Kuen-lin; Russ. J. Phy. Chem. 8, 1299, (1963)
- (24) Rothwell; Dip. Tech. Thesis. R.C.A.T. Salford, (1966).
- (25) Levy, Danford and Agron; J. Chem. Phys. 31, 1458. (1959).
- (26) Orgel; Quart. Revs. 8, 422, (1954).
- (27) Young; Record Chem. Progress 12, 81, (1951).
- (28) Zarakhani and Vinnik; Russ. J. Phys. Chem. 37, 260, (1963)
- (29) Newmann and Brown; J. Am. Chem. Soc, 78, 1843, (1956).
- (30) Sincius; Ph.D., Thesis, Mich. State Univ. Microfilm 62-47, 131.
- (31) Levich; Disc. Farad. Soc, 1, 37, (1947).
- (32) Wrangton and Nilsson; Electrochim. Acta, 7, 121, (1962).
- (33) Bazan and Arvia; Electrochim. Acta, 9, 17, (1964)
- (34) Kolthoff and Hartong; Rec.Trav.Chim, 44, 113, (1925).
- (35) Parks and Beard; J. Am. Chem. Soc. 54, 856, (1932)
- (36) Tourky and Mousa; J. Chem. Soc. 756, (1948).
- (37) Perley; Ind. Eng. Chem. Anal. Ed. 11, 316, (1939).
- (38) Kan and Knappsberg; A. Elek. Chem, 45, 760, (1939).
- (39) Gatty and Spooner; "Electrode Potential Behaviour of Corroding Metals in Aqueous Solutions" Oxford, University Press (1938).
- (40) Tomlinson; J. Elect. Chem. Soc. 111, 592, (1964).
- (41) Electric Storage Battery Co; Brit.Pat.Nos. 786298, 896800.
- (42) Janz and Ives; Reference Electrodes Theory and Practice. Pub. Academic Press. (1961).
- (43) Roberts and Fenwick; J.Am.Chem.Soc. 50, 2125, (1928).
- (44) Ruetschi; U. S. Patent No. 3,265,534 (1966).

- (45) Thilo, Von Erich; Int. Symp. Inorg. Polymers, Special Pub. 15, Chem. Soc. (1961).
- (46) Kaye and Laby; Phys. and Chem. Constants, Pub. Longmans (1956).